DOT/FAA/AR-09/9

Air Traffic Organization
NextGen & Operations Planning
Office of Research and
Technology Development
Washington, DC 20591

Damage Tolerance Evaluation of Full-Scale Sandwich Composite Fuselage Panels

May 2009

Final Report

This document is available to the U.S. public through the National Technical Information Service (NTIS), Springfield, Virginia 22161.

U.S. Department of Transportation
Federal Aviation Administration

NOTICE

This document is disseminated under the sponsorship of the U.S. Department of Transportation in the interest of information exchange. The United States Government assumes no liability for the contents or use thereof. The United States Government does not endorse products or manufacturers. Trade or manufacturer's names appear herein solely because they are considered essential to the objective of this report. This document does not constitute FAA certification policy. Consult your local FAA aircraft certification office as to its use.

This report is available at the Federal Aviation Administration William J. Hughes Technical Center's Full-Text Technical Reports page: actlibrary.faa.gov in Adobe Acrobat portable document format (PDF).

Technical Report Documentation Page

1. Report No.	2. Government Accession No.	3. Recipient's Catalog No.
DOT/FAA/AR-09/9		

4. Title and Subtitle	5. Report Date
DAMAGE TOLERANCE EVALUATION OF FULL-SCALE SANDWICH COMPOSITE FUSELAGE PANELS	May 2009
	6. Performing Organization Code
7. Author(s)	8. Performing Organization Report No.
K.S. Raju and J.S. Tomblin	
9. Performing Organization Name and Address	10. Work Unit No. (TRAIS)
Wichita State University 1845 N. Fairmount Wichita, KS 67260-0093	11. Contract or Grant No.
12. Sponsoring Agency Name and Address	13. Type of Report and Period Covered
U.S. Department of Transportation Federal Aviation Administration Air Traffic Organization NextGen & Operations Planning Office of Research and Technology Development Washington, DC 20591	Final Report
	14. Sponsoring Agency Code ACE-110

15. Supplementary Notes

The Federal Aviation Administration Airport and Aircraft Safety R&D Division Technical Monitor was Peter Shyprykevich.

16. Abstract

This report examines the behavior of full-scale cylindrical sandwich panels with different flaw types under longitudinal and pressurization loads that were investigated experimentally. Test panels were fabricated using Toray T700S-12K-50C/#2510 plain weave carbon fabric prepreg (F6273C-07M, 190 g/m^2) for the facesheets and an overexpanded cell DuPont™ Nomex® honeycomb core (Hexcel Composites, HRH-10/OX-3/16-3.0). Both facesheets had a stacking sequence of [45/0/45] and the core thickness used in the test section was 0.75 inch. The cylindrical panel had an internal radius of 74 inches and measured 125 inches long. An undamaged test panel was subjected to longitudinal loading, pressurization, and a combination of both loads to study the resulting strain distributions in the panel. Test panels with a 10-inch-diameter open hole, 10-inch-long slit along longitudinal direction, 10-inch-long longitudinal notch, 10-inch-long circumferential notch, and a 10-inch-long notch at 45º to the longitudinal axis were tested under different combinations of loads, and the residual strengths were measured.

A total of eight static tests were performed on six full-scale panels. The first test was on an unnotched panel that was subsequently damaged with a longitudinal and cross slits in the top facesheet to induce failure. Because of the apparatus load limitations, failure was achieved only with a 10-inch-longintudinal slit under pure pressure loading of 14 psi. The second panel tested contained a 10-inch-diameter hole in the top facesheet. Failure was initiated at 21.4 psi pressure, but not propagated because of load limitations. The other four panels, with 10- by 1/2-inch notches oriented at three different directions, were tested under longitudinal, pressure, and combined loading until failure. In all cases, failures initiated at the notch. All panels were instrumented with strain gages. Strain gage readings were compared to previously performed finite element analysis modeled as a flat plate. Predictions were also made as to when failure would occur and were compared to test results.

17. Key Words	18. Distribution Statement
Sandwich, Damage tolerance, Combined loading, Notches, Holes, Full-scale	This document is available to the U.S. public through the National Technical Information Service (NTIS), Springfield, Virginia 22161.

19. Security Classif. (of this report)	20. Security Classif. (of this page)	21. No. of Pages	22. Price
Unclassified	Unclassified	101	

Form DOT F 1700.7 (8-72) Reproduction of completed page authorized

TABLE OF CONTENTS

		Page
EXECUTIVE SUMMARY		xi
1.	INTRODUCTION	1
2.	FULL-SCALE AIRCRAFT STRUCTURAL TEST EVALUATION AND RESEARCH FACILITY	3
3.	DESIGN AND FABRICATION OF TEST ARTICLE	6
4.	TEST PROGRAM AND TEST MATRIX	14
4.1	Estimation of Failure Loads	17
4.2	Geometry, Coordinates, and Loads	20
4.3	Test Article Instrumentation	22
5.	RESULTS	26
5.1	Test Panel CP1	26
5.1.1	Longitudinal Loading	27
5.1.2	Pressurization/Hoop Loading	31
5.1.3	Combined Longitudinal and Pressurization Loading	34
5.2	Test Panel CP1A	36
5.3	Test Panel CP1B	38
5.4	Test Panel CP2	44
5.4.1	Longitudinal Loading	44
5.4.2	Combined Longitudinal, Pressurization Loading	49
5.4.3	Pressurization Loading	55
5.5	Test Panel CP3	57
5.6	Test Panel CP4	61
5.7	Test Panel CP5	64
5.8	Test Panel CP6	68
6.	Comparison of Test and Analysis of Panel Failure Loads	74
7.	SUMMARY	75
8.	REFERENCES	76
APPENDIX A—ANALYSIS FOR FAILURE LOAD ESTIMATION		

LIST OF FIGURES

Figure		Page
1	Compressive Residual Strength vs Planar Damage Area for Impact Damaged Sandwich Panels	2
2	Strengths of Sandwich Panels With Open Holes Under Tensile and Compressive Loading	2
3	Full Assembly and Exploded Views of the FASTER Test Fixture	3
4	Schematic of Force Multiplication Lever Assembly With Whiffle-Tree Links Used for Longitudinal and Hoop Loading	4
5	Deformation of a Cylindrical Chord Under Internal Pressure and Loading in a Semi-Monocoque Fuselage Panel Using the FASTER Fixture	5
6	Schematic of Frame Loading Assembly and Radial Reaction Link	6
7	Overall Geometry of the Curved Test Panel	7
8	Geometric Details of Loading Edges	8
9	Tangency of Hoop Loading Edge With the Test Section of the Panel	8
10	Subdivision of Panel Based on Stacking Sequence	10
11	Stacking Sequence in Regions A and B	10
12	Stacking Sequence in Regions C and D	11
13	Pattern Machining for the Mold	11
14	Test Panel During the Layup Process	12
15	A Close-Up of the Honeycomb Core Being Placed on the Top Facesheet	12
16	Test Panel After Curing and Ready to be Machined	13
17	Test Panel After Machining	13
18	Test Panel With Hole in Top Facesheet (Convex Side)	15
19	Test Panel With Circumferential Notch (CP3 and CP4)	15

20	Test Panel With Longitudinal Notch (CP5)	16
21	Test Panel With Off-Axis Notch (CP6)	16
22	Finite Element Model, No Damage	18
23	Finite Element Model, 10-Inch-Diameter Hole	18
24	Finite Element Model, 10-Inch-Longitudinal Notch	19
25	Finite Element Model, 10-Inch-Circumferential Notch	19
26	Geometry and Coordinates Associated With the Test Article	21
27	Far-Field Strain Gage Locations and Orientations Common to all Test Panels	23
28	Strain Gage Locations in the Vicinity of the Open Hole	24
29	Strain Gage Locations in the Vicinity of Longitudinal and Circumferential Notches	25
30	Strain Gage Locations in the Vicinity of the Off-Axis Notch	26
31	Assumed Strain Distribution for Computing the Bending Deformation in the Panel	27
32	Variation of Longitudinal Strain (Top Facesheet) With Applied Longitudinal Loading at Different Locations on the Test Panel	28
33	Variation of Hoop Strain (Top Facesheet) With Applied Longitudinal Loading at Different Locations on the Test Panel	28
34	Variation of Longitudinal Strains as a Function of Hoop Location	29
35	Variation of Longitudinal Strains as a Function of Longitudinal Location	30
36	Bending of Panel in r-z and r-θ Planes Under Pure Longitudinal Loading	30
37	Variation of Hoop Strain (Top Facesheet) With Applied Hoop Loading at Different Locations on the Test Panel	31
38	Variation of Longitudinal Strain (Top Facesheet) With Applied Hoop Loading at Different Locations on the Test Panel	32
39	Variation of Hoop Strains as a Function of the Circumferential Direction	33
40	Variation of Hoop Strains as a Function of the Longitudinal Direction	33

41	Bending of Panel in r-z and r-θ Planes Under Pure Pressurization/Hoop Loading	34
42	Variation of Longitudinal Strain (Top Facesheet) With Applied Loading at Different Locations on the Test Panel	35
43	Variation of Hoop Strain (Top Facesheet) With Applied Loading at Different Locations on the Test Panel	35
44	Bending of Panel in r-z and r-θ Planes Under Combined Loading	36
45	Slit Geometry and Strain Gage Locations for Test Panel CP1A	37
46	Variation of Far-Field Strains With Applied Longitudinal Load	37
47	Strain Profiles Along the Critical Section (z=0) on the Top Facesheet	38
48	Slit Geometry and Strain Gage Locations for Test Panel CP1B	39
49	Variation of Far-Field Hoop Strains With Applied Loading	39
50	Far-Field Bending of Panel in r-θ Plane	40
51	Variation of Hoop Strain Along the Critical Section With Applied Loading	41
52	Hoop Strain Distributions on the Top Surface Prior to and After Failure Initiation	41
53	Hoop Strain Distributions on the Bottom Surface Prior to and After Failure Initiation	42
54	Bending in r-θ Plane Along s=0 Near the Notch Tip	42
55	Fracture Path in the Vicinity of the Notch in the Bottom Facesheet	43
56	Fracture Path in the Vicinity of the Notch in the Top Facesheet	43
57	Far-Field Longitudinal Strains as a Function of Longitudinal Loading in Panel CP2	45
58	Far-Field Hoop Strains as a Function of Longitudinal Loading in Panel CP2	45
59	Longitudinal Strain Distribution Along a Section at a Distance of z=-24 Inches From the Center of the Panel	46
60	Hoop Strain Distribution Along a Section at a Distance of s=+12 Inches From the Center of the Panel	46
61	Bending in r-z Plane at Different Locations in the Test Panel	47

62	Bending in r-θ Plane at Different Locations in the Test Panel	48
63	Observed Bending Deformation of the Panel Based on Strain Gage Data	48
64	Tangential Strains Near the Hole Boundary on the Top Facesheet for Panel CP2 Under Longitudinal Loading	49
65	Tangential Strains Near the Hole Boundary on the Bottom Facesheet for Panel CP2 Under Longitudinal Loading	49
66	Combined Loading of Panel With Open Hole	50
67	Far-Field Longitudinal Strains Under Combined Loading in Panel CP2	51
68	Far-Field Hoop Strains Under Combined Loading in Panel CP2	51
69	Longitudinal Strain Distribution at z=-24 Inches Under Combined Loading	52
70	Hoop Strain Distribution at s=+12 Inches Under Combined Loading	52
71	Bending of Test Panel in the r-z Plane Under Combined Loading	54
72	Bending of Test Panel in the r-θ Plane Under Combined Loading	54
73	Tangential Strains Near the Hole Boundary on the Top Facesheet	55
74	Tangential Strains Near the Hole Boundary on the Bottom Facesheet	55
75	Observed Crack at Hole Boundary Under Pressurization Loading	56
76	Tangential Strains Near the Hole Boundary on the Top Facesheet Under Pressurization Loading	57
77	Planned Loading Sequence for Test Panel CP3	58
78	Applied Loading Sequence for Test Panel CP3	58
79	Far-Field Longitudinal Strains in Panel CP3	59
80	Far-Field Hoop Strains in Panel CP3	59
81	Strains in the Vicinity of the Notch in Panel CP3	60
82	Picture of Observed Failure Mode in One-Half of Panel CP3	61
83	Planned Loading Sequence for Test Panel CP4	62

84	Applied Loading Sequence for Test Panel CP4	62
85	Far-Field Longitudinal Strains in Panel CP4	63
86	Far-Field Hoop Strains in Panel CP4	64
87	Strains in the Vicinity of the Notch in Panel CP4	64
88	Repair Patch on the Interior (Concave) Side of Panel CP5	65
89	Applied Loading Sequence for Test Panel CP5	66
90	Far-Field Longitudinal Strains in Panel CP5	66
91	Far-Field Hoop Strains in Panel CP5	67
92	Hoop Strains in the Vicinity of the Notch on the Top (Convex) Facesheet	68
93	Hoop Strains in the Vicinity of the Notch on the Bottom (Concave) Facesheet	68
94	Applied Loading Sequence for Test Panel CP6	69
95	Far-Field Longitudinal Strains in Panel CP6	70
96	Far-Field Hoop Strains in Panel CP6	70
97	Normal Strains in the Vicinity of the Notch on the Top (Convex) Facesheet	71
98	Normal Strains in the Vicinity of the Notch on the Bottom (Concave) Facesheet	71
99	Longitudinal Strains in the Vicinity of the Notch on the Top (Convex) Facesheet	72
100	Longitudinal Strains in the Vicinity of the Notch on the Bottom (Concave) Facesheet	72
101	Hoop Strains in the Vicinity of the Notch on the Top (Convex) Facesheet	73
102	Hoop Strains in the Vicinity of the Notch on the Bottom (Concave) Facesheet	73
103	Failure Mode in Panel CP6 With Off-Axis Notch	74

LIST OF TABLES

Table		Page
1	Nominal Mechanical Properties of Toray T700S-12K-50C/#2510 Plain Weave Carbon Fabric Prepreg	9
2	Nominal Mechanical Properties of HRH-10/OX-3/36-3.0 Honeycomb Core	9
3	Planned Loading for Panels With Different Damage Types	14
4	Summary of Estimated Failure Loads and Modes for Test Panels With Different Damage Types	20
5	Comparison of Initiation and Final Failure Loads With the Predicted Failure Loads	74

LIST OF ACRONYMS

CLPT	Classical Laminated Plate Theory
FAA	Federal Aviation Administration
FASTER	Full-Scale Aircraft Structural Test Evaluation and Research
MS	Margin Safety
WSU	Wichita State University

EXECUTIVE SUMMARY

This report examines the behavior of full-scale cylindrical sandwich panels with different flaw types under longitudinal and pressurization loads that were investigated experimentally. Test panels were fabricated using Toray T700S-12K-50C/#2510 plain weave carbon fabric prepreg (F6273C-07M, 190 g/m^2) for the facesheets and an overexpanded cell DuPont™ Nomex® honeycomb core (Hexcel Composites, HRH-10/OX-3/16-3.0). Both facesheets had a stacking sequence of [45/0/45], and the core thickness used in the test section was 0.75 inch. The cylindrical panel had an internal radius of 74 inches and measured 125 inches long. An undamaged test panel was subjected to longitudinal loading, pressurization, and a combination of both loads to study the resulting strain distributions in the panel. Test panels with a 10-inch-diameter open hole, 10-inch-long slit along longitudinal direction, 10-inch-long longitudinal notch, 10-inch-long circumferential notch, and a 10-inch-long notch at 45º to the longitudinal axis were tested under different combinations of loads, and the residual strengths were measured.

A total of eight static tests were performed on six full-scale panels. The first test was on an unnotched panel that was subsequently damaged with a longitudinal and cross slits in the top facesheet to induce failure. Because of the apparatus load limitations, failure was achieved only with a 10-inch-longintudinal slit under pure pressure loading of 14 psi. The second panel tested contained a 10-inch-diameter hole in the top facesheet. Failure was initiated at 21.4 psi pressure, but not propagated because of load limitations. The other four panels, with 10- by 1/2-inch notches oriented at three different directions, were tested under longitudinal, pressure, and combined loading until failure. In all cases, failures initiated at the notch. All panels were instrumented with strain gages. Strain gage readings were compared to previously performed finite element analysis modeled as a flat plate. Predictions were also made as to when failure would occur and were compared to test results.

1. INTRODUCTION.

Sandwich construction is widely used in airframe structural applications due to the distinct advantages they offer over other metallic and composite (monolithic laminate) structural configurations in terms of stiffness, stability, specific strength, corrosion resistance, ease of manufacture and repair, and above all, weight savings. However, the sandwich structures are very susceptible to localized transverse loads, due to their inherent construction [1-3]. Some of these loads are accidental in nature [1 and 2], and could be inflicted on the airframe structure during various stages of the aircraft's life [1 and 2]. The response of sandwich structures to the accidental loads, the resulting damage states, their detectability and the effects of the damage states on the residual properties have been widely investigated using experimental and analytical methods [1 and 3]. However, most damage resistance and tolerance investigations have been confined to laboratory coupons, with limited studies on scaling effects [4 and 5], while the studies on full-scale sandwich airframe components are rare. Most previous investigations of fuselage type structures under combined loading conditions have been limited to semi-monocoque metallic structures [6-8].

The damage tolerance of sandwich panels has been previously investigated by subjecting the damaged specimens to uniaxial in-plane compressive loads. The sandwich panels were observed to fail in contrasting modes, depending on the nature of the initial damage magnitude and morphology [1 and 3]. However, the compressive residual strength was found to correlate well with the planar damage size, with the asymptotic portion of the residual strength degradation curve being populated by damage states due to larger diameter (3″) impactors, as shown in figure 1. While the impact damage states produce a significant strength reduction, it was determined that the strength reduction due to an open-hole damage, which represents the situation where no load path exists through the damage zone, produces strength reduction that is a lower bound on the residual strength of a panel for a given planar flaw size [5]. Further, the reduction in tensile strength of the panel with open-hole damage, although lower, the characteristics with damage size were comparable to that under compressive loading, as illustrated in figure 2 [5].

The sandwich construction in an airframe may, in general, be subjected to a combination of in-plane axial and shear loads and out-of-plane normal loads resulting from pressurization of the fuselage, with the curvature of the structure adding to the complexity of the problem. The particular combination of loads may be a function of the location on the airframe and the external loading within the mission envelope. It is thus desireable to obtain an understanding of the behavior of critical damage states [3] in a curved sandwich structure under combined loading cases.

In this study, the strength of cylindrical sandwich panels under combined longitudinal and pressurization loading was investigated experimentally. The influence of flaws, such as open hole and through-thickness notches in single facesheets, on the strength of the panel under different loading scenarios were studied. The notches are representative of damage occurring due to rotor burst incidents, while the open hole damage represents a failed repair patch. The details of the Federal Aviation Administration (FAA) full-scale panel testing facility, test panel design and fabrication, test procedures, results and key observations are enumerated in this report.

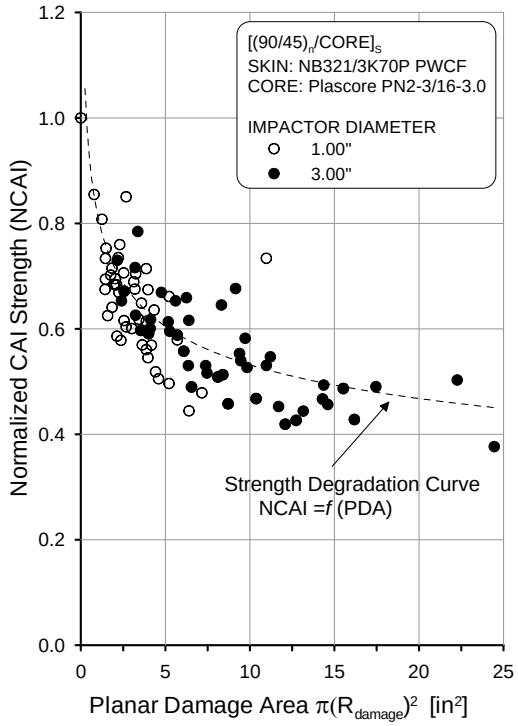

Figure 1. Compressive Residual Strength vs Planar Damage Area for Impact Damaged Sandwich Panels [1]

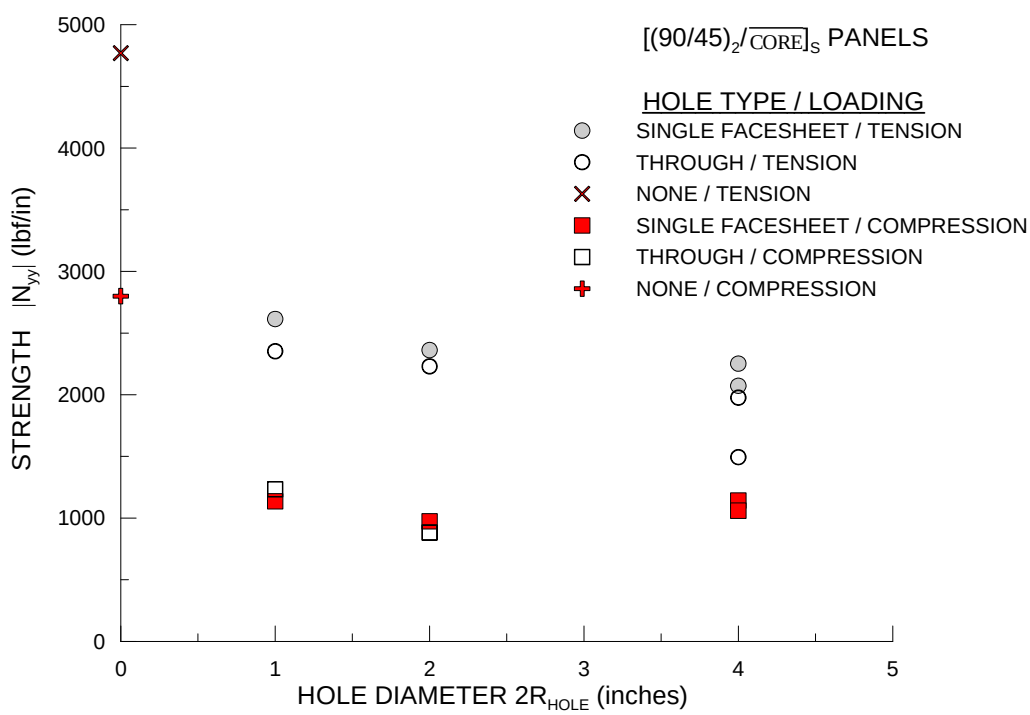

Figure 2. Strengths of Sandwich Panels With Open Holes Under Tensile and Compressive Loading [5]

2. FULL-SCALE AIRCRAFT STRUCTURAL TEST EVALUATION AND RESEARCH FACILITY.

A full-scale curved panel test was studied in detail by visiting the Full-Scale Structural Test Evaluation and Research (FASTER) facility at the FAA William J. Hughes Technical Center in Atlantic City, New Jersey, and by reviewing previous test reports [6]. This study was intended to obtain the requirements and constraints on the test panel geometry and applied loading. The FASTER test fixture consists of mechanisms to introduce different combinations of loads on a cylindrical chord of an airframe fuselage structure. The test fixture can apply longitudinal, reactive hoop, shear and pressurization loads on a curved (cylindrical) test article. The test fixture can accommodate a specimen width of 73 inches and a length of 125 inches. The planar dimensions include the end attachment tabs used for load introduction. The fixture can accommodate specimens with curvatures ranging between 62 and 130 inches. The FASTER test fixture consists of a base structure, longitudinal load assembly, hoop load assembly, shear fixture assembly and pressurization box that houses frame load assemblies [6]. The above assemblies are shown in the exploded view in figure 3. The required forces are generated using water and air as fluid medium. The external loads are generated by applying water pressure to bladder type actuators, as illustrated in figure 4. A detailed description of the hydraulic and pneumatic systems, associated controls, and data acquisition system has been reported elsewhere [6]. In this section, the details of the load introduction mechanisms, the load limits, load introduction into a typical test article, and constraints on the test article geometry are discussed.

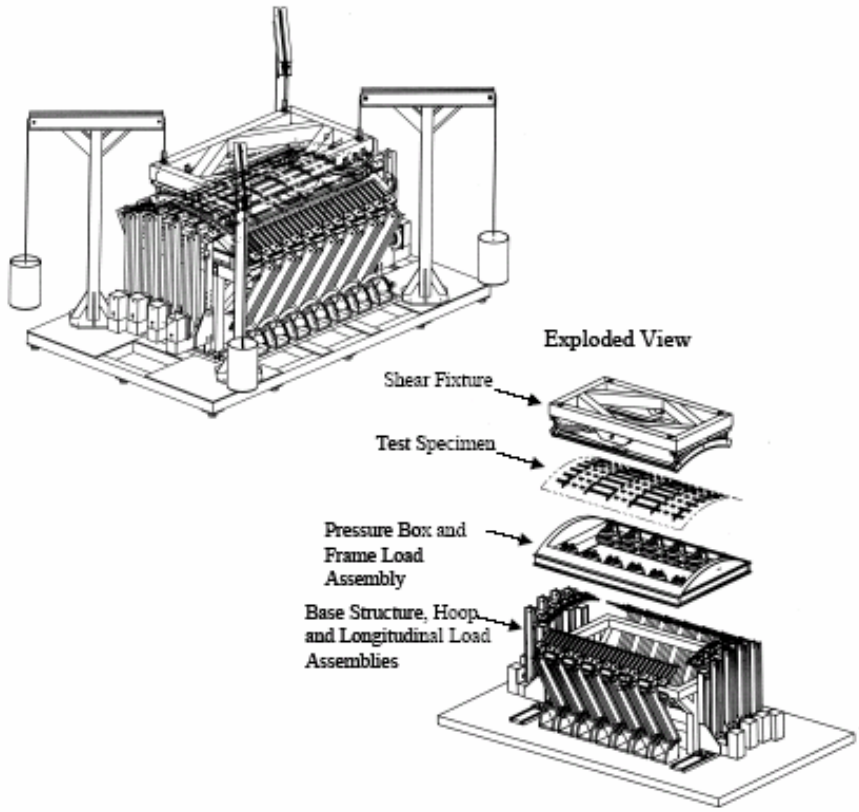

Figure 3. Full Assembly and Exploded Views of the FASTER Test Fixture [6]

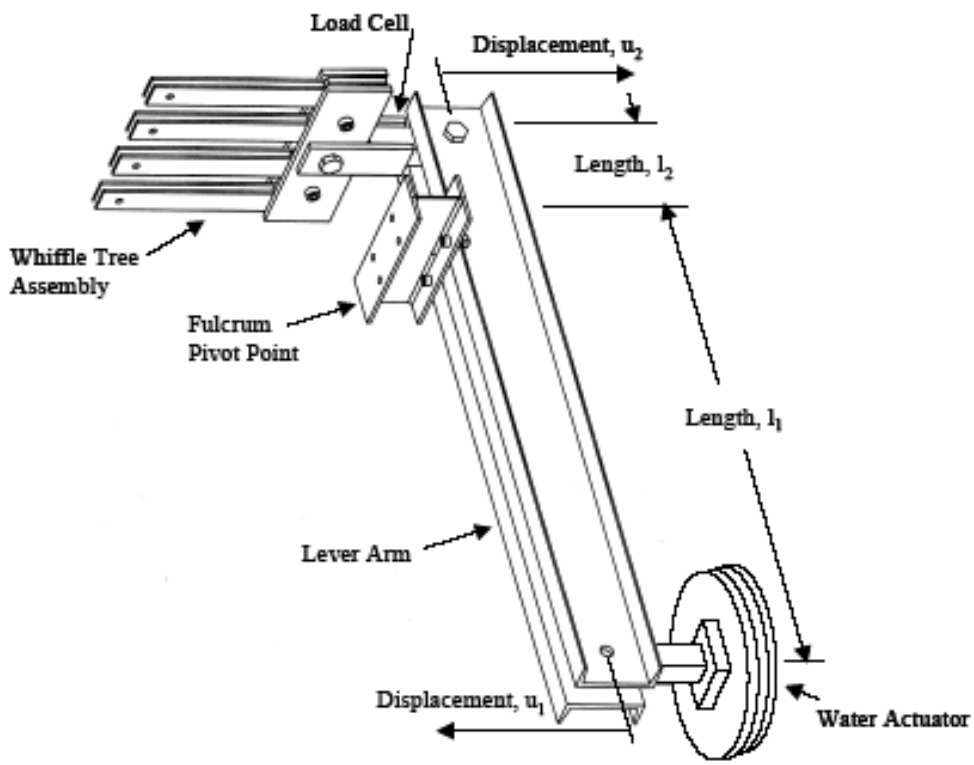

Figure 4. Schematic of Force Multiplication Lever Assembly With Whiffle-Tree Links Used for Longitudinal and Hoop Loading [6]

The longitudinal and hoop loading are applied by a force multiplier lever mechanism that is actuated by pressurized water, as shown in figure 4. The longitudinal and hoop loading are introduced into the test article though a two-tier coaxial whiffle-tree assembly shown in figure 4. The longitudinal loads are introduced at 16 locations along the hoop edge of the test article. The test fixture can apply a maximum longitudinal load of 1800 lbf/in. The running load is based on the length of the load introduction region and not the test section of the panel. This running load translates to a point load of approximately 6500 lbf each (based on test section width of 56″), applied at 16 locations, evenly distributed along the hoop edges of the test article.

The hoop loading in the skin is generated by applying internal pressure and constraining the circumferential displacements by applying tangential loads (reactive) along the longitudinal edges. The cylindrical panel will deform in a self-similar fashion if the pressure load is applied over the entire chord with a tangential reaction at the edge, which would be the ideal situation, as shown in figure 5. However, due to physical constraints, the pressure load cannot be applied over the entire chord, and the tangential reactive force at the free edge will produce a moment that tends to bend the cylindrical panel resulting in radial displacements, as shown in the same figure. However, this can be alleviated by providing a radial reaction (and/or a reactive moment), as shown. Since the tangential reactions are applied at some distance from the edge of pressurization, a radial reaction is necessary to keep the test article in equilibrium, as shown in figure 5. The radial reaction for the test article is provided by connecting the frames to a radial

reaction link[1], which is fixed to the pressurization box. The radial reaction is applied to the frame at the same point where the tangential loads are introduced into the frames. A total of 12 radial reaction links are available (two per frame) at a spacing of 19″ along the length of the fixture. The reaction links along with the hoop loading assemblies equilibrate a total pressurization force resulting from internal pressure. The hoop loading mechanisms are the primary reacting mechanisms, while the radial reactions account for the moments generated due to the hoop reactions not being tangential at the edge of pressurization.

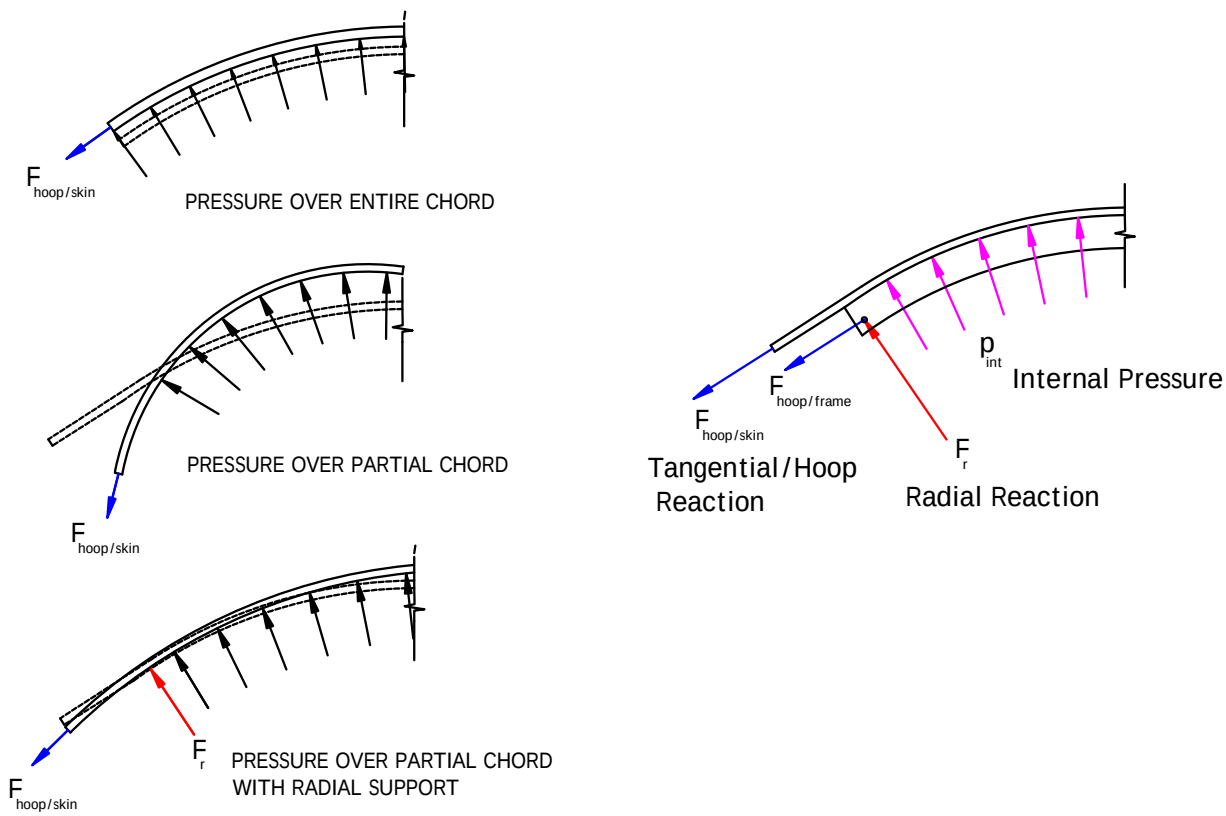

Figure 5. Deformation of a Cylindrical Chord Under Internal Pressure and Loading in a Semi-Monocoque Fuselage Panel Using the FASTER Fixture

The hoop loads corresponding to a given internal pressure (and internal radius of the test article) are induced through the hoop loading mechanisms. The reactive hoop loads are introduced into the test article at 28 locations along the longitudinal edges. The maximum hoop loads that can be achieved are 1800 lbf/in, which is slightly less than the hoop load (1950 lbf/in) in a test article of internal radius of 130″ and subjected to a maximum internal pressure of 15 psi. Further, the contribution of the frames in resisting the pressurization loads is simulated by loading the frames independently using the frame loading mechanisms, as shown in figure 6.

The pressurization loading of the test article is accomplished by pumping water at the desired pressure into the pressurization chamber. The maximum internal pressure that can be generated

[1] The radial reaction link is primarily intended to constrain the displacement of the frame loading points along the tangential direction [6].

is 25 psi. The pressurized water is contained within the chamber by using an elastomeric rubber seal bonded to the test article and fastened to the edge of the pressure box, as shown in figure 6. The elastomeric seal accommodates radial displacement of the test article and tangential displacement of the longitudinal edges while containing the pressurized water.

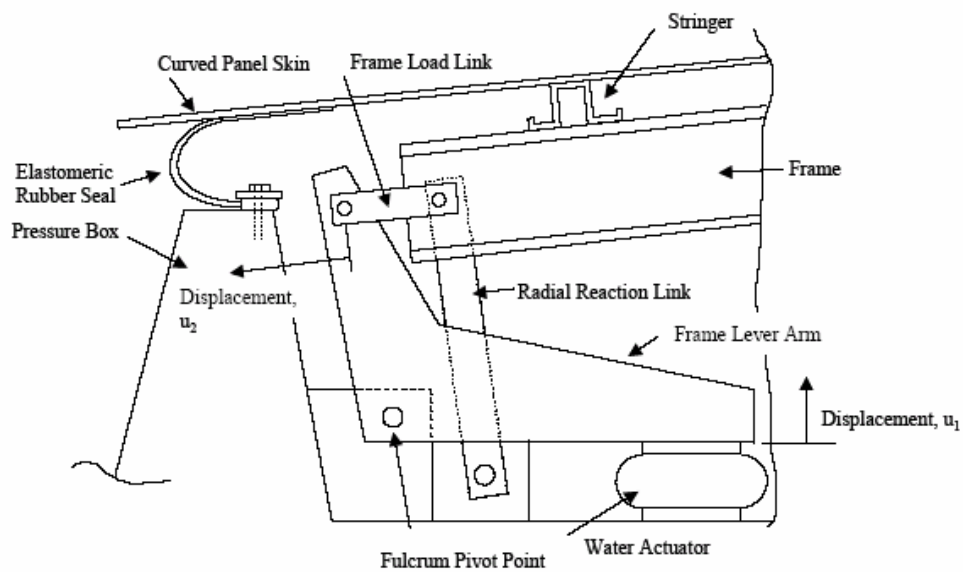

Figure 6. Schematic of Frame Loading Assembly and Radial Reaction Link [6]

In summary, the FASTER fixture is capable of applying longitudinal loads, pressurization, and associated hoop reactions. The fixture can also load the frames independently in the tangential direction. The test setup can subject a test article to both quasi-static and dynamic loading at a maximum rate of 0.2 Hz.

3. DESIGN AND FABRICATION OF TEST ARTICLE.

The test article was designed to have an internal radius of 74 inches, a longitudinal length of 125 inches, and circumferential length of 76.2 inches. These dimensions were required for proper interface of the test article with the pressurization chamber. The overall geometry of the test panel is shown in figure 7. The loading edges of the panel contain 0.5-inch-diameter holes for load introduction. The holes were spaced at 3.5-inch intervals for longitudinal loads and 4.0-inch intervals for hoop load introduction. These dimensions were dictated by the geometry of the whiffle-tree assembly. Relief slits were introduced between the loading holes to alleviate the effects of stiffened edges on the load distribution in the panel. In the absence of the slits, the load distribution would be nonuniform due to the edge effects. The geometry of the relief slits along the longitudinal and circumferential edges are shown in figure 8. Further, the hoop loading edge of the test panel was required to be tangential to the test section of the panel. The point of tangency was to coincide with the edge of internal pressure application. Lack of tangency would lead to bending moments resulting in bending deformation of the panel under pressurization loading. Thus, the hoop loading edge was made flat and tangential to the test section, as shown in figure 9.

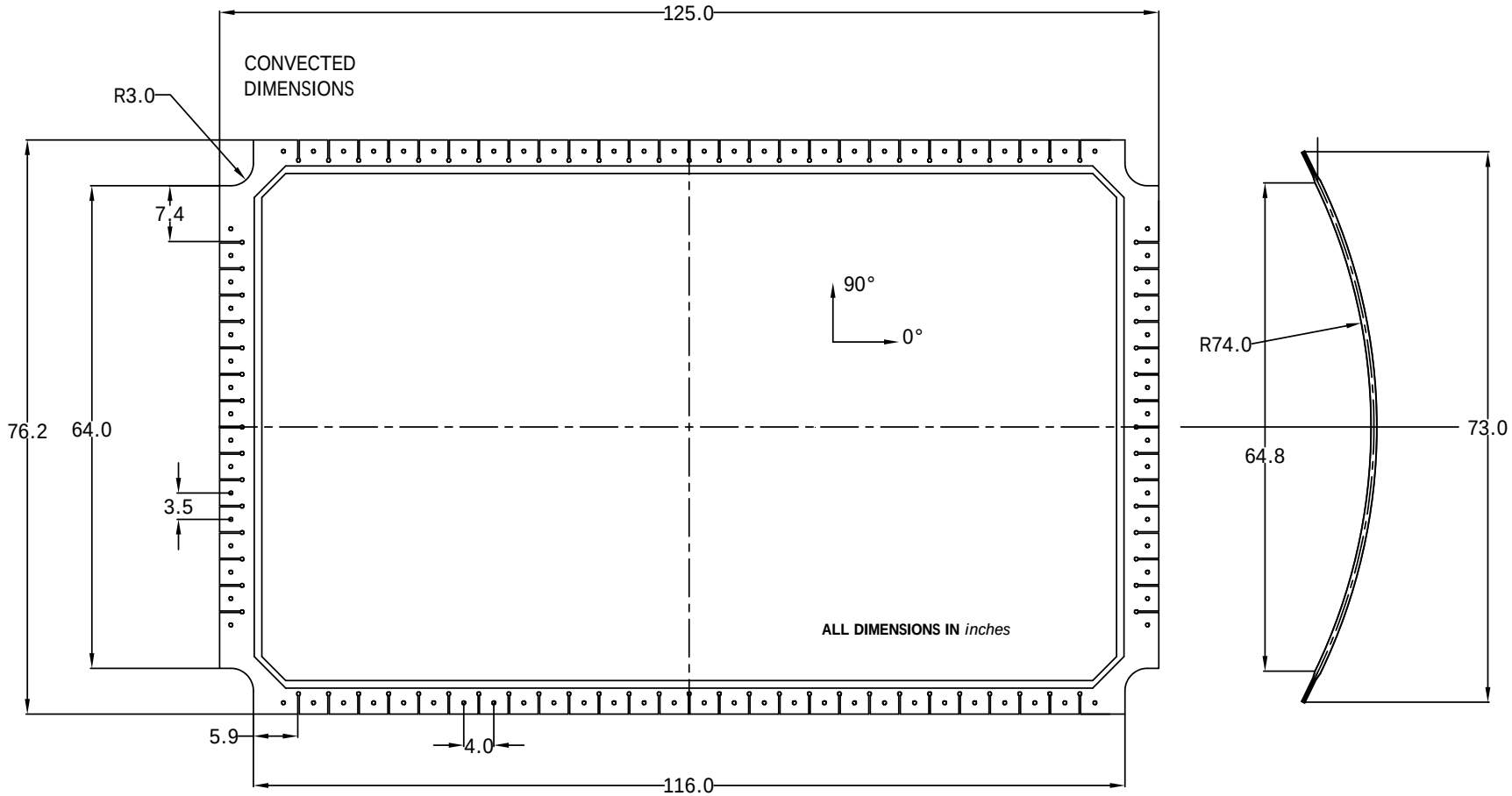

Figure 7. Overall Geometry of the Curved Test Panel

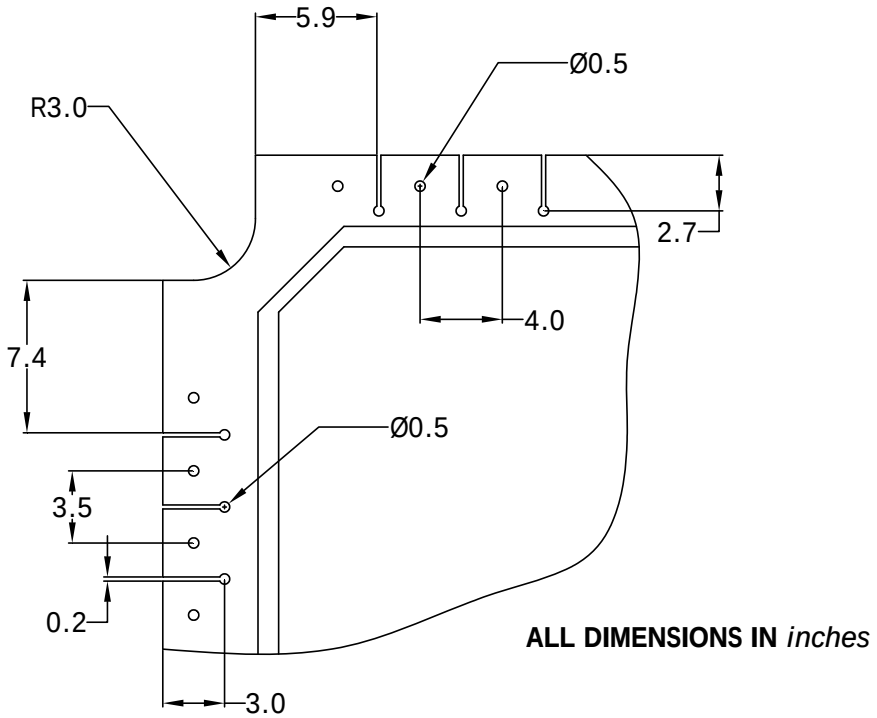

Figure 8. Geometric Details of Loading Edges

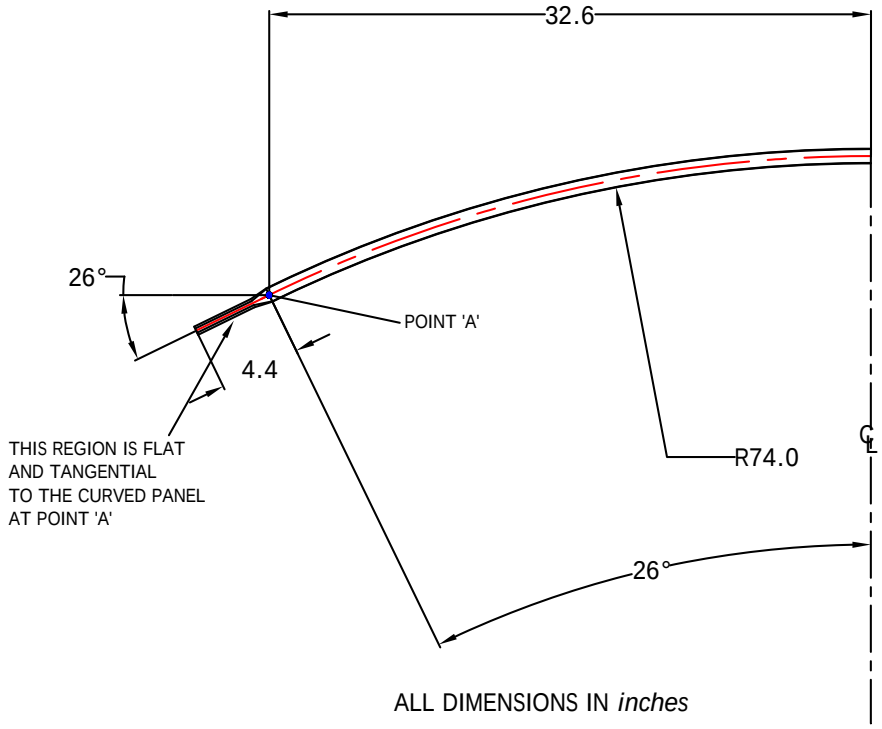

Figure 9. Tangency of Hoop Loading Edge With the Test Section of the Panel

The test articles were fabricated using Toray T700S-12K-50C/#2510 plain weave carbon fabric prepreg (F6273C-07M, 190 g/m^2) for the facesheets and an overexpanded cell DuPont™ Nomex® honeycomb core (Hexcel Composites, HRH-10/OX-3/16-3.0). The overexpanded cell core is preferred as it drapes easily over the cylindrical mold surface. The facesheet to core bonding was achieved by using EA9696 film adhesive (0.060 psf). The honeycomb core along the load introduction region was potted using Hysol® EA9394 epoxy paste adhesive. The nominal ply mechanical properties of the facesheet material is presented in table 1. The mechanical properties of the core material are presented in table 2.

Table 1. Nominal Mechanical Properties of Toray T700S-12K-50C/#2510 Plain Weave Carbon Fabric Prepreg [9]

Property	Value
Nominal cured ply thickness t_{PLY} (in.)	0.0083
In-plane Modulus E_{11} (Msi)	8.3
In-plane Modulus E_{22} (Msi)	8.1
In-plane Shear Modulus G_{12} (Msi)	0.62
Poisson's Ratio ν_{12}	0.085
In-plane Tensile Strengths F_{11}^T, F_{22}^T (ksi)	116
In-plane Compressive Strengths F_{11}^C, F_{22}^C (ksi)	108
In-plane Shear Strength S_{12}^C (ksi)	22
In-plane Tensile Strain ε_{11}^T (microstrain)	13975
In-plane Compressive Strain ε_{11}^C (microstrain)	13012
In-plane Tensile Strain ε_{22}^T (microstrain)	14320
In-plane Compressive Strain ε_{22}^C (microstrain)	13333
In-plane Shear Strain ε_{12} (microstrain)	35483

Table 2. Nominal Mechanical Properties of HRH-10/OX-3/36-3.0 Honeycomb Core [10]

Property	Value
Nominal Density (lb/ft^3)	3.0
Nominal Cell size (in.)	0.1875
Out-of plane Compressive Modulus E_{33}^C (ksi)	17
Out-of-plane Compressive Strength F_{33}^C (psi)	285
Plate Shear Modulus 'L' Direction (ksi)	3.0
Plate Shear Strength 'L' direction (psi)	116
Plate Shear Modulus 'W' direction (ksi)	6.0
Plate Shear Strength 'W' direction (psi)	90
L ~ Ribbon Direction W ~ Transverse Direction	

The stacking sequence in the test region of the panel was $\lfloor 45/0/45/\overline{CORE} \rfloor_S$. However, the panel was reinforced along the longitudinal and hoop edges to increase the bearing strength of the panel. To alleviate the interlaminar stresses, the additional plies in the tab region were terminated gradually towards the interior of the panel. The test article was subdivided into four regions (A, B, C, and D) based on the stacking sequence of the facesheets, as shown in figure 10. The stacking sequences in the different regions of the panel are shown in figures 11 and 12. In addition, the core was tapered from 0.75 inch in the test region to 0.25 inch in the load introduction region. This was necessitated by the constraint on the maximum thickness (0.5 inch) of the part that could be engaged by the whiffle-tree assembly.

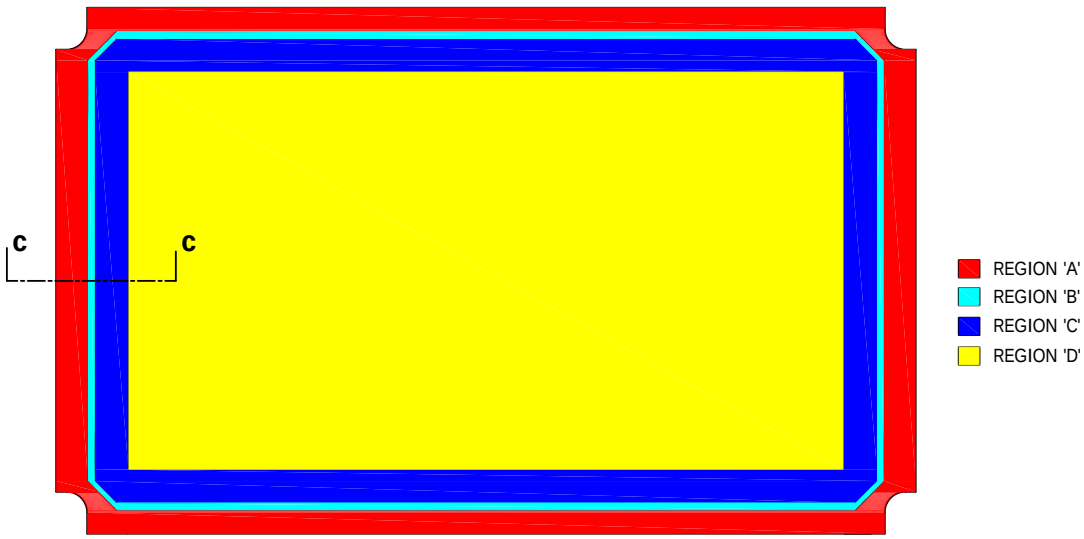

Figure 10. Subdivision of Panel Based on Stacking Sequence

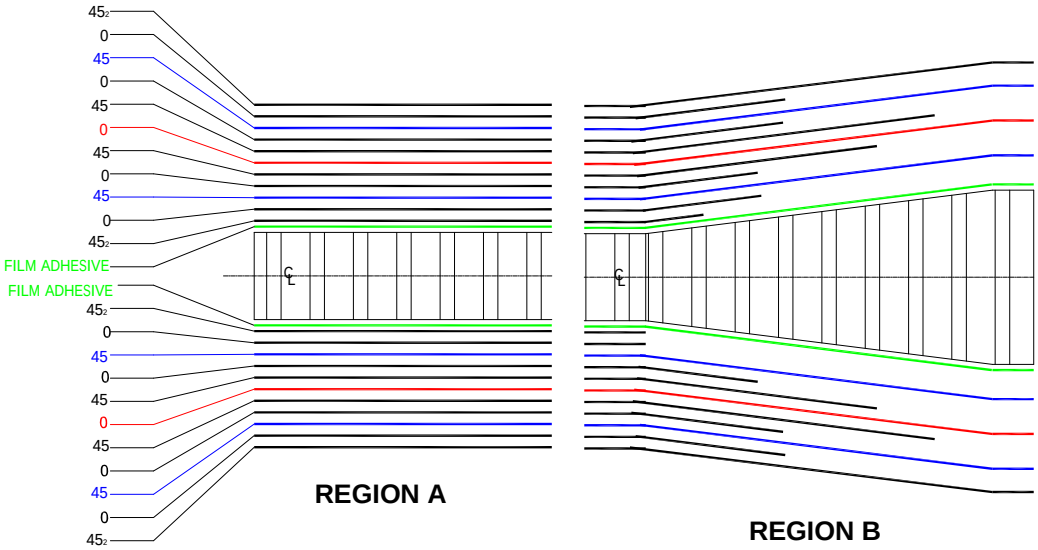

Figure 11. Stacking Sequence in Regions A and B

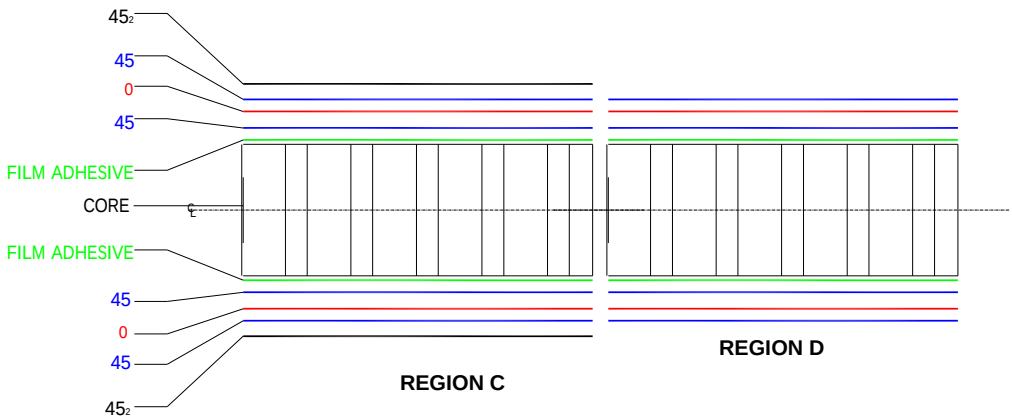

Figure 12. Stacking Sequence in Regions C and D

The mold for the test panels and the test panels themselves, were fabricated at the Adam Aircraft Co., Denver, Colorado. The various stages of the mold fabrication and subsequent panel layup are shown in figures 13 through 17. The test panels were cured in an oven at 350°F per the prepreg manufacturer recommended cure cycle [9]. The load introduction holes, relief slits, and any desired flaw types (open hole, notch, etc.) were machined once the panel was cured.

Figure 13. Pattern Machining for the Mold

Figure 14. Test Panel During the Layup Process

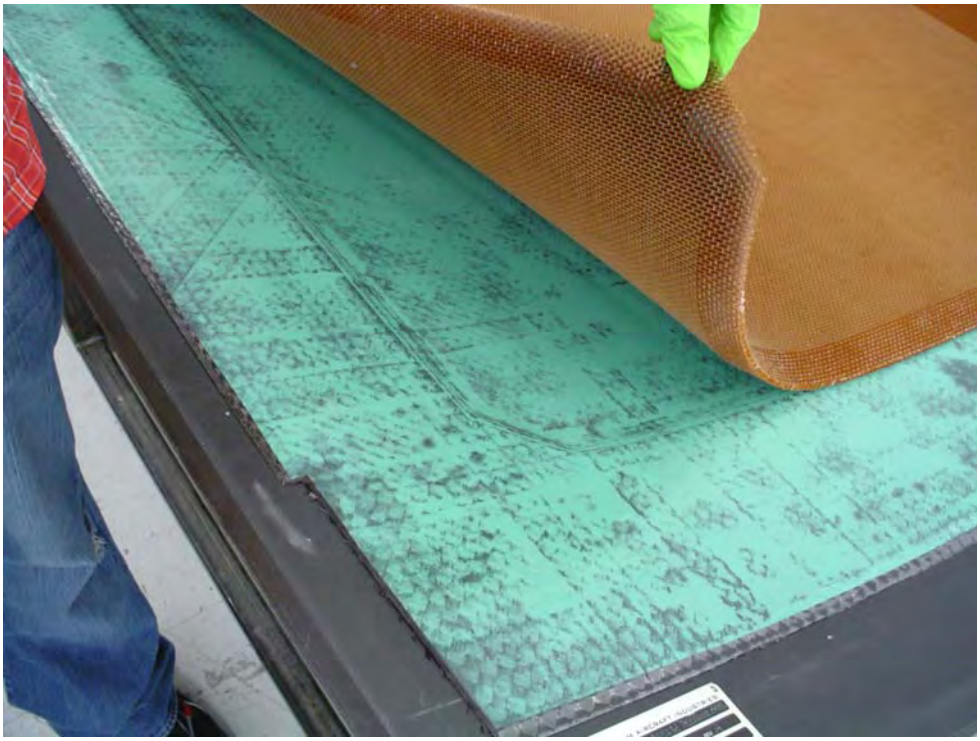

Figure 15. A Close-Up of the Honeycomb Core Being Placed on the Top Facesheet

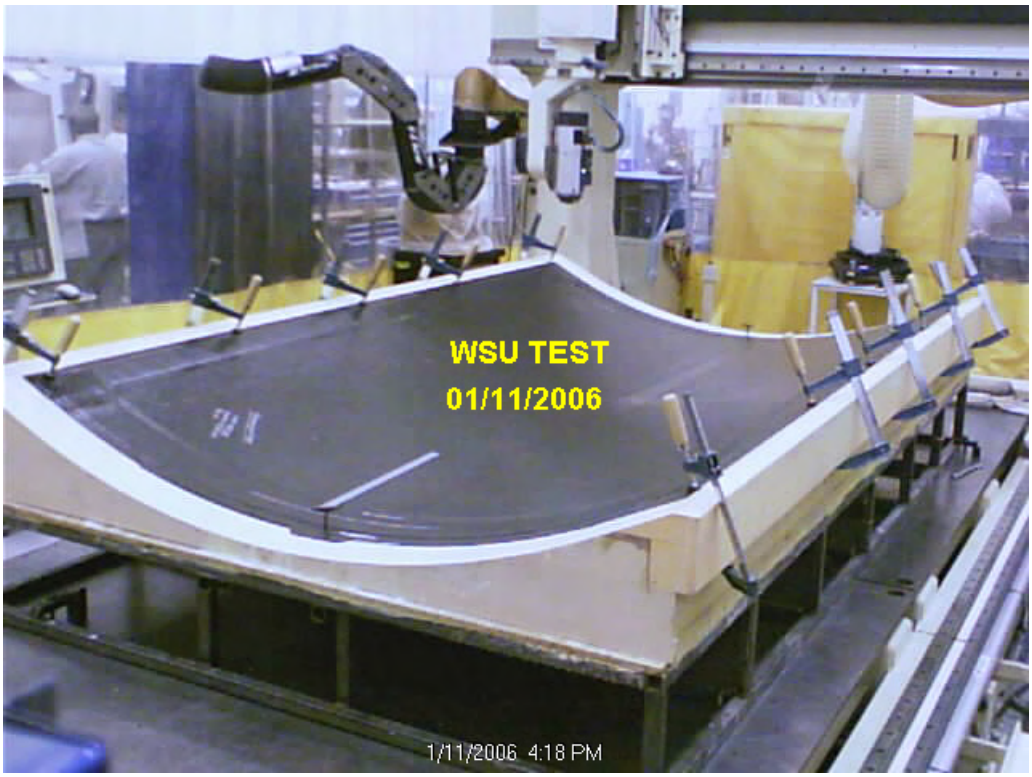

Figure 16. Test Panel After Curing and Ready to be Machined

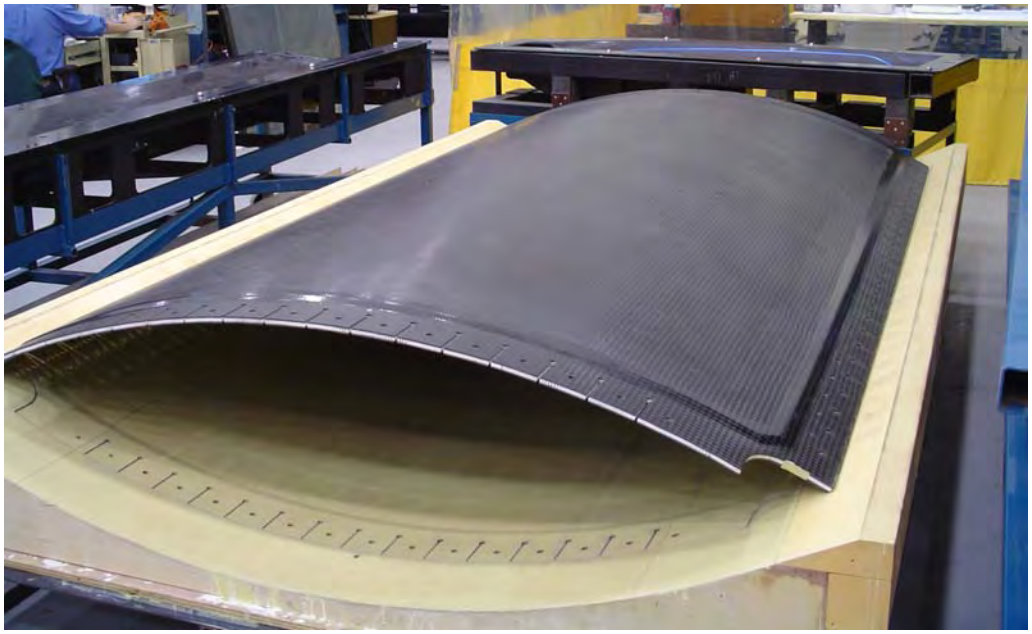

Figure 17. Test Panel After Machining

4. TEST PROGRAM AND TEST MATRIX.

The objective of the test program was to evaluate the damage tolerance of curved sandwich panels representative of fuselage structures under combined longitudinal and pressurization loading. Before flawed panels were tested, an unnotched/pristine panel was subjected to different combinations of loadings to ensure even load distribution in the panel and evaluate the deformations and strain distributions under such loadings. In addition, this panel was used to exercise the digital image correlation technique for full-field strain measurements. Subsequently, test panels with different flaws were tested (or attempts were made) to failure under predetermined loading scenarios. The different flaw types investigated in the current study included saw cut notches, open-hole in a single facesheet and through notches along longitudinal, hoop and off-axis directions. The different panel types and planned loading for each case are summarized in table 3. The geometry of the panels with different flaw types are shown in figures 18 to 21.

Table 3. Planned Loading for Panels With Different Damage Types

Panel No.	Damage Type	Load Cases
CP1	Unnotched/baseline	Longitudinal (500 lbf/in) Hoop (500 lbf/in) Hoop + Longitudinal (1000 lbf/in)
CP1A	3″ x 3″ cross slit, top facesheet	Longitudinal (to failure)
CP1B	10″ x 1/16″ longitudinal slit, through-thickness	Hoop loading (to failure)
CP2	10″ diameter hole in top facesheet	Longitudinal loading Combined loading Hoop loading
CP3	10″ x 1/2″ circumferential notch, through-thickness (both facesheets)	Pressurize to 8 psi and hold, increase longitudinal load to failure
CP4	10″ x 1/2″ circumferential notch, through-thickness (both facesheets)	Pure longitudinal loading to failure
CP5	10″ x 1/2″ longitudinal notch, through-thickness (both facesheets)	Pressurization to failure
CP6	10″ x 1/2″ 45º off-axis notch, through-thickness (both facesheets)	Longitudinal + Hoop (1:1) to failure

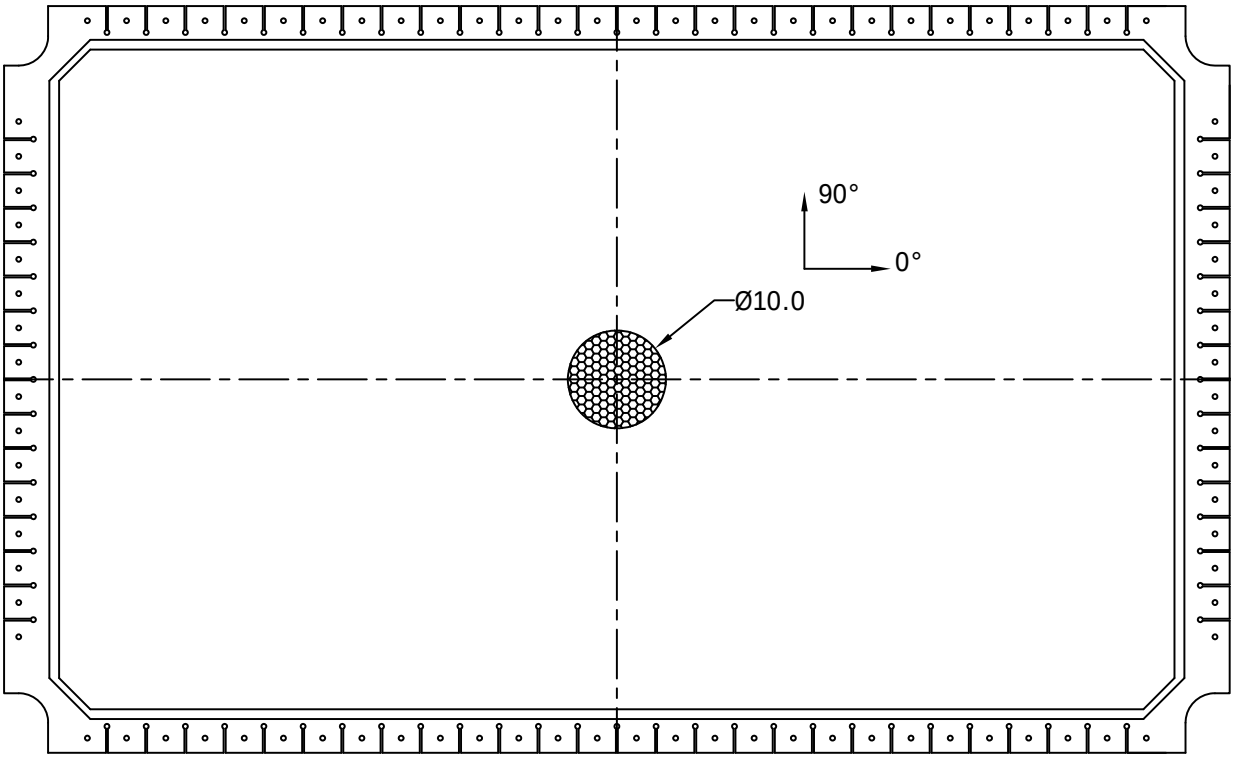

Figure 18. Test Panel With Hole in Top Facesheet (Convex Side)

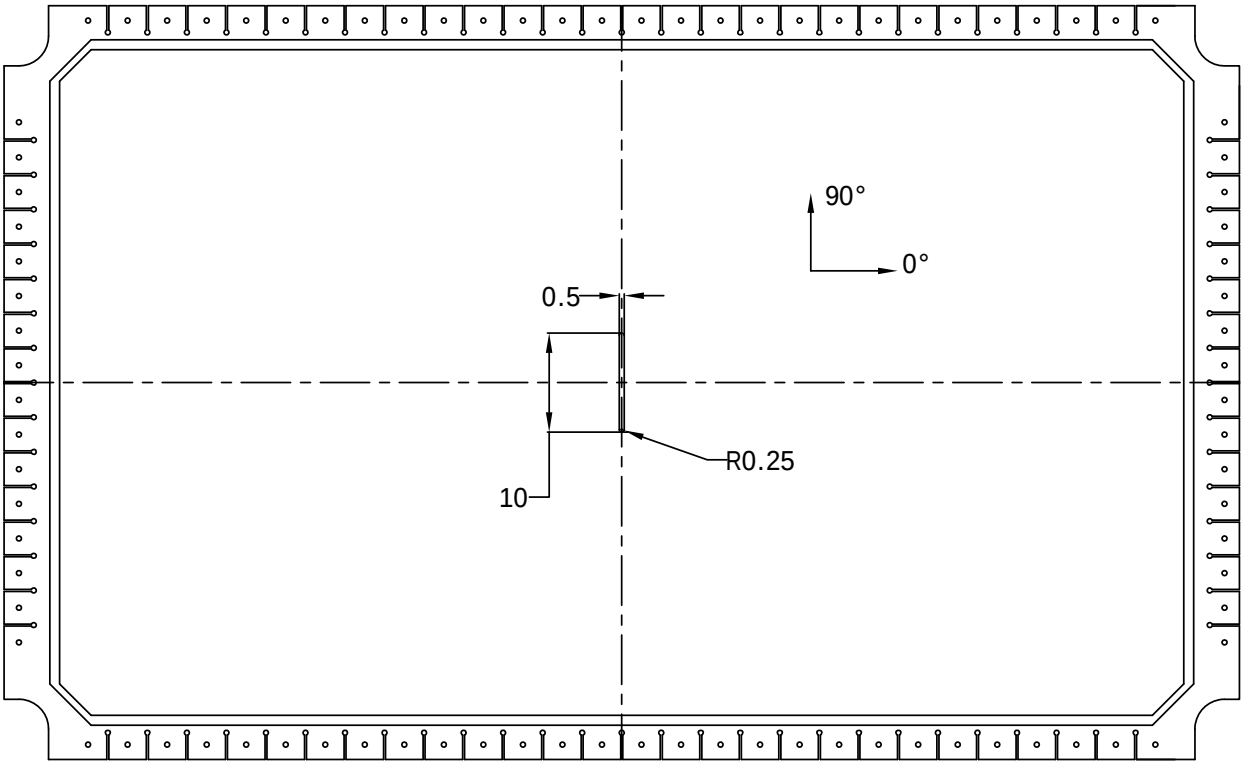

Figure 19. Test Panel With Circumferential Notch (CP3 and CP4)

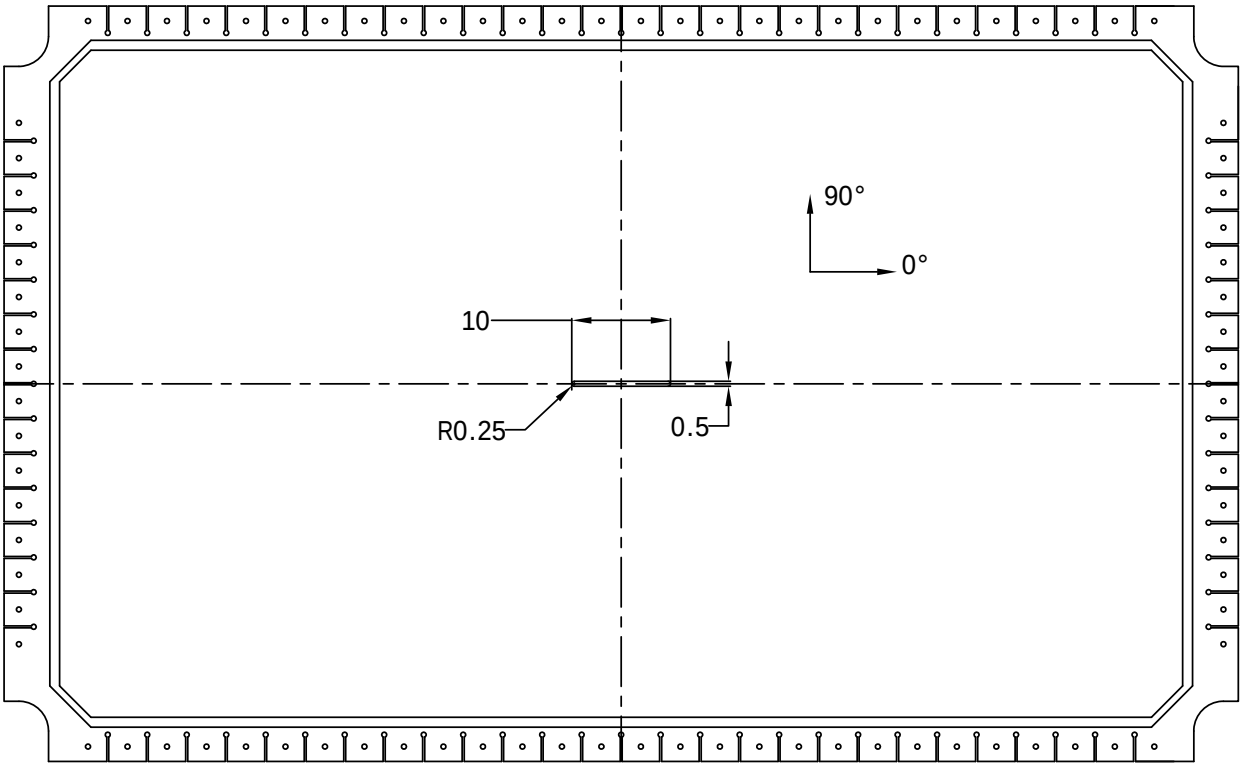

Figure 20. Test Panel With Longitudinal Notch (CP5)

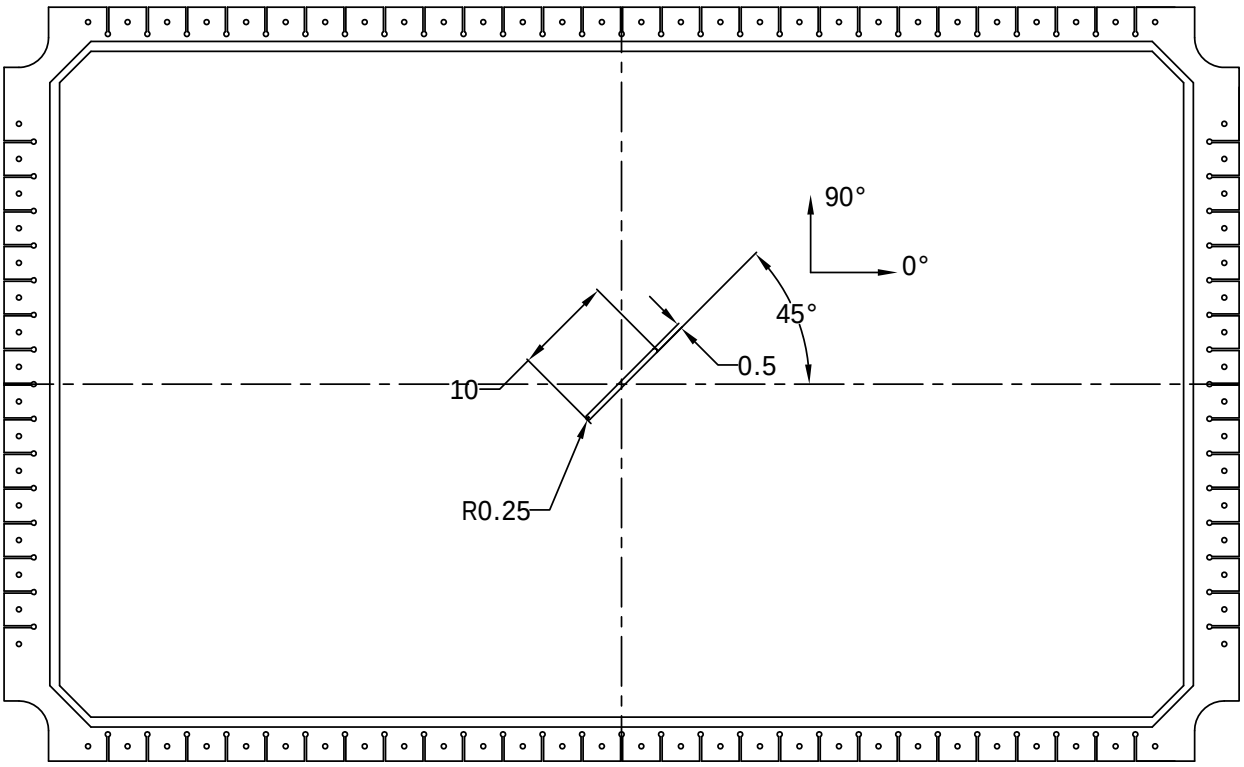

Figure 21. Test Panel With Off-Axis Notch (CP6)

4.1 ESTIMATION OF FAILURE LOADS.

Prior to panel testing, estimates of failure loads and modes were obtained based on finite element analysis. The analysis was completed by an independent consultant [11]. The test panel geometry, material properties, and loading configurations were provided to the consultant.

NASTRAN linear static finite element models were constructed for each panel configuration. These models consist of CQUAD4 plate elements with PCOMP and MAT8 representation of the composite material properties. For the undamaged model, a nominal 1-inch mesh size was used. For models with damage, a local mesh size of 0.15 inch was used for the first 1.5 inches from the edge of the hole.

The long edges of the models were constrained against deflections in the hoop and radial (normal to element plane) directions. For models with longitudinal loading, one of the short sides was constrained against deflections in the longitudinal (global y) direction. The opposite side was loaded with the 1000 lb/in load. For models with pressure loading only, the long sides were constrained against deflections in the hoop and radial directions, and the short sides were constrained against deflections in the longitudinal direction. To account for the pressure load within holes, distributed nodal forces were applied around the perimeter of the holes. The total load to be distributed was calculated by multiplying the surface area taken by the hole by 13.5 psi. This total load was applied about the radial component of a cylindrical coordinate system as a distributed normal force to the nodes along the perimeter of the hole.

The finite element models are shown in figures 22 through 25. Based on the finite element analyses, the failure loads for different loading scenarios were predicted and are summarized in table 4. The details of the failure prediction and the location of the failures for each case may be found in appendix A.

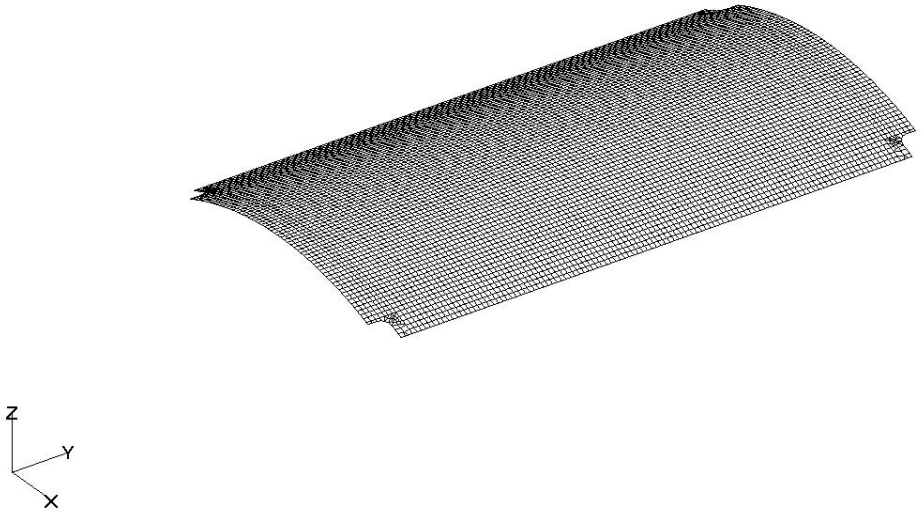

Figure 22. Finite Element Model, No Damage

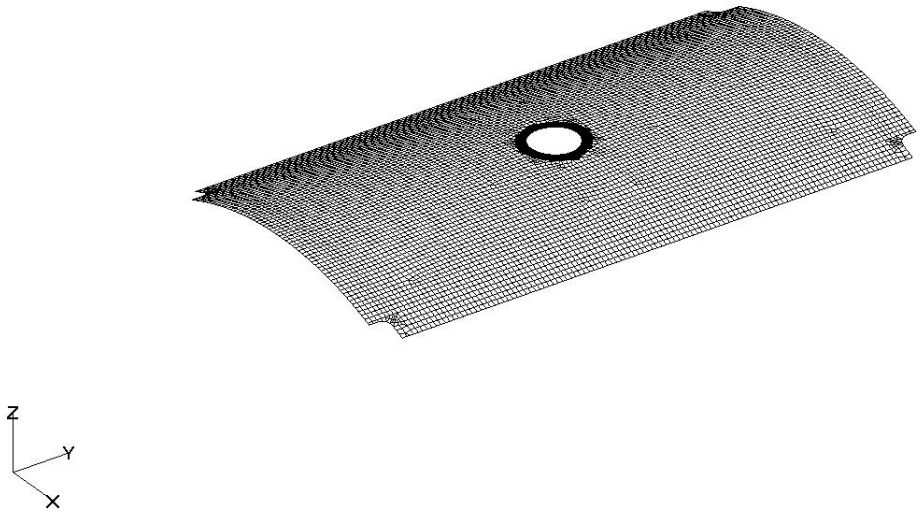

Figure 23. Finite Element Model, 10-Inch-Diameter Hole

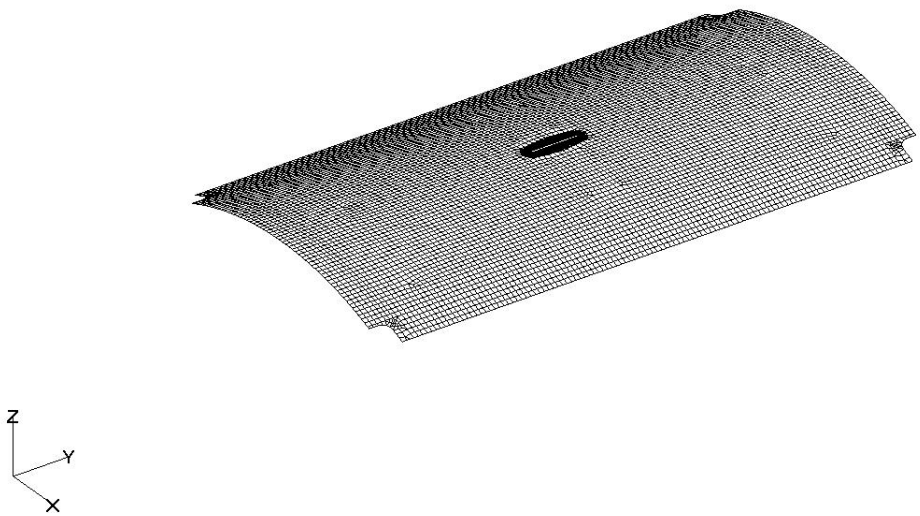

Figure 24. Finite Element Model, 10-Inch-Longitudinal Notch

Figure 25. Finite Element Model, 10-Inch-Circumferential Notch

Table 4. Summary of Estimated Failure Loads and Modes for Test Panels With Different Damage Types

Test Case No.	Damage Type	Loading Type	Failure Mode	Panel Capability	
				Longitudinal Load (lbf/in)	Pressure Load (psi)
1	None	Longitudinal	Principal wrinkling	2170	
		Pressure	Core shear		44.8
		Longitudinal + Pressure	Core shear	2930	39.6
2	10″ diameter hole	Longitudinal	Compression wrinkling	1630	
		Pressure	ε_{22}^{T} fiber strain		16
		Longitudinal + Pressure	ε_{22}^{T} fiber strain	1288	17.4
3	10″ × 1/2″ Longitudinal notch (both facesheets)	Pressure	ε_{22}^{T} fiber strain		6.2
		Longitudinal + Pressure	ε_{22}^{T} fiber strain	468	6.3
4	10″ × 1/2″ Circumferential notch (both facesheets)	Longitudinal	ε_{11}^{T} fiber strain	1058	
		Longitudinal + Pressure	ε_{11}^{T} fiber strain	905	12.2

The test panels were tested at the FASTER facility. The recorded data during each test was subsequently analyzed by Wichita State University (WSU) and FAA personnel. The details of the tests conducted on different panels and the results are discussed in the following sections.

4.2 GEOMETRY, COORDINATES, AND LOADS.

The test panel geometry is described using an r-θ-z coordinate system, as shown in figure 26. The origin of the coordinate system lies in an r-θ plane that cuts the test article in half. The z direction shown in the figure is parallel to the cylindrical axis of the panel. The coordinates s or θ and z are used to identify the locations of points on the convex and concave surfaces of the test panel.

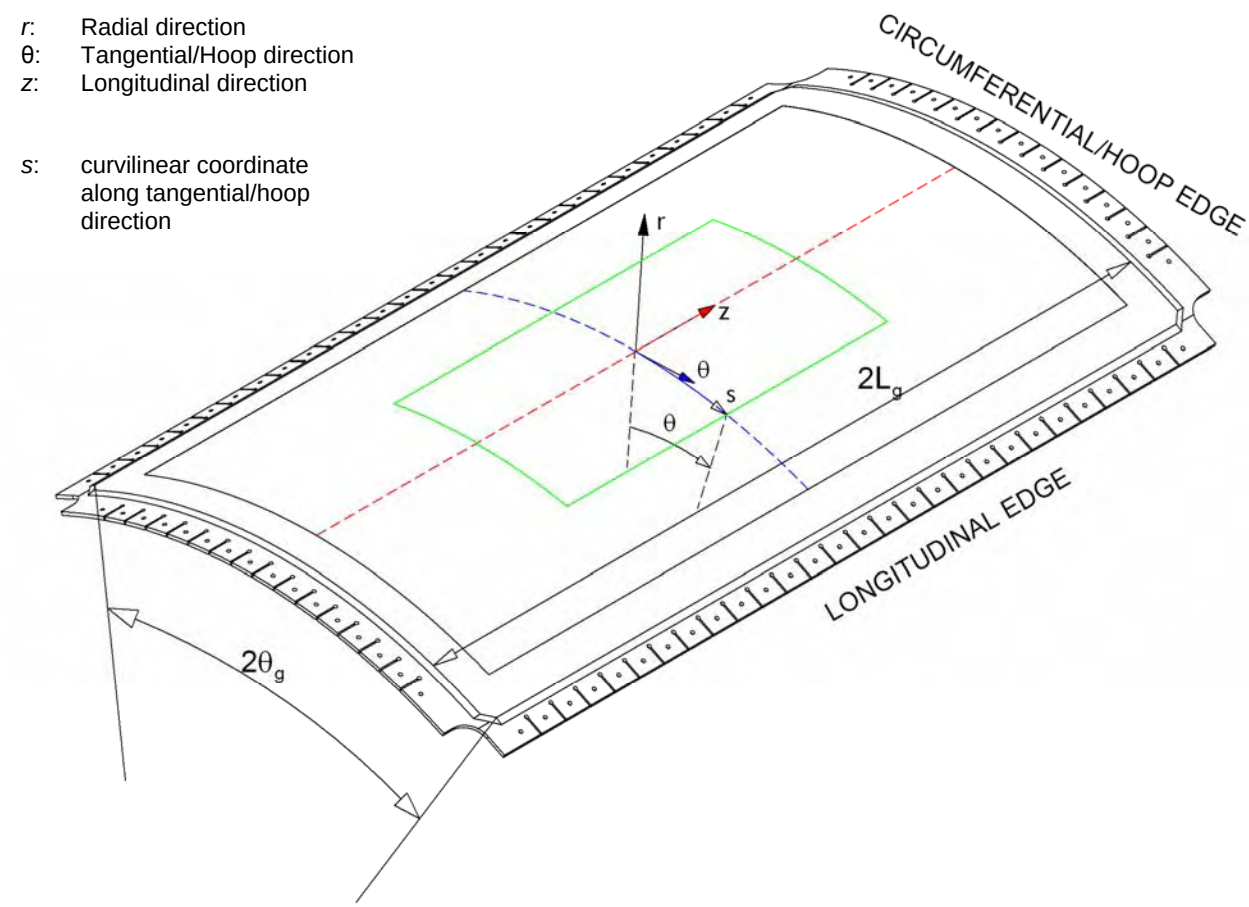

Figure 26. Geometry and Coordinates Associated With the Test Article

The load introduction into the test article occurs over suitable reinforced edges, as shown in figure 26. The longitudinal loads are introduced along the circumferential (or hoop) edge corresponding to $z=\pm L$, where $2L$ is the length of the panel. The hoop reaction loads are introduced along the longitudinal edge of the panel corresponding to $\theta_g = \pm 26^{\circ}$. (Note that the panel surface of the longitudinal edge is tangential to the curved portion at $\theta_g = \pm 26^{\circ}$.)

The loads introduced along the longitudinal and circumferential edges are converted to equivalent running loads $N_{\theta\theta}$ and N_{zz}, respectively. Due to the constraints associated with the test fixture, the load introduction regions are slightly narrower than the dimensions of the test panel between the core ramps. Thus, the running loads for all tests will be defined as the total load divided by the length (or width) of the panel between the ramps. For the geometry of the present panels, the longitudinal and hoop running loads are defined by the following equations:

$$N_{zz} = \frac{\sum_{i=1}^{4} \left(P_{long} \right)_i}{\left(2 \frac{\pi \times \theta_g}{180} \right) R_m} \tag{1a}$$

$$N_{\theta\theta} = \frac{\sum_{i=1}^{7} \left(P_{hoop} \right)_i}{2L_g} \approx \frac{p_{\text{int}}}{R_m} \tag{1b}$$

where, θ_g is the nominal angle between rz-planes corresponding to the two ramps along the longitudinal edge, R_m is the mean radius, $2L_g$ is the nominal length of the panel between the ramps along the circumferential edges, and p_{int} is the internal pressure. For the test panels used in the present investigation, the mean radius R_m = 74.4 inches and the longitudinal gage length $2L_g$=113.8 inches. These defined running loads will be used primarily for the presentation of test results and caution must be exercised when using these values for comparison with mathematical models in which the load introduction regions have not been incorporated in the analysis. Since the load introduction regions have a much higher stiffness, albeit over a narrow region, the load carried by this region may not be negligible.

4.3 TEST ARTICLE INSTRUMENTATION.

The test panels were instrumented with several strain gages to obtain a measure of the uniformity of load distribution across the length and width of the panel. The strain gages were oriented primarily along the longitudinal (z) and tangential (θ or *s*) directions. The longitudinal direction was designated as the 0º direction, as it coincides with the 0º fiber orientation, while the tangential direction is labeled as 90º direction, as it coincides with the 90º fiber orientation. The strain gages were mounted back-to-back at most locations, to obtain a measure panel bending during the tests. The typical locations of far-field strain gages installed on test panels are shown in figure 27. The dimensions shown in the figure are convected dimensions measured along the curved surface of the panel. In addition, strain gages were bonded in the vicinity of discrete damage (open-hole and notch) at the center of the panel. The details of their locations and orientations are shown in figures 28 through 30. These strain gages were used to obtain a real-time measure of damage initiation/propagation near the notches/holes under investigation.

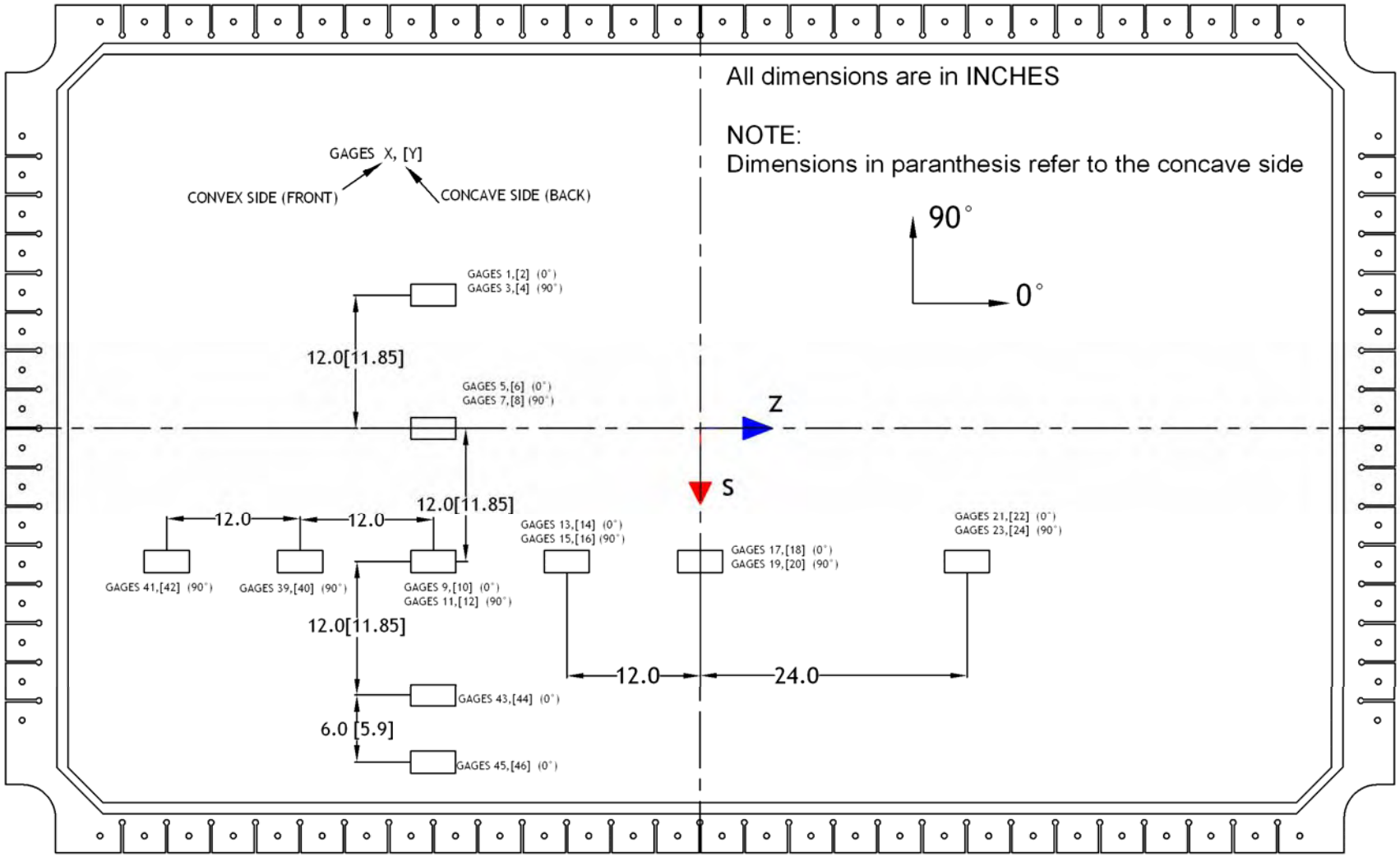

Figure 27. Far-Field Strain Gage Locations and Orientations Common to all Test Panels

Micro-Measurements [12] CEA-06-250UN-350 (350Ω resistance, Gage factor: 2.085, Transverse sensitivity: +(0.4±0.2)%) strain gages were bonded to the surface of the panel using MBond-200 adhesive. The strain gages have a grid length of 0.25 inch and grid width of 0.12 inch, over which the strain value will be averaged.

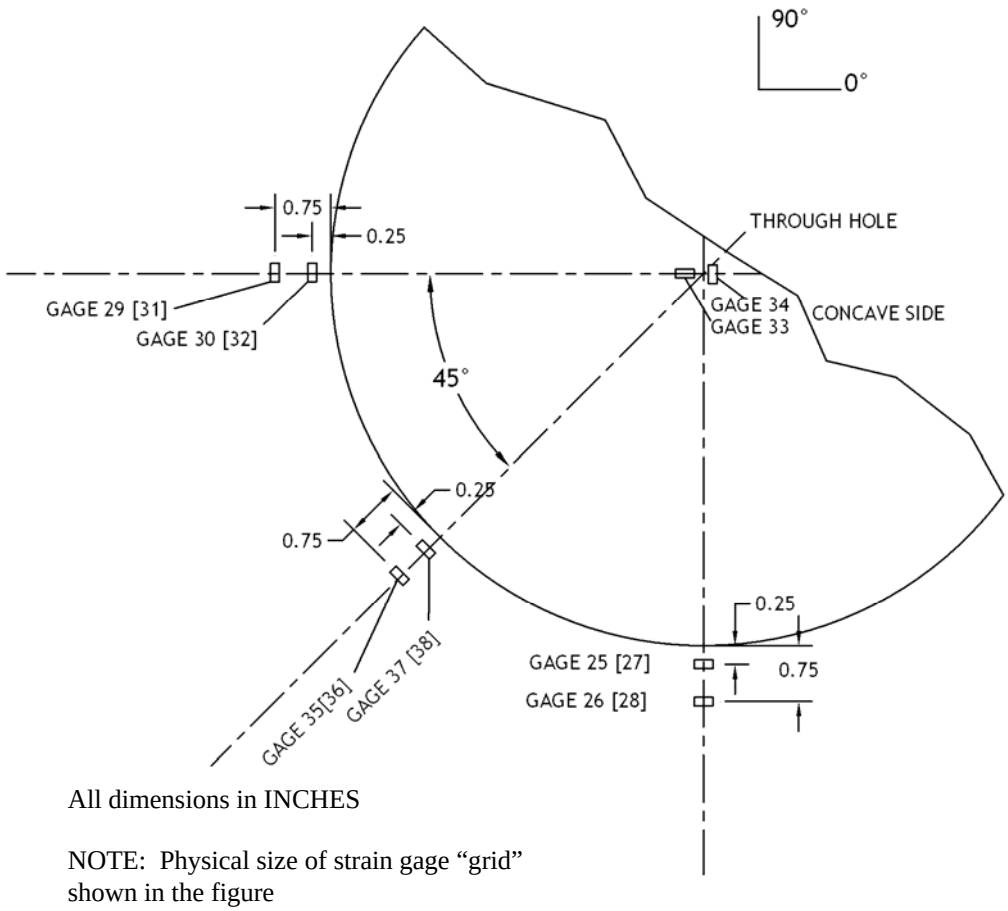

All dimensions in INCHES

NOTE: Physical size of strain gage "grid" shown in the figure

Figure 28. Strain Gage Locations in the Vicinity of the Open Hole

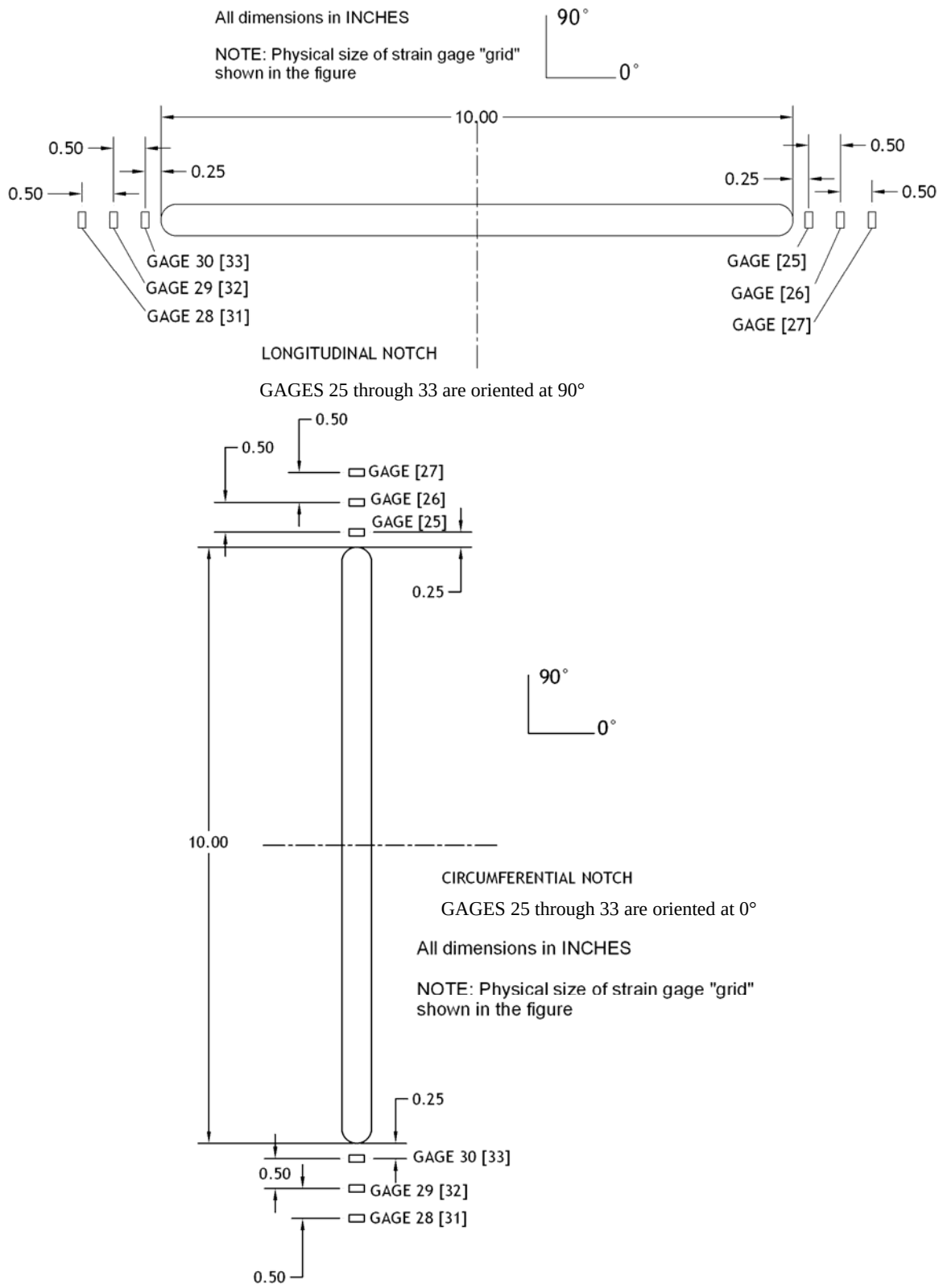

Figure 29. Strain Gage Locations in the Vicinity of Longitudinal and Circumferential Notches

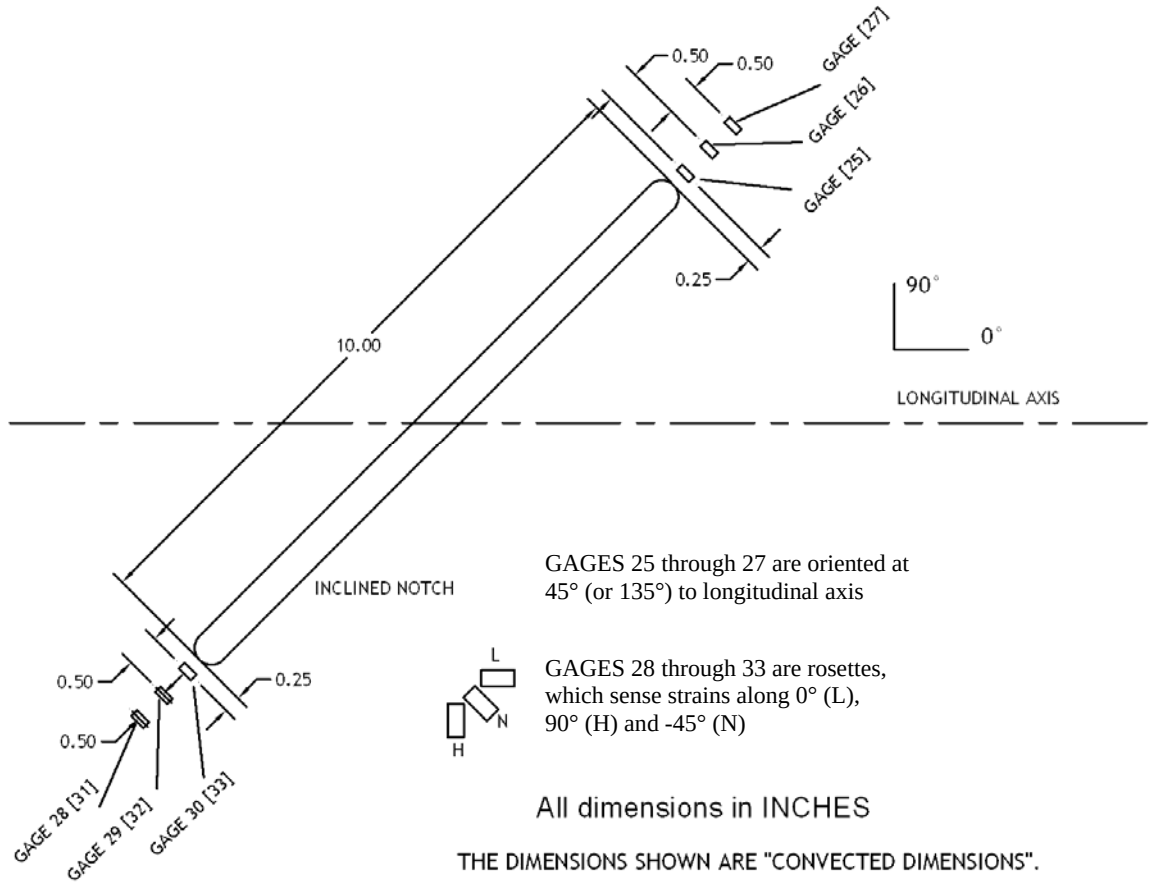

Figure 30. Strain Gage Locations in the Vicinity of the Off-Axis Notch

5. RESULTS.

In this section, the results and observations from individual tests are discussed. In each case, the type of applied loading and resulting far-field strains and their comparison with classical laminated plate theory predictions for a flat plate without flaws are discussed. The initiation and final failure of the panels are discussed in terms of the recorded strain gage data close to the flaw boundaries. In addition to the strain gage data, digital image correlation was used to obtain full-field strain/displacement measurements at selected load steps. The full-field data may be found in reference 13.

5.1 TEST PANEL CP1.

The test panel CP1 (without flaw or damage) was used to obtain a measure of the strain distributions and check the uniformity of strains under pure longitudinal loading, pure hoop loading, and combined longitudinal and hoop loading. The strain gage readings were recorded at discrete load steps and analyzed. In each case, the longitudinal and hoop strains were compared with the strain values obtained using Classical Laminated Plate Theory (CLPT). The nominal ply properties presented in section 3 were used in computing the strains based on CLPT. The CLPT predictions are for a flat plate and do not account for the curvature of the test article or the increased stiffness of the loading region. The back-to-back strain gage readings were used to

obtain a measure of bending of the panel in the r-θ plane and the r-z planes using the following equation A linear distribution of in-plane normal strains is assumed across the thickness, as shown in figure 31.

$$\% \, Bending = \frac{0.5\left(\varepsilon_{top} - \varepsilon_{bottom}\right)}{0.5\left(\varepsilon_{top} + \varepsilon_{bottom}\right)} \times 100 \tag{2}$$

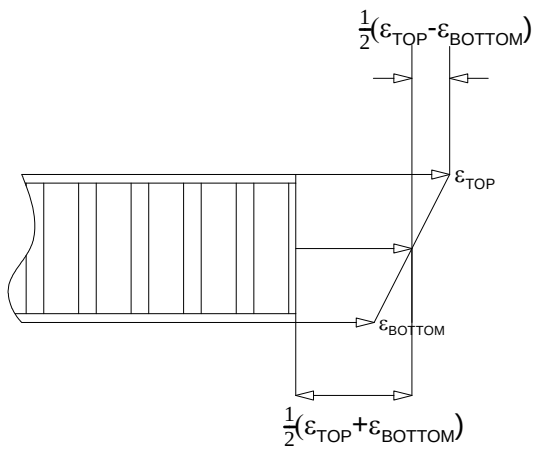

Figure 31. Assumed Strain Distribution for Computing the Bending Deformation in the Panel

The longitudinal strains ε_{zz} were used to obtain a measure of bending in the r-z plane, and the hoop strains $\varepsilon_{\theta\theta}$ were used to measure bending in the r-θ plane.

5.1.1 Longitudinal Loading.

The test panel was loaded longitudinally to a maximum load of 415 lbf/in. Ideally, for such loading, neither internal pressure nor hoop reaction loading has to be applied. However, to support the test article in the fixture, the longitudinal edge was engaged by the hoop loaders, and the pressure box was filled with water but without applying any significant pressure on the panel. Thus, some constraint effects may be present during the test. The variation of longitudinal strains with applied loading are plotted in figure 32. As shown, the longitudinal strains compare reasonably well with the CLPT predictions. The differences in the figure can be attributed to the presence of stiffened regions along the hoop and longitudinal edges. The measured hoop strains arising due to Poisson effects were lower than that predicted by the CLPT for a flat panel (see figure 33). In addition, a slight nonlinearity may be observed in the measured hoop response and may be attributed to the presence of stiffened edges and constraint provided by the hoop loaders.

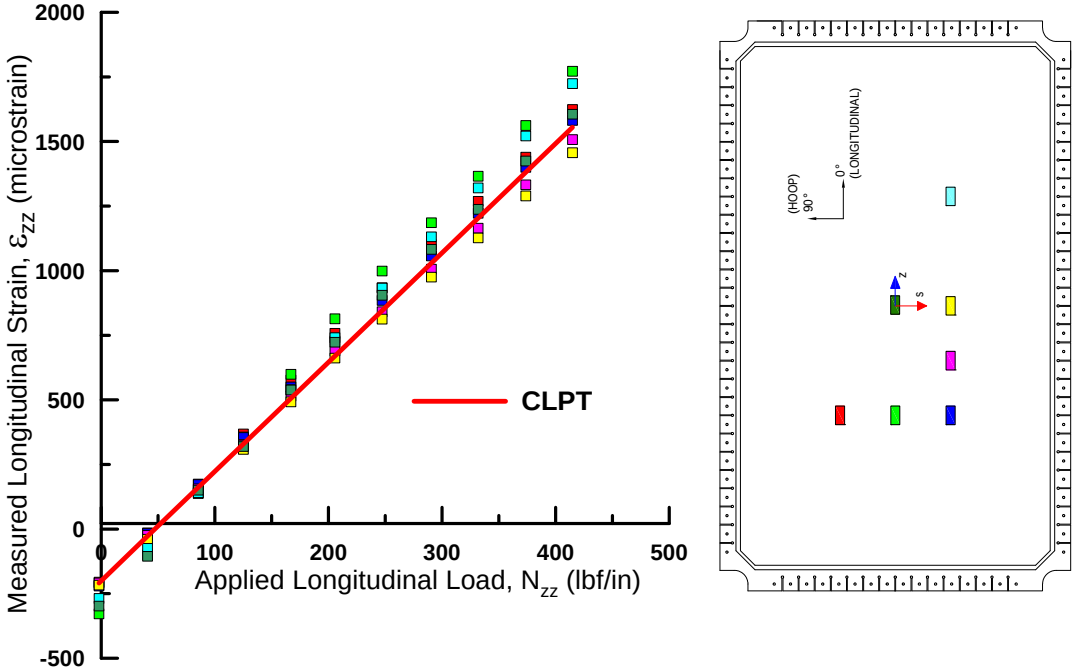

Figure 32. Variation of Longitudinal Strain (Top Facesheet) With Applied Longitudinal Loading at Different Locations on the Test Panel

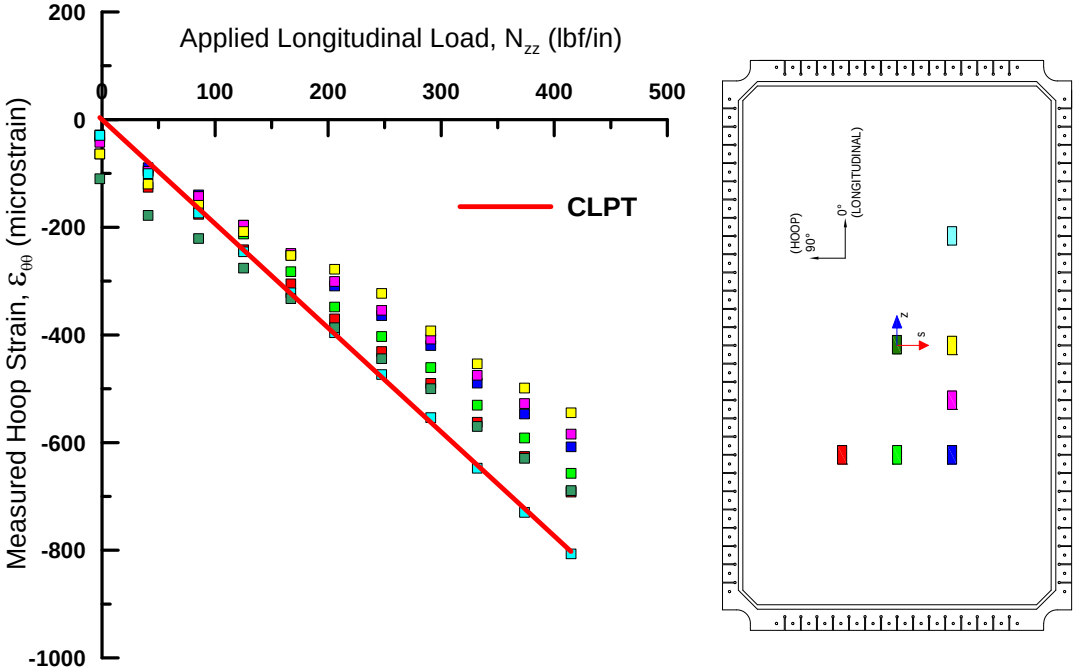

Figure 33. Variation of Hoop Strain (Top Facesheet) With Applied Longitudinal Loading at Different Locations on the Test Panel

The distribution of strains along the longitudinal and hoop directions are plotted in figures 34 and 35. The longitudinal strains tended to peak along the centerline of the panel (θ=s=0) as the load increased, as shown in figure 34. The longitudinal strain distribution as a function of the longitudinal location is plotted at different load levels in figure 35. The longitudinal strain tended to dip slightly at the center plane (z=0) of the panel. These variations of the longitudinal strains imply bending of the panel and some edge effect due to the presence of the stiffened load introduction region.

The bending of the panel in the r-θ and r-z planes as a function of the longitudinal loading are plotted in figure 36. Unfortunately, due to inferior application of protective coating on the strain gages on the interior (concave side) of the panel, water seepage occurred, resulting in electrical shorting of the strain gage circuit. Thus, most gages on the interior were rendered ineffective. However, two sets of gages along the longitudinal and hoop directions were intact, and strains at these locations were recorded during the tests. Under longitudinal loading, the bending in the r-z plane was less than 5% at the two locations where back-to-back-strains were measured. The bending deformation in r-z plane tended to be constant with increasing load. However, in the r-θ plane, the bending deformation decreased with increasing longitudinal loading. The bending deformation was negative and in the neighborhood of -10% for the range of applied loading. Thus, for longitudinal loading, the radius of curvature of the panel tends to decrease in the r-z plane, while it increases (or panel tends to become flat) in the r-θ plane.

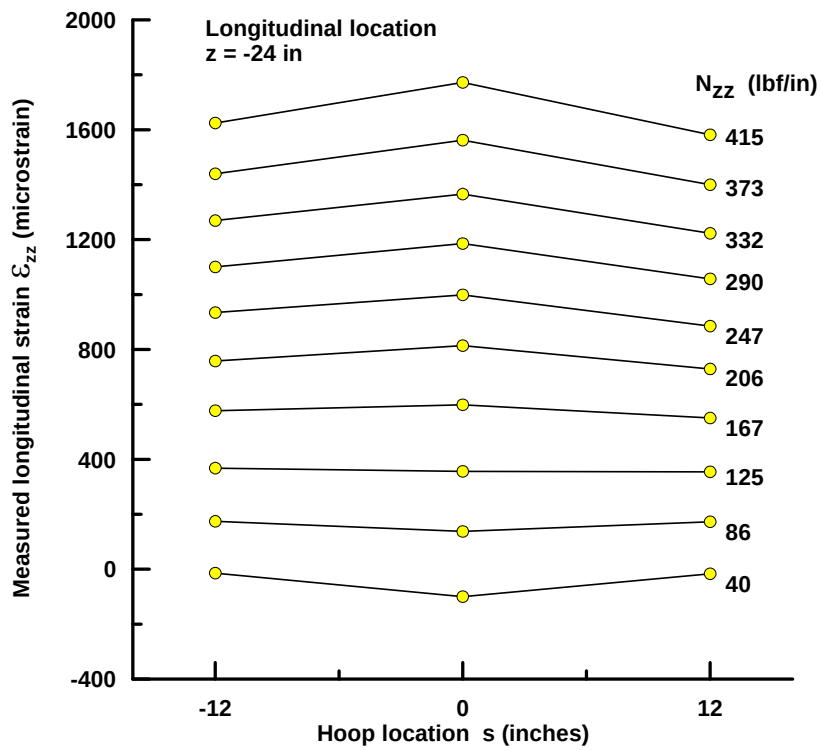

Figure 34. Variation of Longitudinal Strains as a Function of Hoop Location

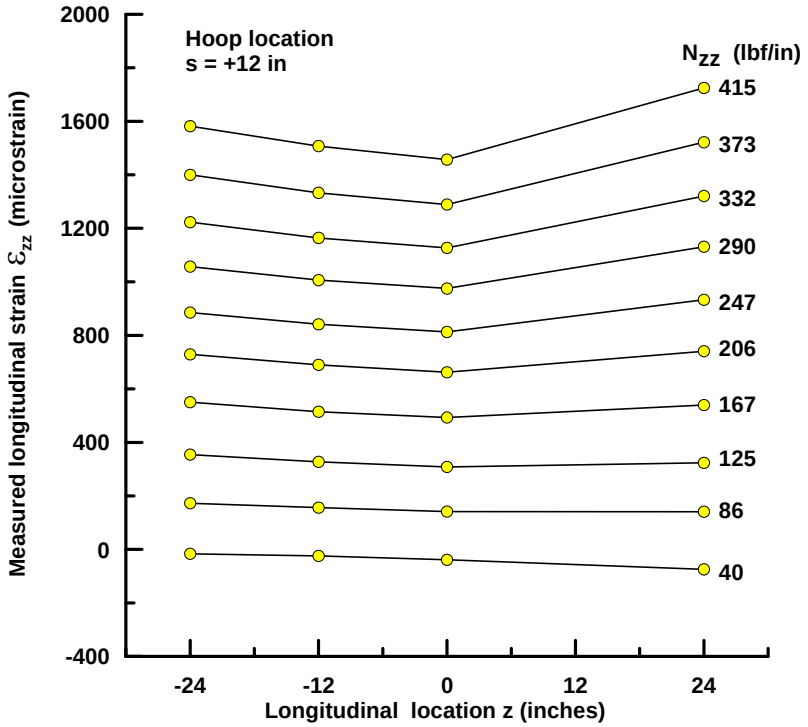

Figure 35. Variation of Longitudinal Strains as a Function of Longitudinal Location

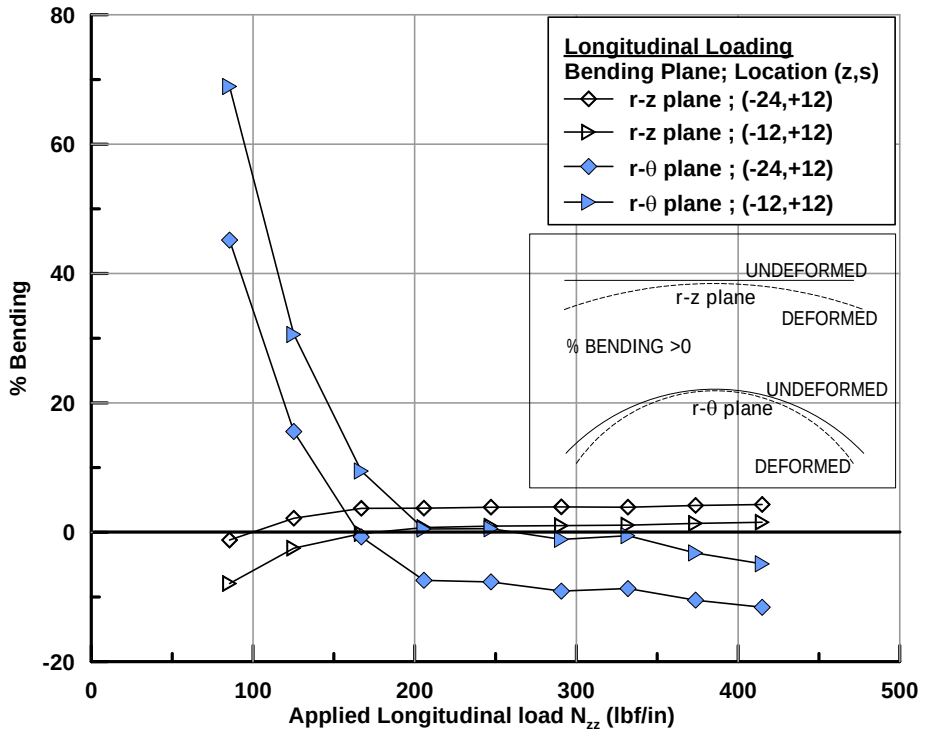

Figure 36. Bending of Panel in r-z and r-θ Planes Under Pure Longitudinal Loading

5.1.2 Pressurization/Hoop Loading.

The test panel was incrementally loaded to a maximum internal pressure of 6.73 psi, which corresponds to a hoop load of 498 lbf/in. Similar to the case of longitudinal loading, the longitudinal loaders were engaged to the specimen even though they were not required. The variation of hoop and longitudinal strains at different locations on the top surface (convex side) of the panel are plotted as a function of the hoop load in figures 37 and 38, respectively. It can be observed that the strains along the direction of applied load compare well with the CLPT prediction (for a flat panel). However, the longitudinal strains tend to be lower than that predicted by CLPT. This can be attributed to the geometric, as well as constraint effects (due to stiffened loading edges and engaging of longitudinal loaders), which are not accounted for in the CLPT predictions.

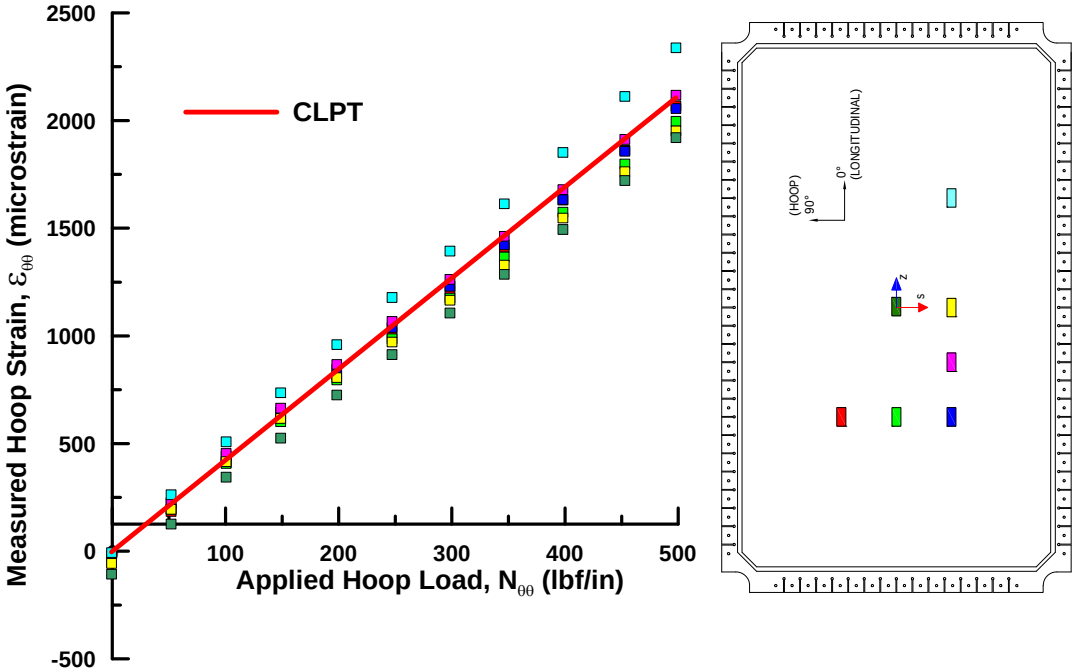

Figure 37. Variation of Hoop Strain (Top Facesheet) With Applied Hoop Loading at Different Locations on the Test Panel

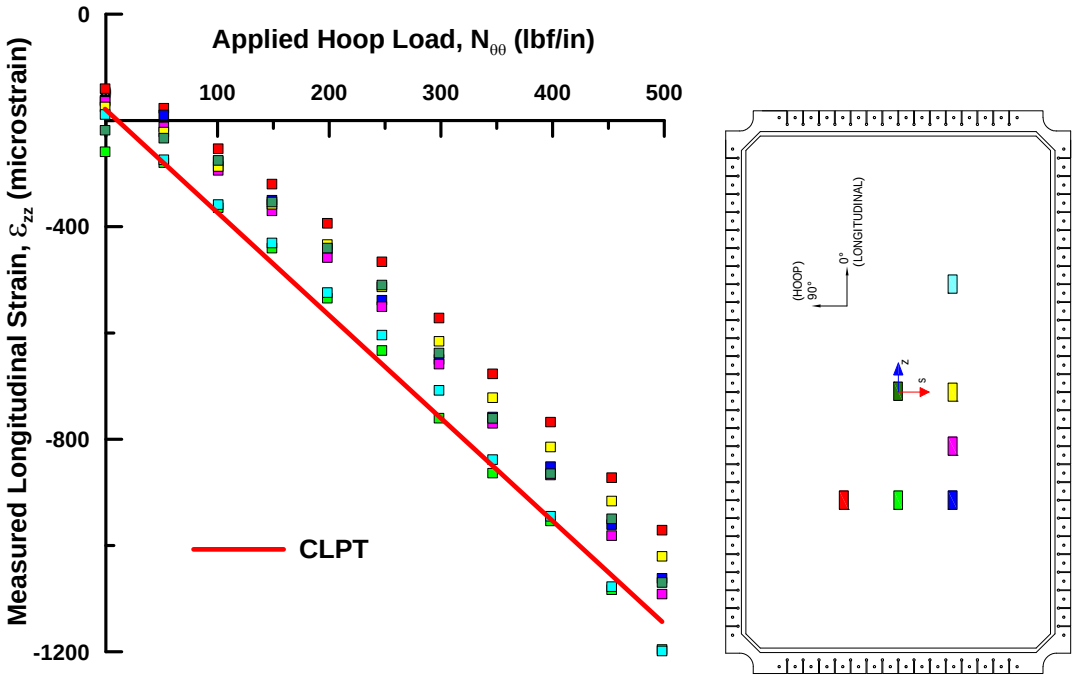

Figure 38. Variation of Longitudinal Strain (Top Facesheet) With Applied Hoop Loading at Different Locations on the Test Panel

The distribution of strains along the longitudinal and hoop directions are plotted in figures 39 and 40. With increasing loads, the hoop strains were observed to remain uniform along the tangential direction, as shown in figure 39. The hoop strain distribution along the longitudinal direction is plotted at different load levels in figure 40. The hoop strain tended to dip slightly at the center plane (z=0) of the panel. Further, the hoop strains were consistently higher at z=+24 inches in comparison to the other locations.

The bending of the panel in the r-θ and r-z planes are plotted in figure 41. Under pressurization loading, the bending in the r-z plane was about +10% at the two locations where back-to-back-strains were measured. The bending deformation in r-z plane tended to be constant with increasing load. However, in the r-θ plane, the bending deformation approached +4% and +8% with increasing load, as shown in figure 41. Thus for pressurization loading, the radius of curvature of the panel tends to decrease in both the r-z and r-θ planes. Under pressurization/hoop loading, under ideal circumstances, the radius of curvature of the cylindrical panel must increase with internal pressure. The opposite trend observed in the current experiments is due to the physical difficulty in applying the internal pressure exactly to point of tangency of the load introduction region to the cylindrical portion of the panel. In addition, the presence of radial supports, which were intended to measure the imbalance in the system of forces, may have actually constrained the panel in an undesirable manner. Thus, in the discussion of individual experimental results in the following section, the bending data will be presented. This data will be useful when correlating the results from idealized numerical models with the experimental data in the future.

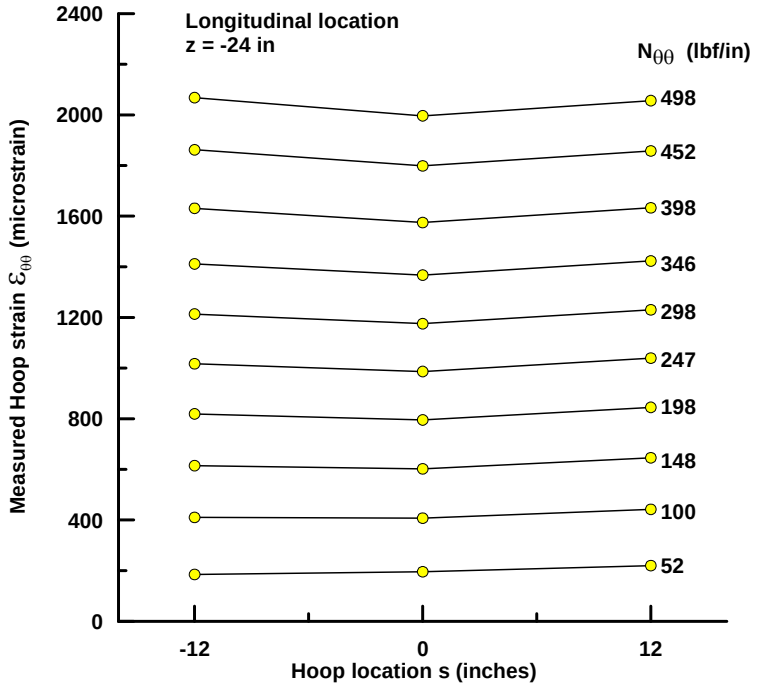

Figure 39. Variation of Hoop Strains as a Function of the Circumferential Direction

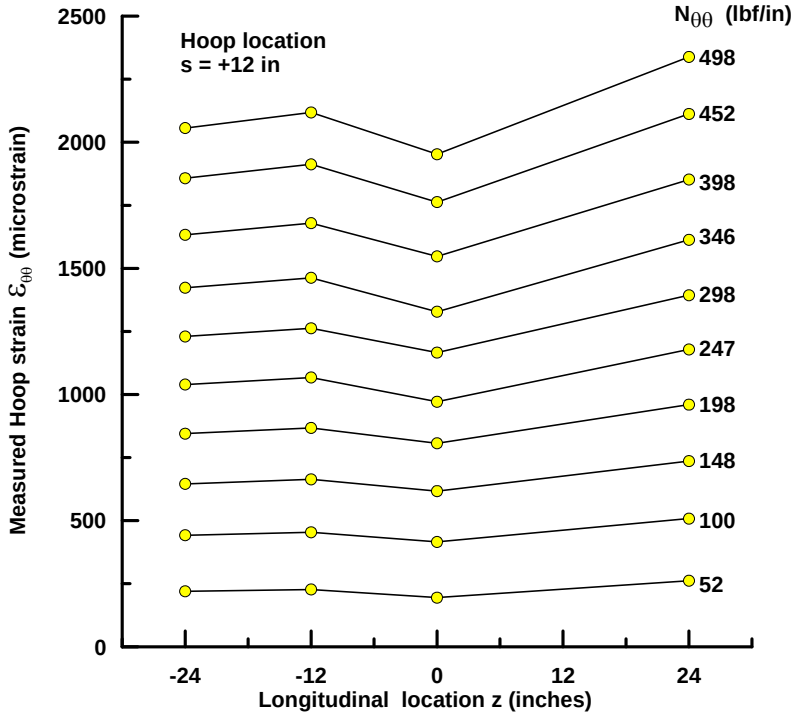

Figure 40. Variation of Hoop Strains as a Function of the Longitudinal Direction

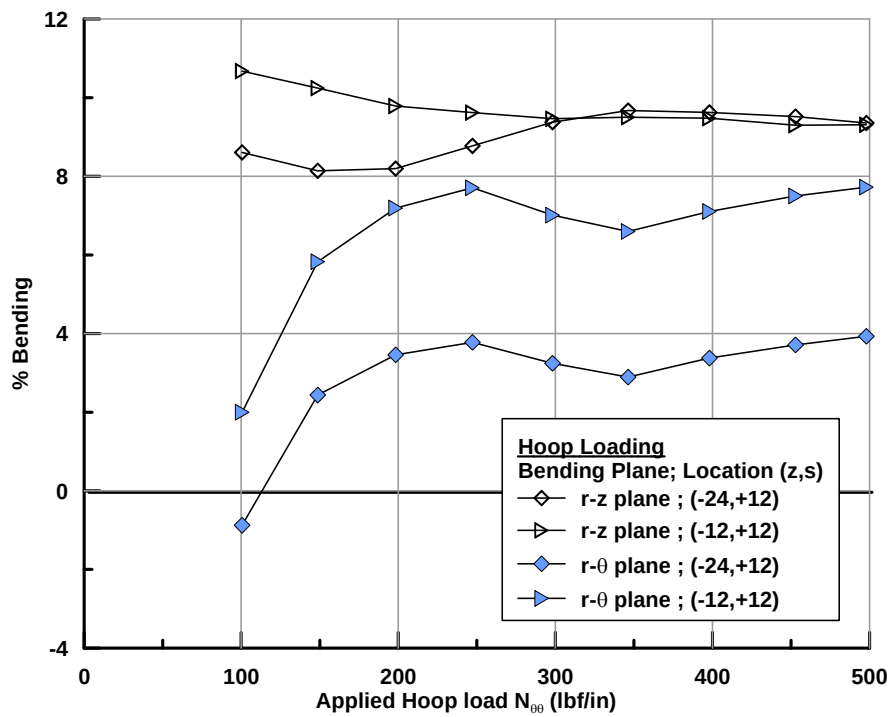

Figure 41. Bending of Panel in r-z and r-θ Planes Under Pure Pressurization/Hoop Loading

5.1.3 Combined Longitudinal and Pressurization Loading.

The test panel was subjected to a combined loading scenario with the longitudinal and pressurization loads applied incrementally to maximum values of 829 lbf/in and 13.46 psi, respectively. The variation of longitudinal and hoop strains measured on the top surface of the panel are plotted as a function of the applied loading in figures 42 and 43, respectively. Both longitudinal and hoop strain compare reasonably with the CLPT predicted strains for combined loading. The variation of longitudinal strains with respect to applied loading was slightly nonlinear when compared to the hoop strains. The uniformity of longitudinal and hoop strains under combined loading were similar to those under pure longitudinal and pure hoop loading previously discussed.

The bending of the panel in the r-z and r-θ planes at two locations in the panel are summarized and plotted in figure 44. The bending in the r-z plane was negative (which tends to make the panel concave upwards) at z = -12, while at z = -24, the bending was slightly positive. The bending in the r-θ planes at both locations where back-to-back strains were measured, was about +20%. The strain data indicate that the test panel forms a saddle shape due to deformation under combined longitudinal and pressurization loads.

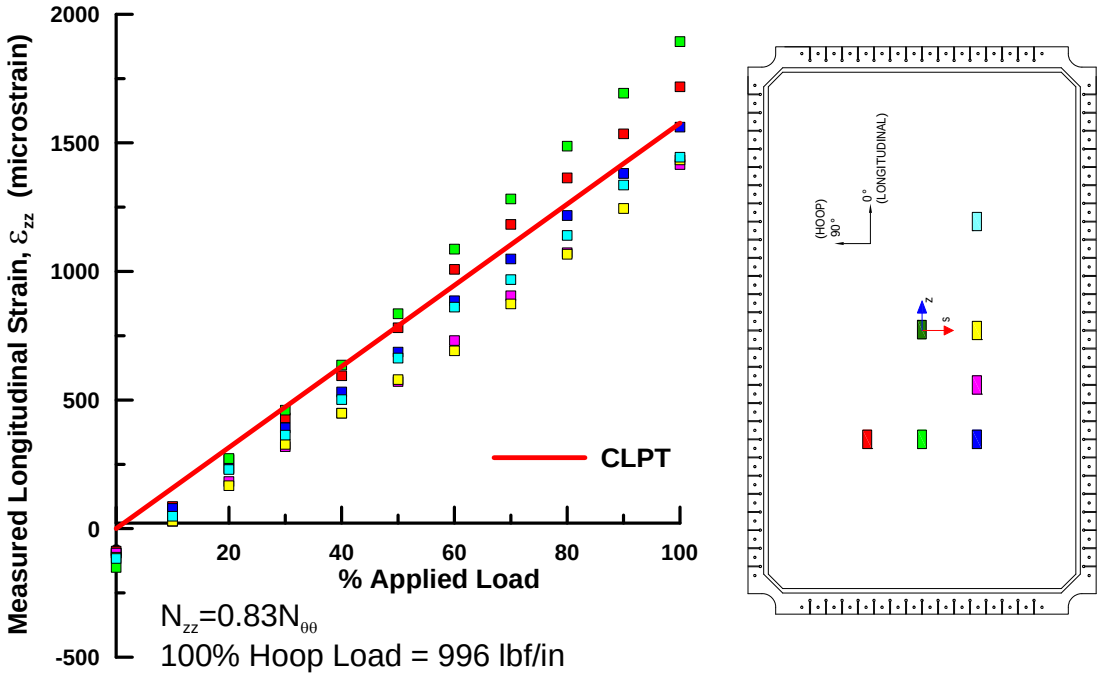

Figure 42. Variation of Longitudinal Strain (Top Facesheet) With Applied Loading at Different Locations on the Test Panel

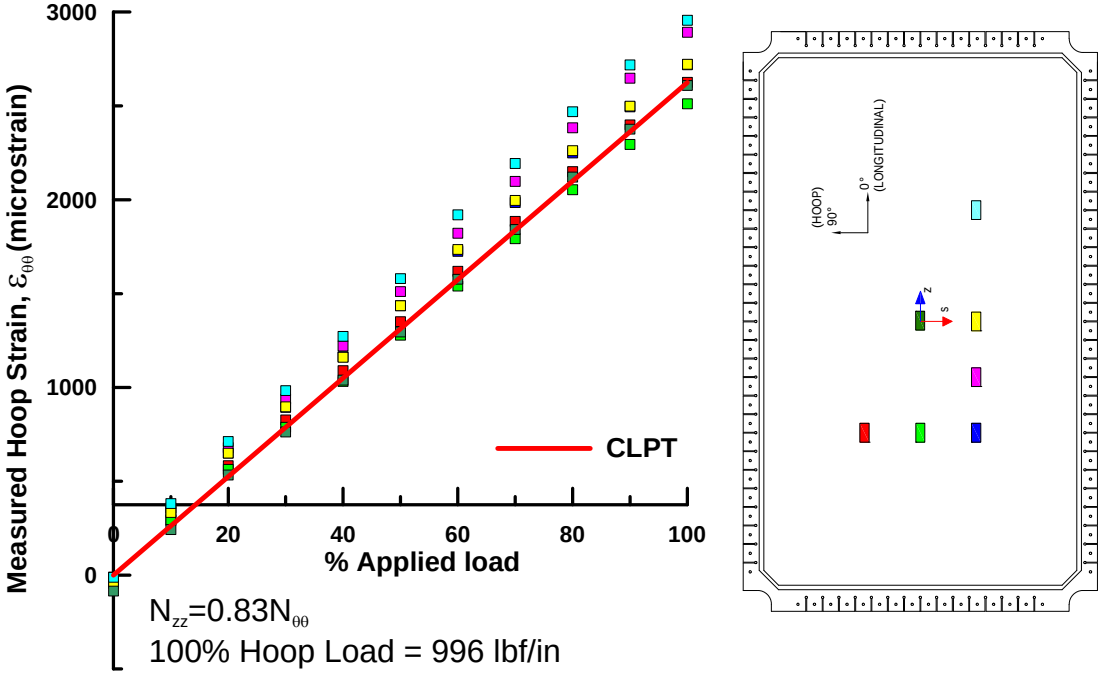

Figure 43. Variation of Hoop Strain (Top Facesheet) With Applied Loading at Different Locations on the Test Panel

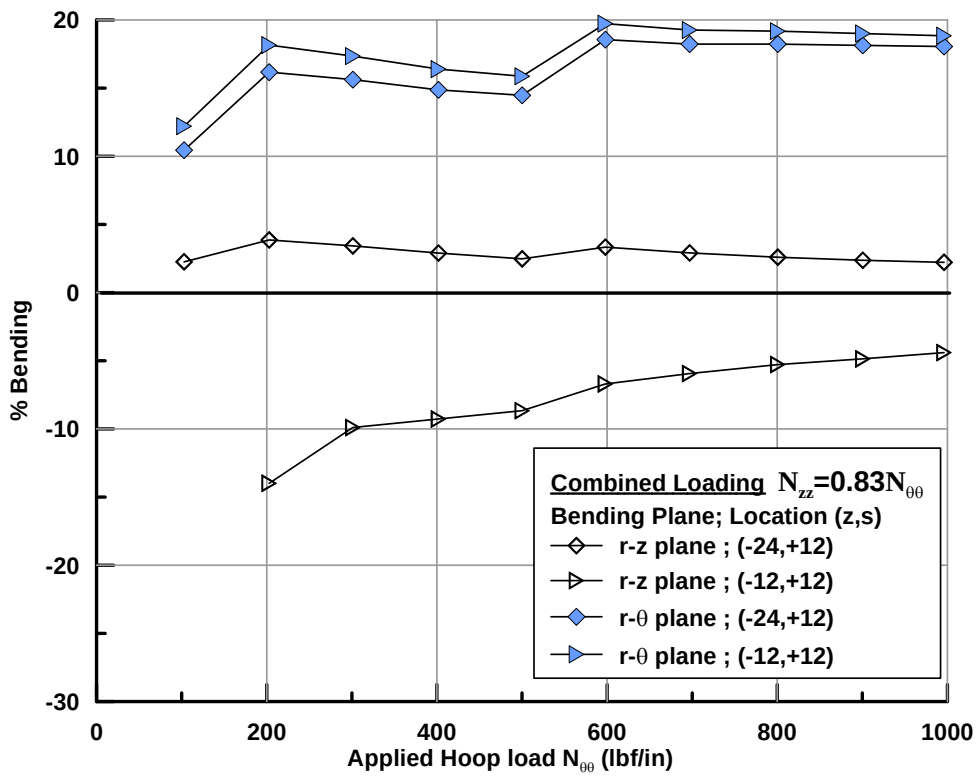

Figure 44. Bending of Panel in r-z and r-θ Planes Under Combined Loading

5.2 TEST PANEL CP1A.

Test panel CP1 was inflicted with a saw-cut damage (slit) in the top facesheet while it was still mounted in the test fixture and designated CP1A. A 3-in. by 3-in. cross slit aligned with the longitudinal and hoop directions were cut in the facesheet, in situ, at the center of the panel. The geometry of the flaw and additional strain gages used to monitor the strains near the slit are shown in figure 45. The test panel was subjected to longitudinal loading in incremental manner up to a maximum value of 1250 lbf/in. Due to mechanical constraints on the loading mechanism of the test apparatus, additional loading was not possible and the test was discontinued. No failure initiation was observed in the panel under the prescribed loading. However, the variation of far-field strains and strains in the vicinity of the slit, with applied loading, are presented in this section.

The far-field longitudinal strains are plotted as a function of the applied loading in figure 46. Similar to the unnotched panel, the strains compare reasonably with the CLPT predictions. The strain profile across the critical section (z = 0) is plotted as a function of the distance from the slit tip in figure 47. The strain profiles are presented at different load steps as indicated in the figure. The strain concentration is not as severe as would be expected for a slit. Since the slit was cut in the top facesheet alone, the loads are transmitted through the bottom facesheet, thereby alleviating the strain concentration near the slit. However, since the strain gage on the bottom facesheet was rendered unusable (due to reasons discussed in the section 5.1.1), the preceding argument cannot be corroborated. Since the failure strains for the facesheet is about 13900 $\mu\varepsilon$, the applied loading was insufficient to cause failure initiation from the slit.

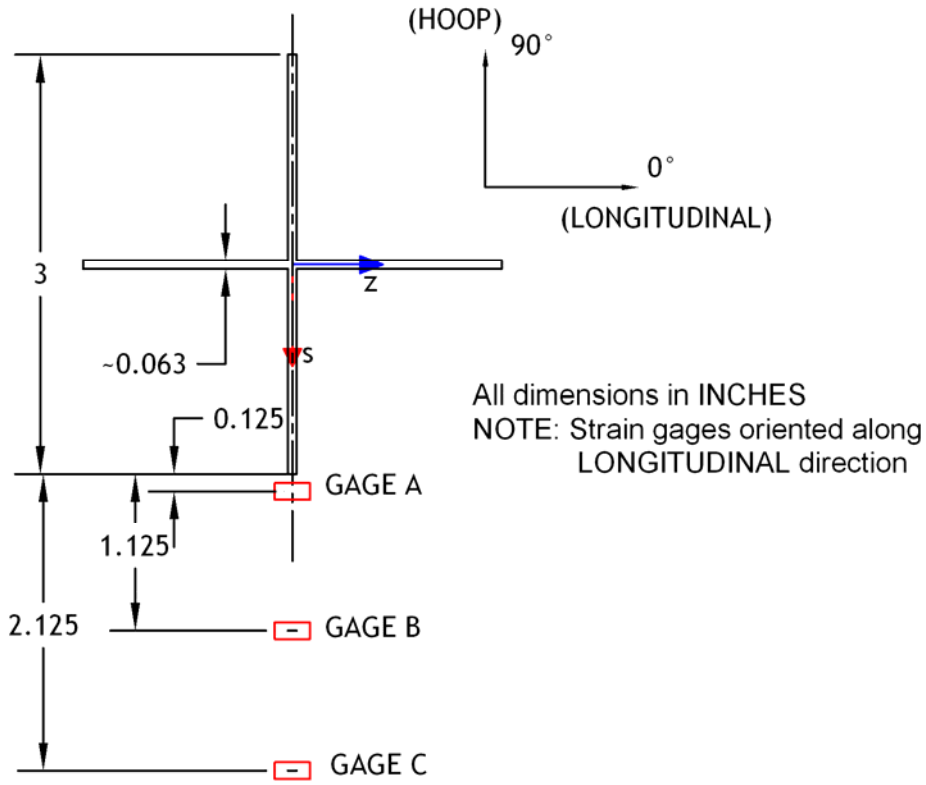

Figure 45. Slit Geometry and Strain Gage Locations for Test Panel CP1A

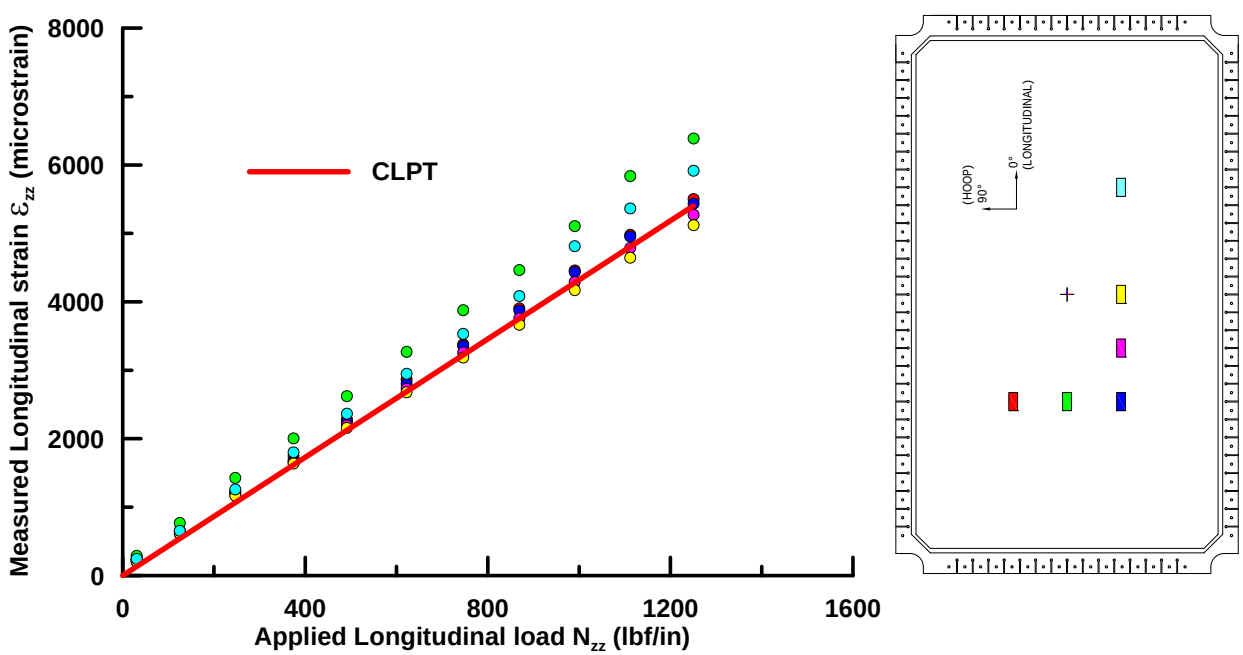

Figure 46. Variation of Far-Field Strains With Applied Longitudinal Load

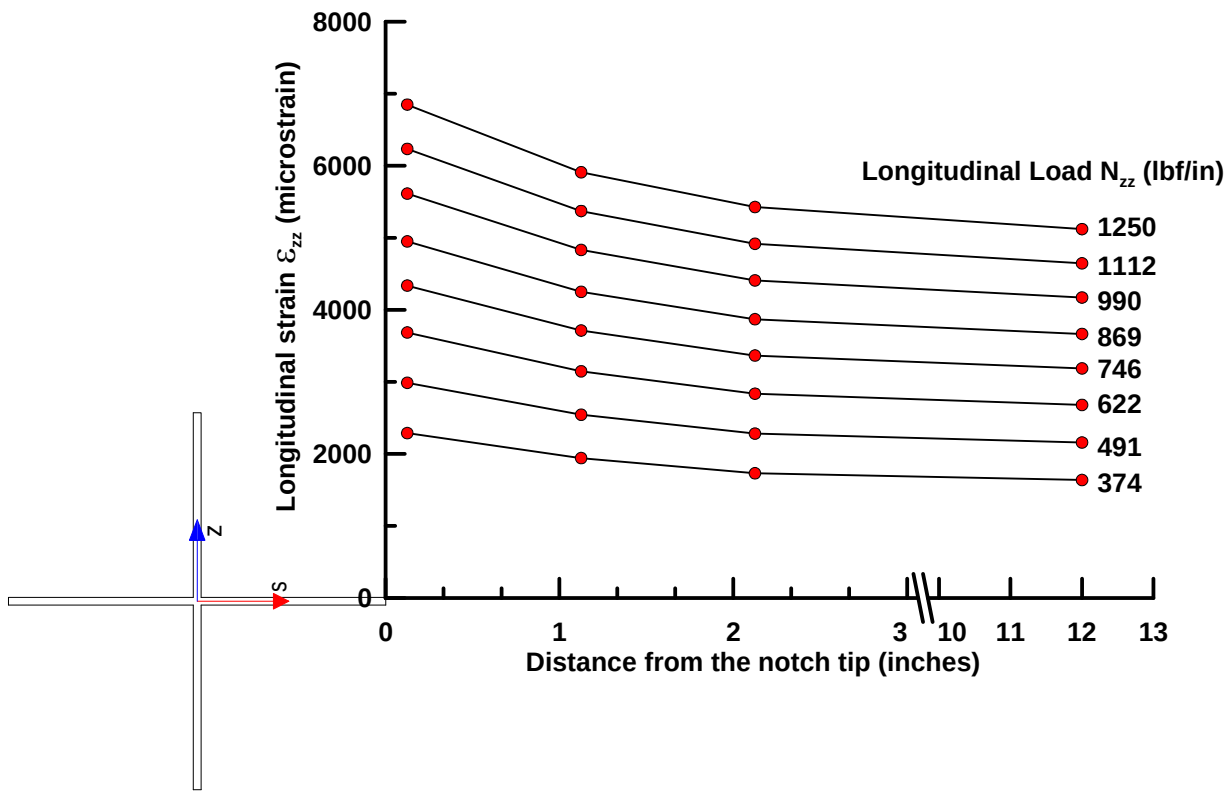

Figure 47. Strain Profiles Along the Critical Section (z=0) on the Top Facesheet

5.3 TEST PANEL CP1B.

Since the panel configuration CP1A strength was higher than the loading capability of the test apparatus, it was decided to extend the slit along the longitudinal direction to a length of 10 inches. The panel was designated CP1B. The geometry of the slit and additional strain gages that were used are shown in figure 48. The test panel was then subjected to pressurization/hoop loading until panel fracture occurred. The test panel suffered a fracture across the critical section (~s=0) at a hoop load of 1038 lbf/in, with the failure initiation occurring at about 600 lbf/in. The loading and failure process observed in the test panel is discussed in terms of the strain gage data in the following paragraphs.

The variation of far-field hoop strains as a function of the applied hoop loading is plotted in figure 49. It may be observed that the far-field strain gages compare well with the CLPT predictions for the given loading. The strain gage in the load path between the slit and the longitudinal edge of the panel (yellow data points), recorded lower strains compared to the others. This is expected, as the load path goes around the slit and the material beside the slit (along the load direction) is stressed less.

The bending of the panel in the r-θ plane at locations far removed from the slit were plotted as a function of applied load, as shown in figure 50. The panel exhibited significant bending at some locations (up to +40%) prior to initiation of failure. After failure initiation, the bending of the

panel along s=+12 inches settled to about +10% or less, while the gages along s=0 indicated a bending of about +20%.

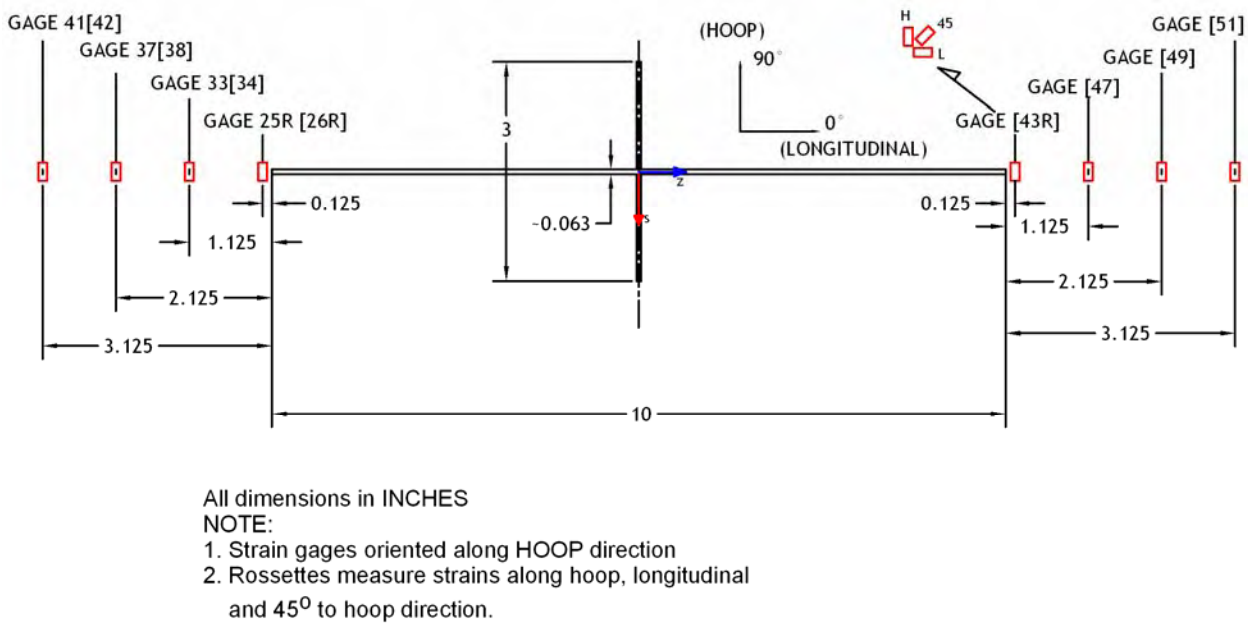

Figure 48. Slit Geometry and Strain Gage Locations for Test Panel CP1B

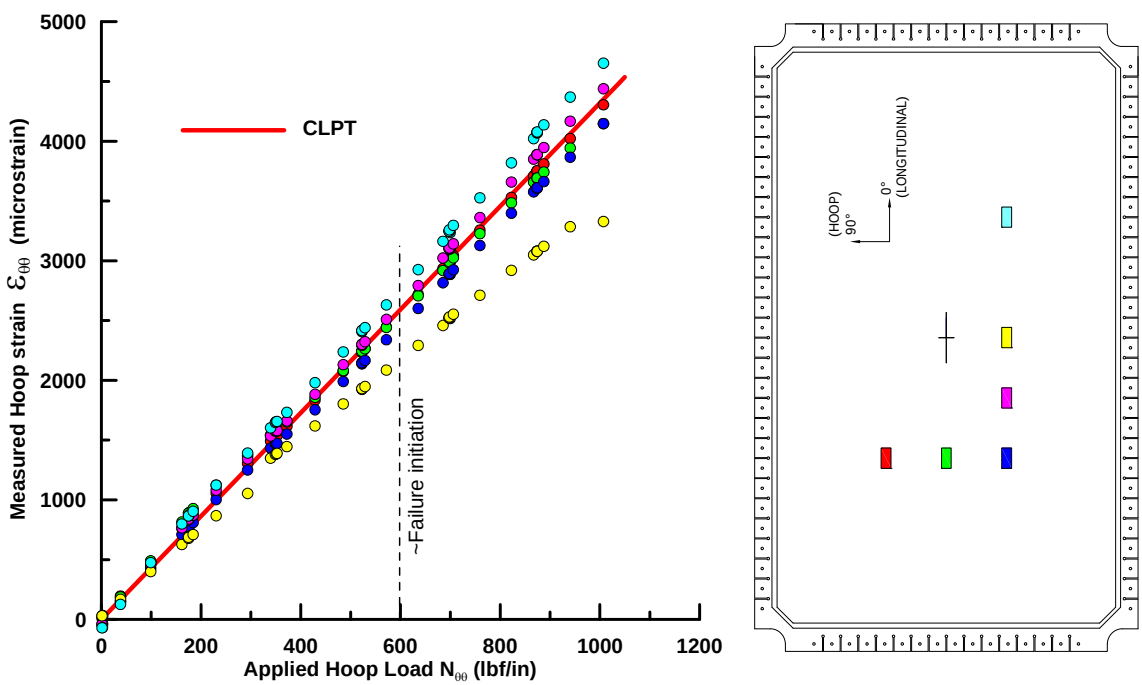

Figure 49. Variation of Far-Field Hoop Strains With Applied Loading

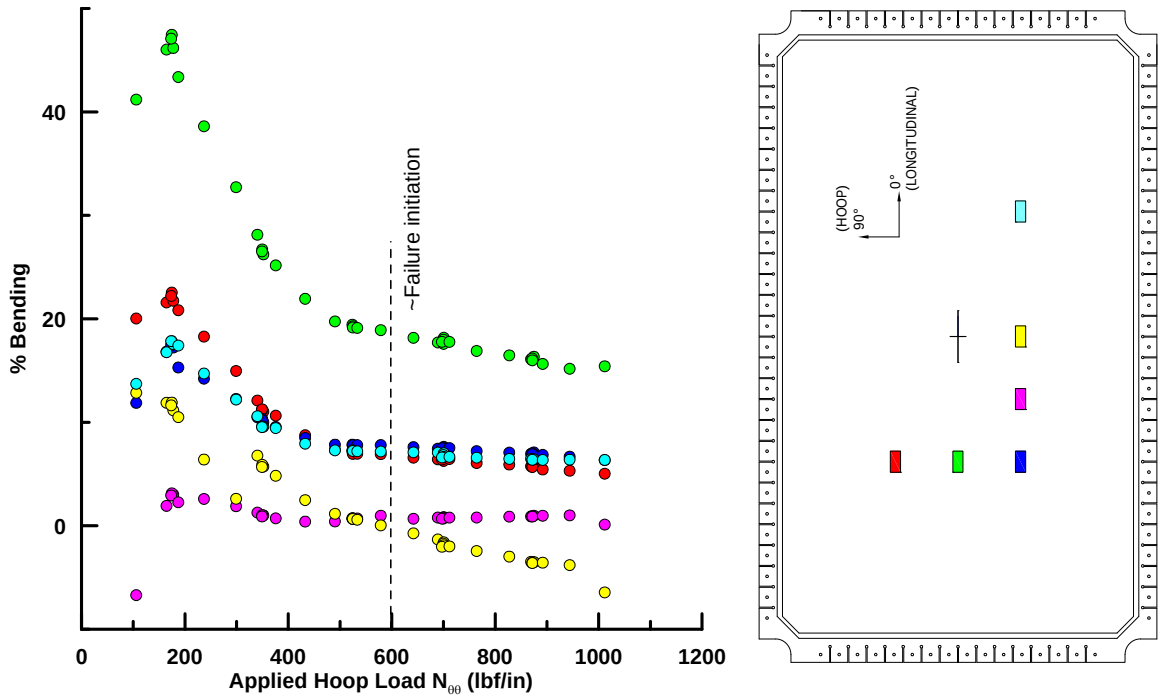

Figure 50. Far-Field Bending of Panel in r-θ Plane

The strains measured in the immediate vicinity of the slit were plotted as a function of the applied loading, as shown in figure 51. From this figure, the failure initiation loads can be roughly estimated as 600 lbf/in. Note that the strain gage nearest to the slit is located at a distance of 0.125 in. from the slit. Thus, failure at the slit tip could have occurred at a slightly lower load. The strain profiles (top and bottom facesheet) at selected load levels were plotted as a function of distance from the slit tip, prior to failure initiation and after failure initiation, as shown in figures 52 and 53. Prior to failure initiation, the strain distribution indicates the strain concentration near the slit. After failure initiates and propagates, some strain gages indicate a lower strain level. This happens when the fracture plane bypasses (above or below) the location of the strain gage. When the fracture path passes though the gage, either the gage is severed or the lead wire solder snaps resulting in the loss of strain gage signal. The missing strain data in figure 53 corresponds to such a situation. The strain distributions on the top and bottom facesheets are similar up to the point of failure initiation. After, failure initiation, the strain distributions differ due to the differences in fracture path in the two facesheets.

The bending of panel in the r-θ plane in the vicinity of the slit along the section s=0 was plotted as a function of applied load, as shown in figure 54. In comparison to the far-field locations, the magnitude of bending was much higher prior to failure initiation. After failure initiation, the amount of bending decreased to below +20%. However, no trends could be established between the magnitude of bending and distance from the slit tip. The pictures of fractured facesheets in the vicinity of the slit are shown in figures 55 and 56. The fracture paths are surrounded by a diffuse damage region of matrix cracks and fiber failures characteristic of shear failure. The fracture path was tortuous in nature, which is characteristic of laminates with majority of plies at ±45° to the loading direction.

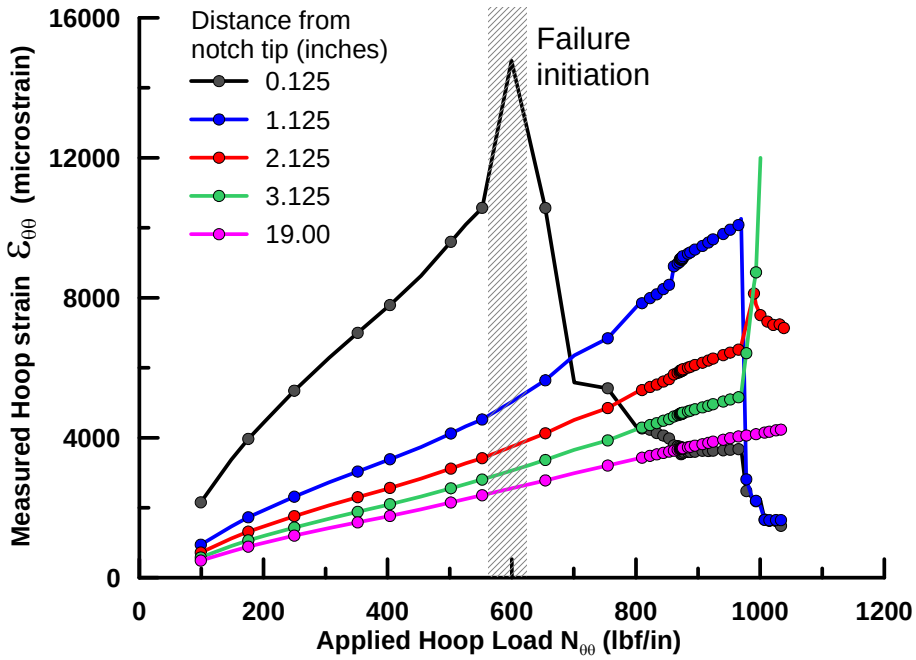

Figure 51. Variation of Hoop Strain Along the Critical Section With Applied Loading

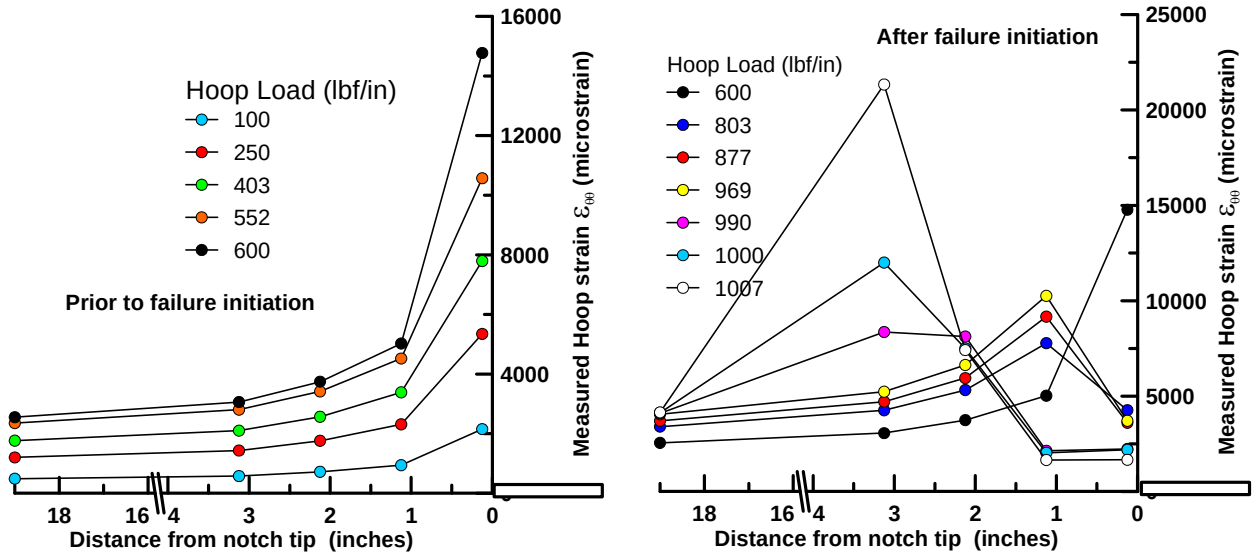

Figure 52. Hoop Strain Distributions on the Top Surface Prior to and After Failure Initiation

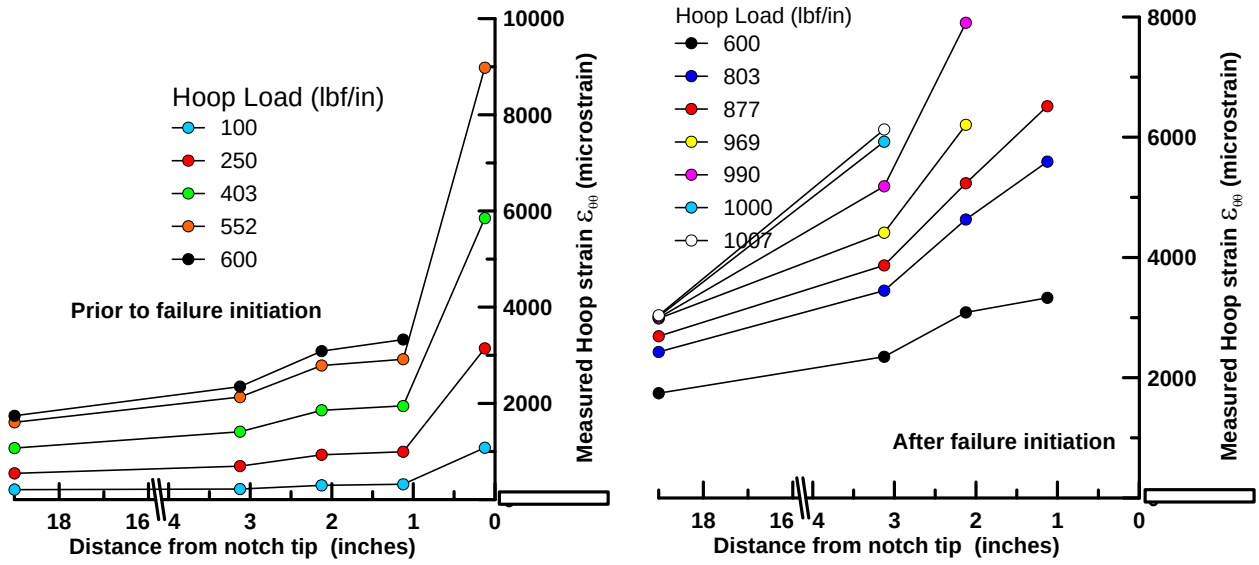

Figure 53. Hoop Strain Distributions on the Bottom Surface Prior to and After Failure Initiation

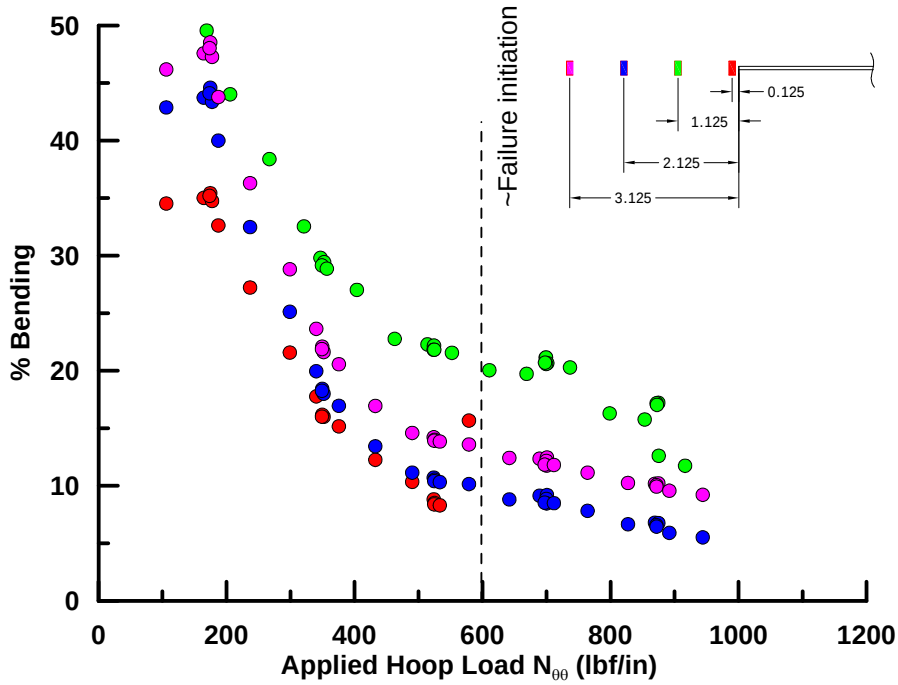

Figure 54. Bending in r-θ Plane Along s=0 Near the Notch Tip

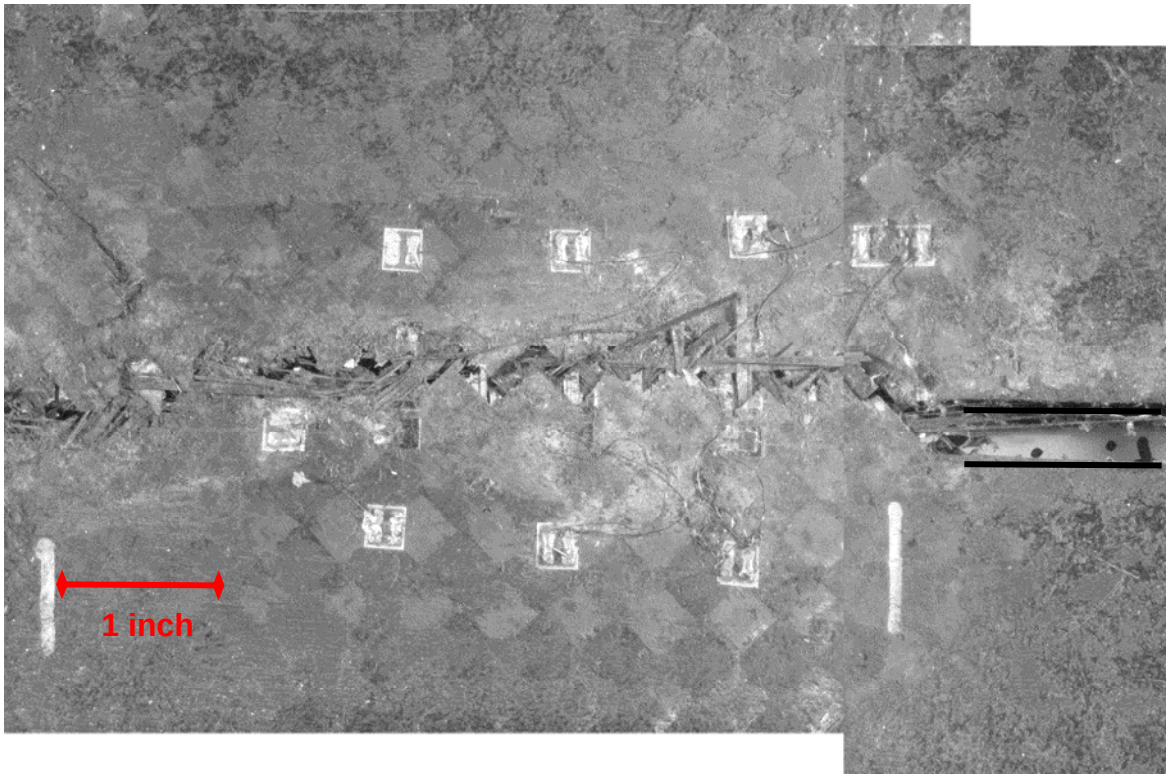

Figure 55. Fracture Path in the Vicinity of the Notch in the Bottom Facesheet

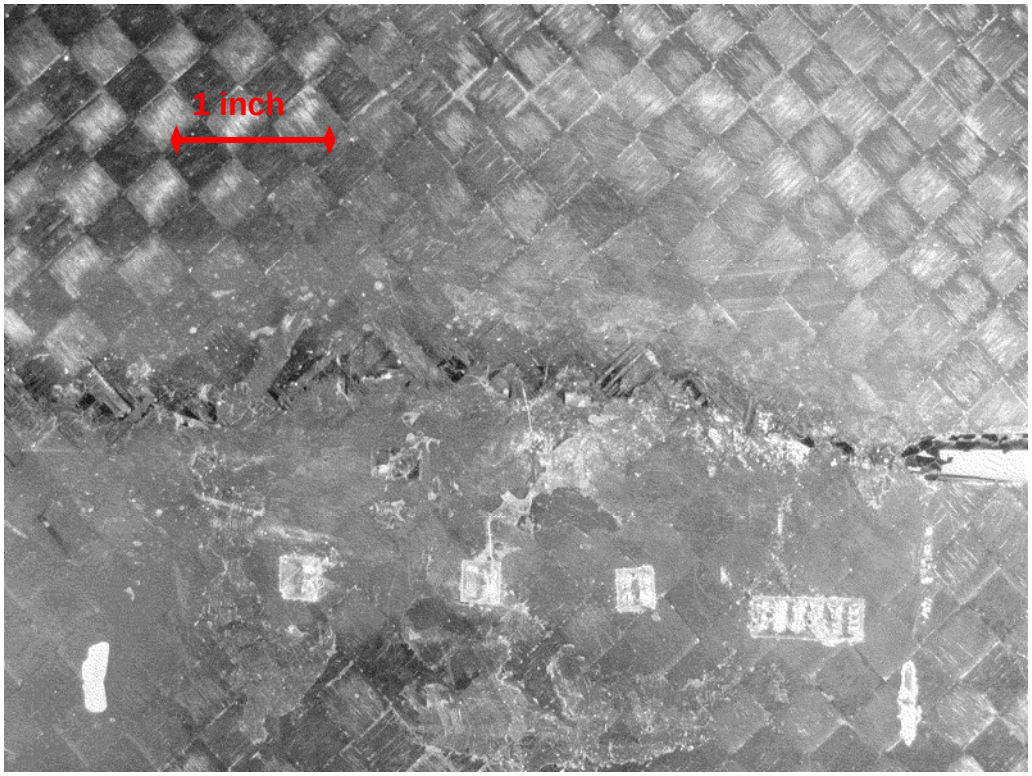

Figure 56. Fracture Path in the Vicinity of the Notch in the Top Facesheet

5.4 TEST PANEL CP2.

The test panel CP2 consisted of a 10-inch-diameter hole in the top facesheet. The core was left intact in the region of the hole. The test panel was intended to be loaded under uniaxial tension until failure. However, due to the limitations and constraints of the test apparatus, loading in the longitudinal direction was limited to 1250 lbf/in. Three longitudinal loading tests were performed on the test article without any failure initiation. Subsequently, the test panel was loaded biaxially (longitudinal + pressurization/hoop). The loads were applied incrementally with the ratio of longitudinal to hoop loads being 0.83. The loading-unloading exercise was performed three times. No failure was initiated in the panel at the maximum load combination of 1160 lbf/in longitudinal and 1400 lbf/in hoop (18.85 psi internal pressure) during each test. Next, the test panel was subjected to two loading-unloading tests of pure pressurization/hoop loading to a maximum value of 1400 lbf/in (18.9 psi internal pressure). Finally, the test panel was subjected to an internal pressure of 21.2 psi (1570 lbf/in hoop load). A small crack was initiated during this test. The crack could not be propagated further due to lack of additional loading capacity of the test apparatus. The far-field and near-field strain distributions for each loading case are discussed in the following sections. The data presented in the following sections represent one of the three tests for each load case. Test data for the additional runs may be found in reference 13.

5.4.1 Longitudinal Loading.

The test panel was loaded in the longitudinal direction to a maximum load of 1250 lbf/in. The loading was limited by the geometric constraints on the loading arms, which limited the amount of specimen elongation that could be accommodated. No failure of the test specimen was observed during this test. However, the strain gage data collected during the tests have been used make observations about the load/strain distributions and deformations of the test panel.

The far-field longitudinal and hoop strains are plotted as a function of the applied longitudinal loading, as shown in figures 57 and 58. Both longitudinal and hoop strains compare well with CLPT predictions for a flat panel. The hoop strains for the open-hole panel correlated better with CLPT when compared to the pristine (unnotched) panel (CP1). It should be noted that the panel with hole in a single facesheet is inherently unbalanced. The stretching-bending coupling arising out of this imbalance has resulted in higher hoop strains relative to the unnotched panel and thus, exhibits a better correlation with CLPT.

The variations of longitudinal and hoop strains across the width and length of the panel at selected load levels are shown in figures 59 and 60. The longitudinal strains are not uniform across the width of the panel, as shown in figure 59. This can be attributed to the edge effects due to the stiffened longitudinal edge and to the fact that the load is introduced over a slightly narrower region along the loading edge and has to redistribute itself. The hoop strain distribution along the length of the panel was observed to be nonuniform, but no trends could be identified.

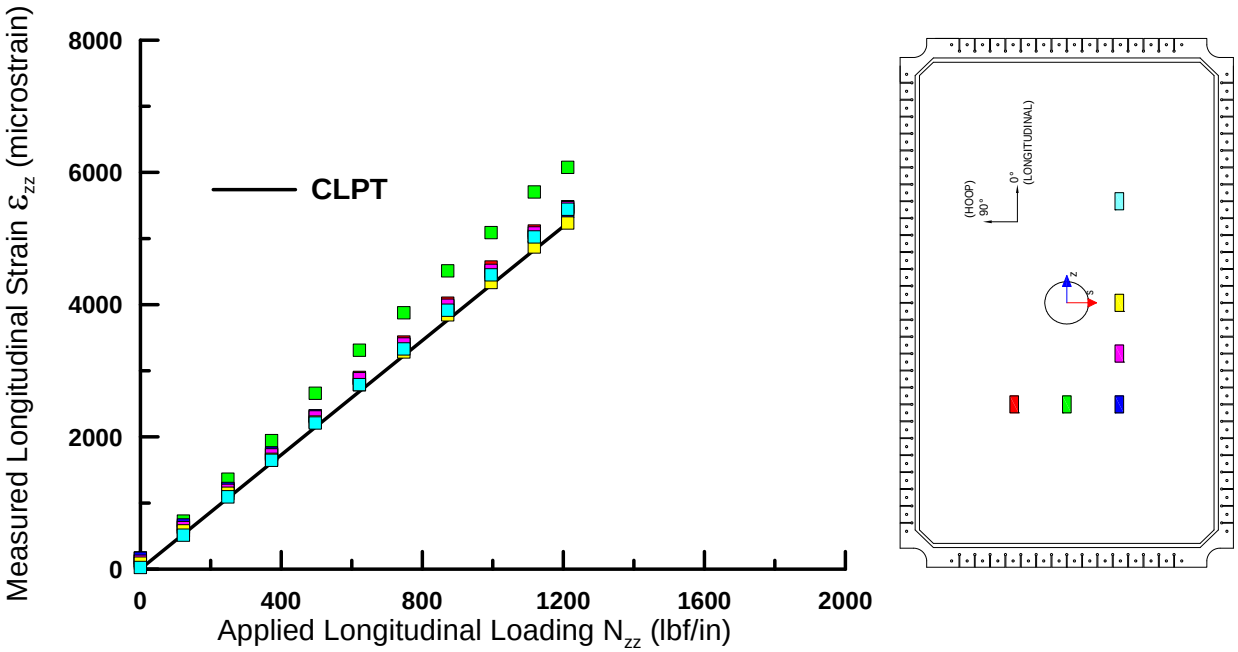

Figure 57. Far-Field Longitudinal Strains as a Function of Longitudinal Loading in Panel CP2

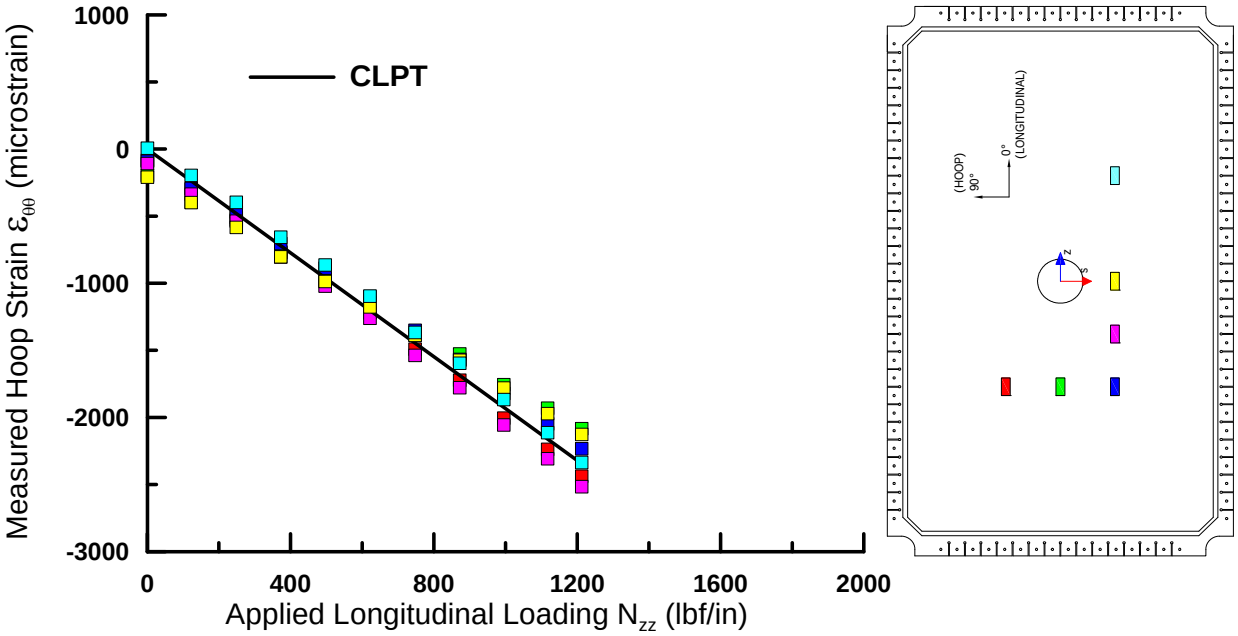

Figure 58. Far-Field Hoop Strains as a Function of Longitudinal Loading in Panel CP2

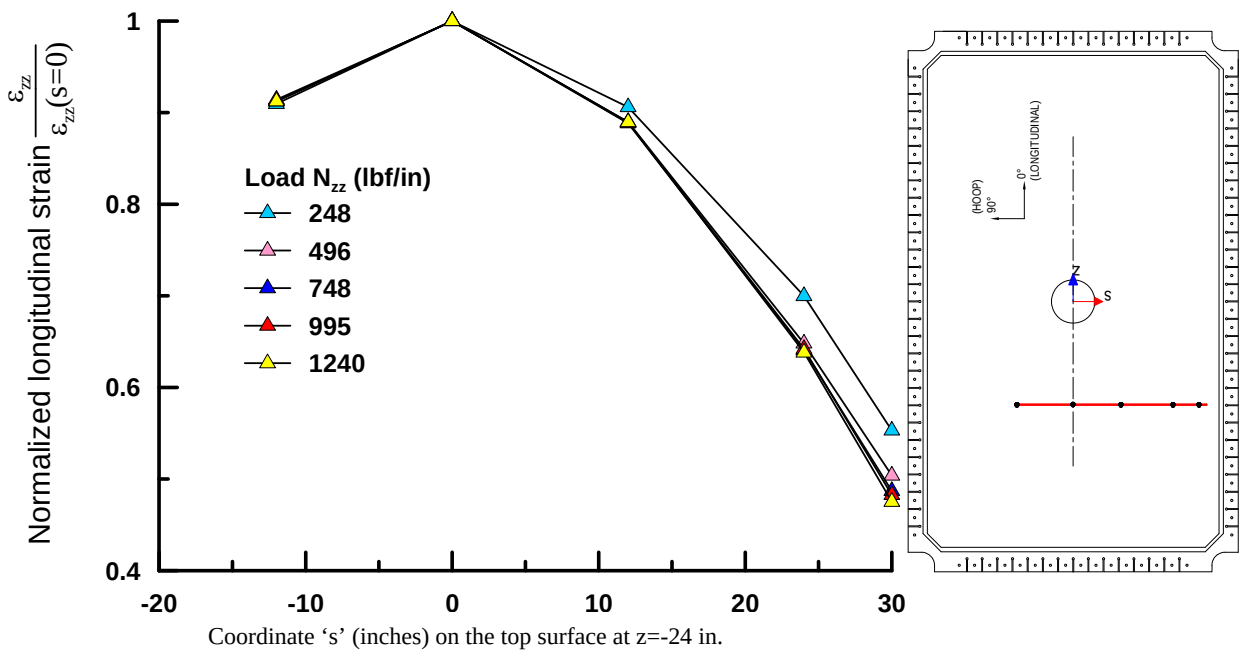

Figure 59. Longitudinal Strain Distribution Along a Section at a Distance of z=-24 Inches From the Center of the Panel

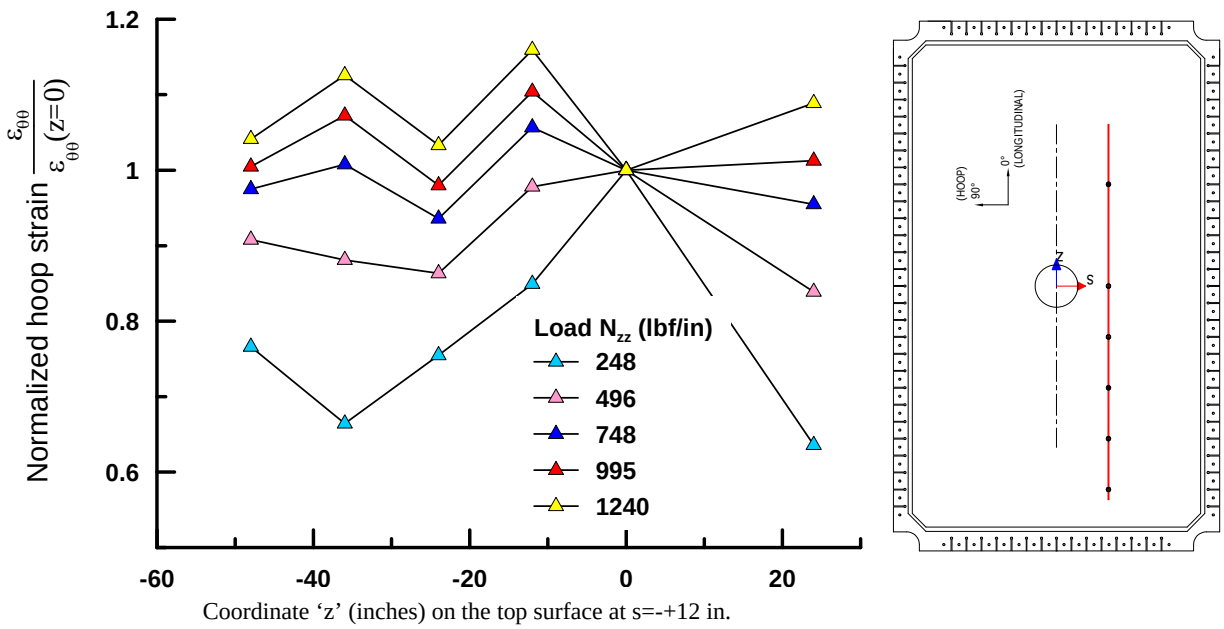

Figure 60. Hoop Strain Distribution Along a Section at a Distance of s=+12 Inches From the Center of the Panel

Due to the presence of stiffened longitudinal edges, the test article experienced bending due to the resultant of the load not passing through the modulus weighted centroid of the cross-section. The data from the far-field strain gages along the longitudinal direction have been used to estimate the amount of bending in the test panel in the r-z plane and r-θ plane along which the strain gages were mounted. The bending in the r-z plane was observed to be positive and ranged

between 0 to 10% at various locations, as shown in figure 61. The bending in the r-θ plane decreased with increasing load levels and reached negative values approaching -20%, as shown in figure 62. This implies that that the panel tends to deform such that the radius of curvature decreases in the r-z plane and increases in the r-θ plane. Thus, the panel deforms from a cylindrical surface to a nondevelopable surface. The deformed shapes are shown in figure 63.

The strains tangential to the hole boundary on the top and bottom facesheet were plotted as a function of the applied longitudinal loads, as shown in figures 64 and 65, respectively. At the maximum applied load of 1250 lbf/in, the tangential strains (along loading direction, ϕ=0º) at a distance of 0.25 inch from the boundary, reached about 10,000 $\mu\varepsilon$. This was well below the material failure strain presented in table 1. Strain concentration effects were observed on the top facesheet, with the strain gages nearest to the hole boundary indicating higher strain levels when compared to gages further away from the boundary. The tangential strains (C and D in figure 64) at ϕ=90º, which ideally must be compressive in nature, tended to approach zero with increasing load levels. This may be attributed to the local buckling of the facesheet resulting in outward bulging of the facesheet, which imposes a tensile component of strain. On the bottom facesheet, the strain distributions were markedly different from the top facesheet because the load was off-loaded from the top to the bottom skin. The strains were highs relative to far-field strains. The difference between strain readings at 0.25 and 0.75 inch from the hole boundary were negligible at the three locations (ϕ=0º, 45º, and 90º) where strains were measured indicating there was no effect of strain concentration on the bottom skin, as expected. In addition, at ϕ=90º, the strains are compressive and increase in magnitude with applied loading, as shown in the figure 65.

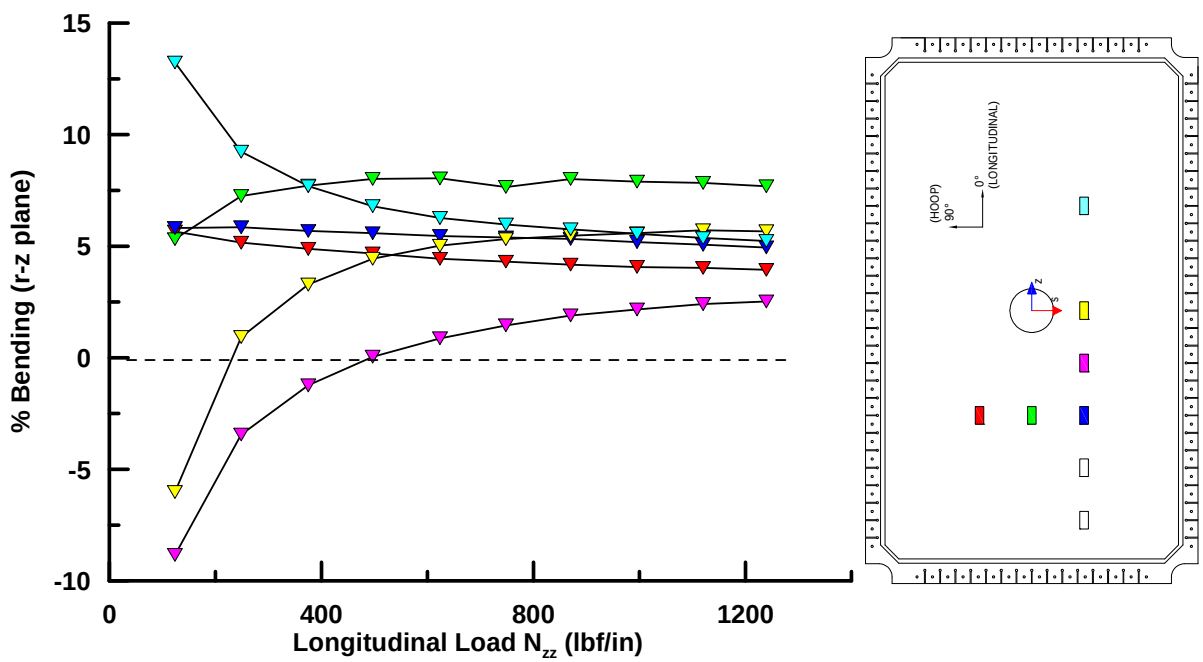

Figure 61. Bending in r-z Plane at Different Locations in the Test Panel

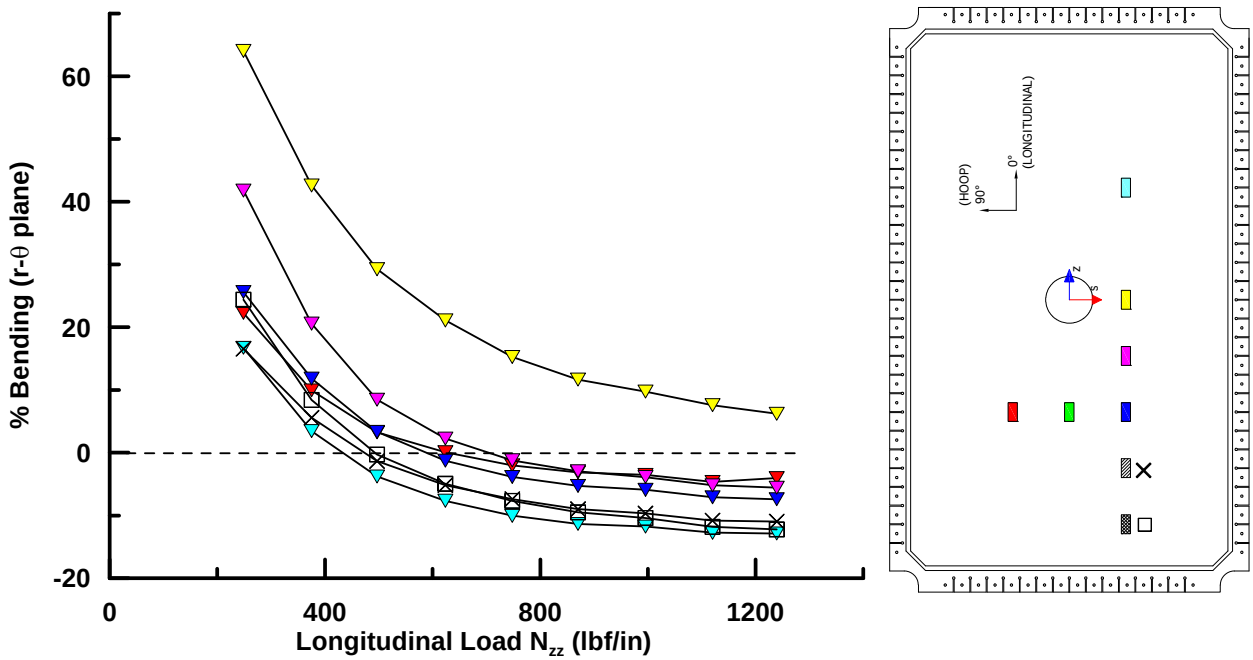

Figure 62. Bending in r-θ Plane at Different Locations in the Test Panel

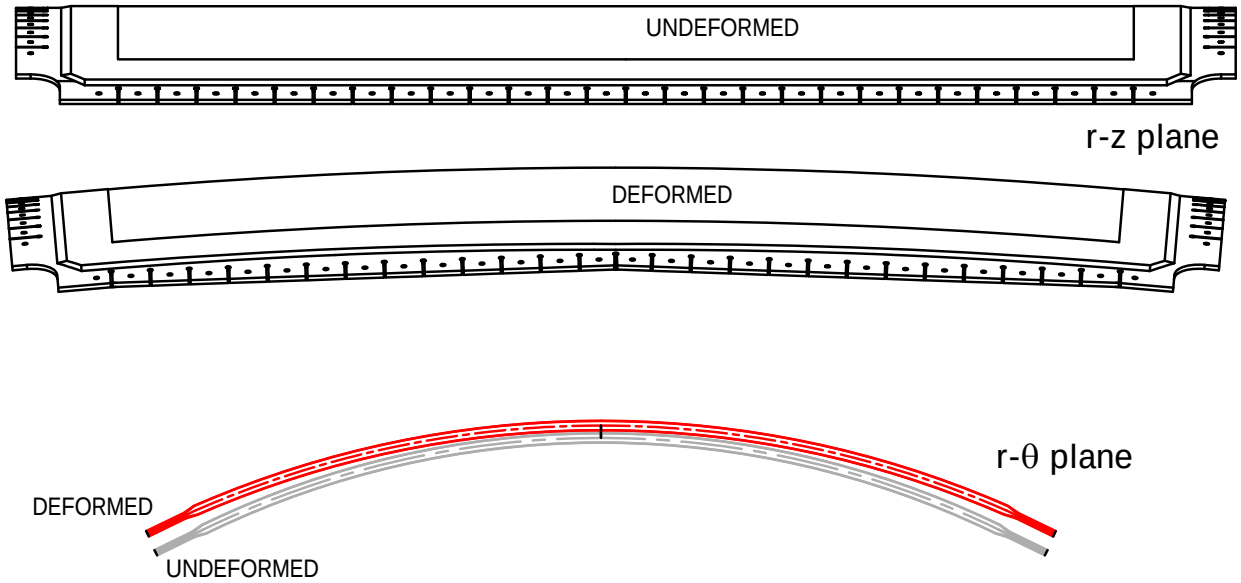

Figure 63. Observed Bending Deformation of the Panel Based on Strain Gage Data

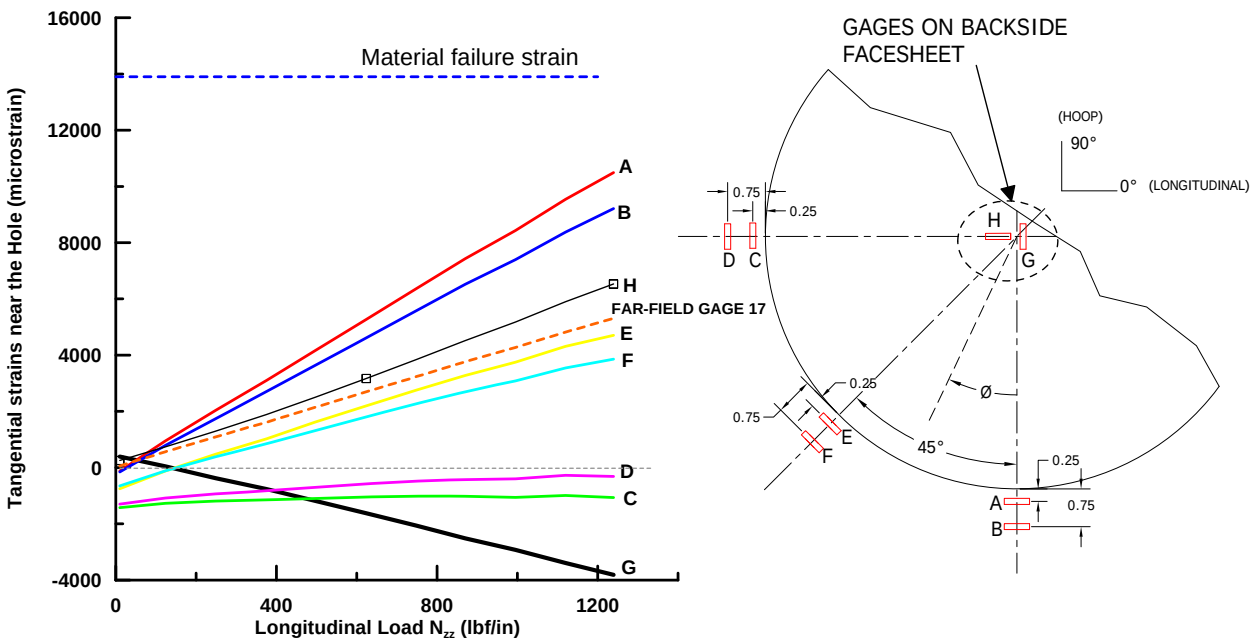

Figure 64. Tangential Strains Near the Hole Boundary on the Top Facesheet for Panel CP2 Under Longitudinal Loading

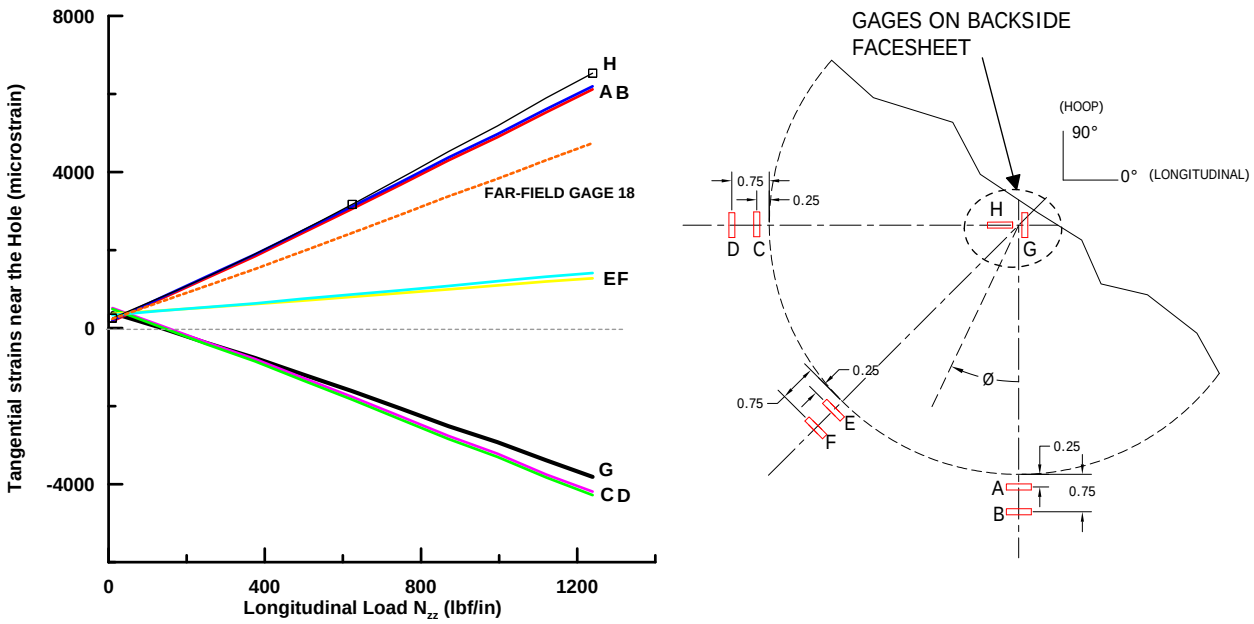

Figure 65. Tangential Strains Near the Hole Boundary on the Bottom Facesheet for Panel CP2 Under Longitudinal Loading

5.4.2 Combined Longitudinal, Pressurization Loading.

Following the longitudinal loading tests, the test panel was subjected to combined longitudinal and pressurization loading. The longitudinal load and internal pressure were increased proportionally to maximum values of 1373 lbf/in and 22.7 psi, respectively. The load

application is shown in figure 66. The maximum hoop load caused by the internal pressure is 1676 lbf/in. The ratio of hoop load to longitudinal load at each load step was to 1.2. The longitudinal and pressure loading were limited to the aforementioned maximum values due to the constraints on the panel deformations that could be accommodated by the longitudinal and hoop loaders. Thus, no failure of the specimen was observed during the test. The combined loading was repeated three times and the results from the third cycle will be discussed in this section.

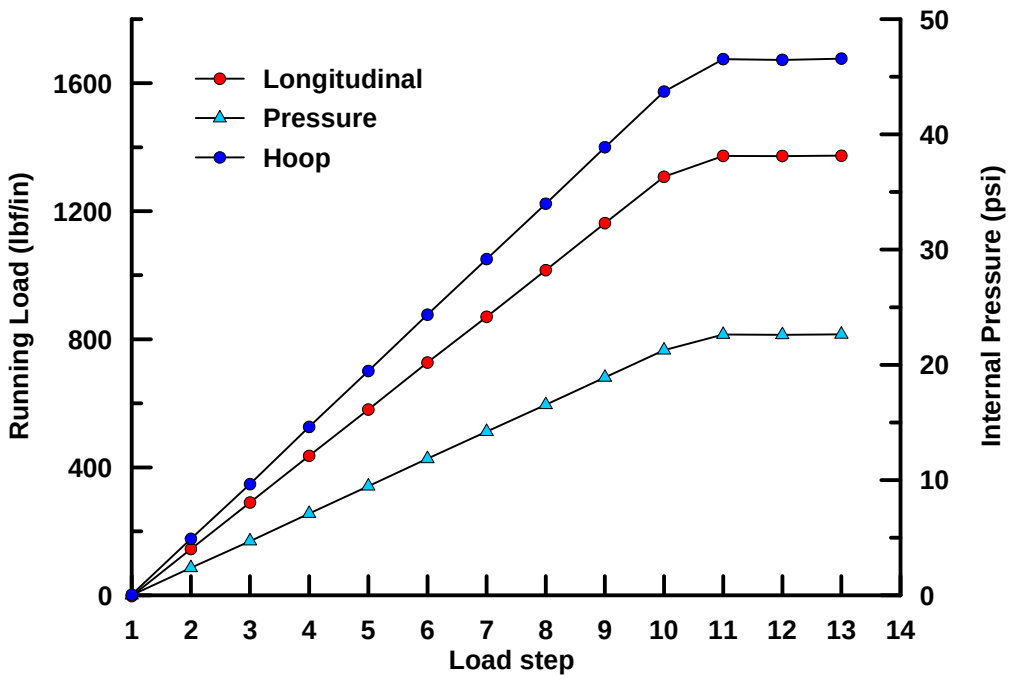

Figure 66. Combined Loading of Panel With Open Hole

The far-field longitudinal and hoop strains were plotted as a function of the applied longitudinal loading, as shown in figures 67 and 68. Similar to the previous loading case, both longitudinal and hoop strains compared well with CLPT predictions for a flat panel.

The variations of longitudinal and hoop strains across the width and length of the panel, at selected load levels are shown in figures 69 and 70. The longitudinal strains are not uniform across the width of the panel, as shown in figure 69. This can be attributed to the edge effects due to the stiffened longitudinal edge and the fact that the load is introduced over a slightly narrower region along the loading edge and has to redistribute itself. Further, the longitudinal strain distribution appears to be asymmetric when compared to the longitudinal loading case discussed in the previous section. The hoop strains increase away form the center of the panel (z=0) and continuously decrease towards the edge of the panel. A clear trend in the distribution exists when compared to the pure longitudinal loading.

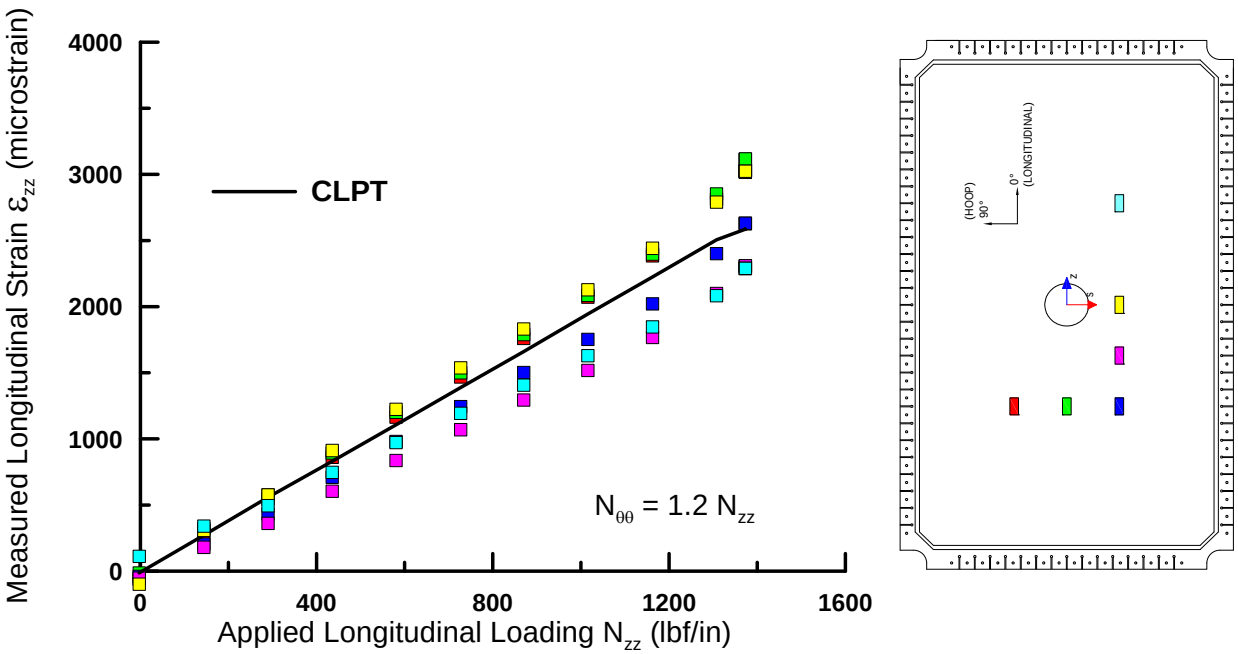

Figure 67. Far-Field Longitudinal Strains Under Combined Loading in Panel CP2

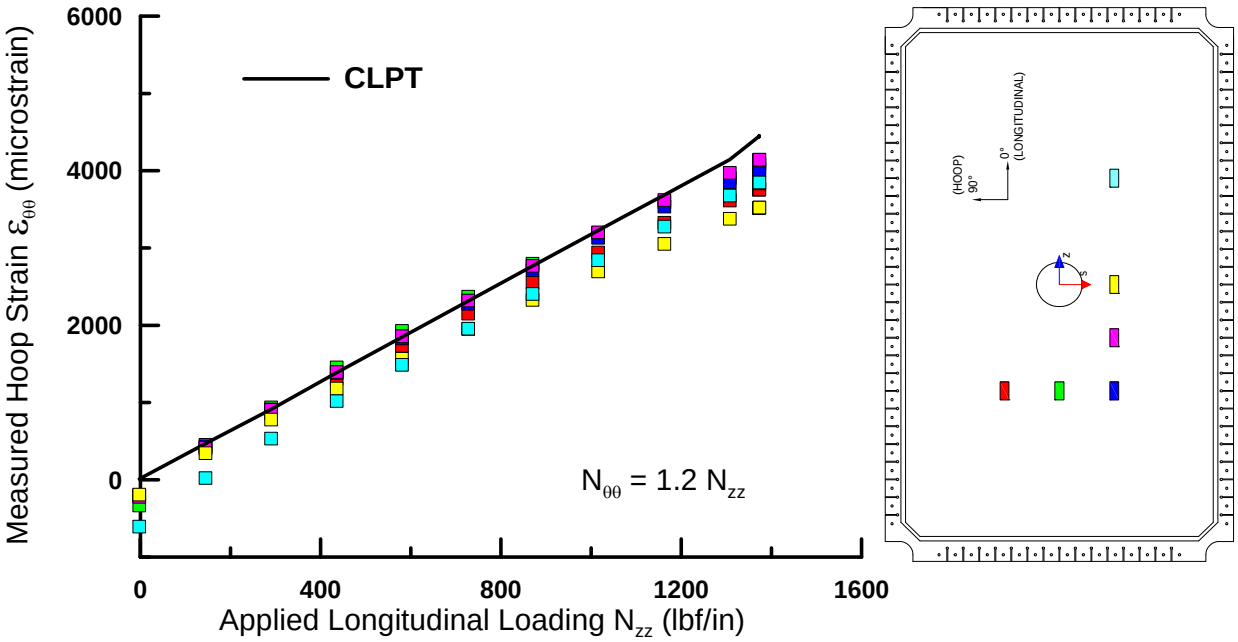

Figure 68. Far-Field Hoop Strains Under Combined Loading in Panel CP2

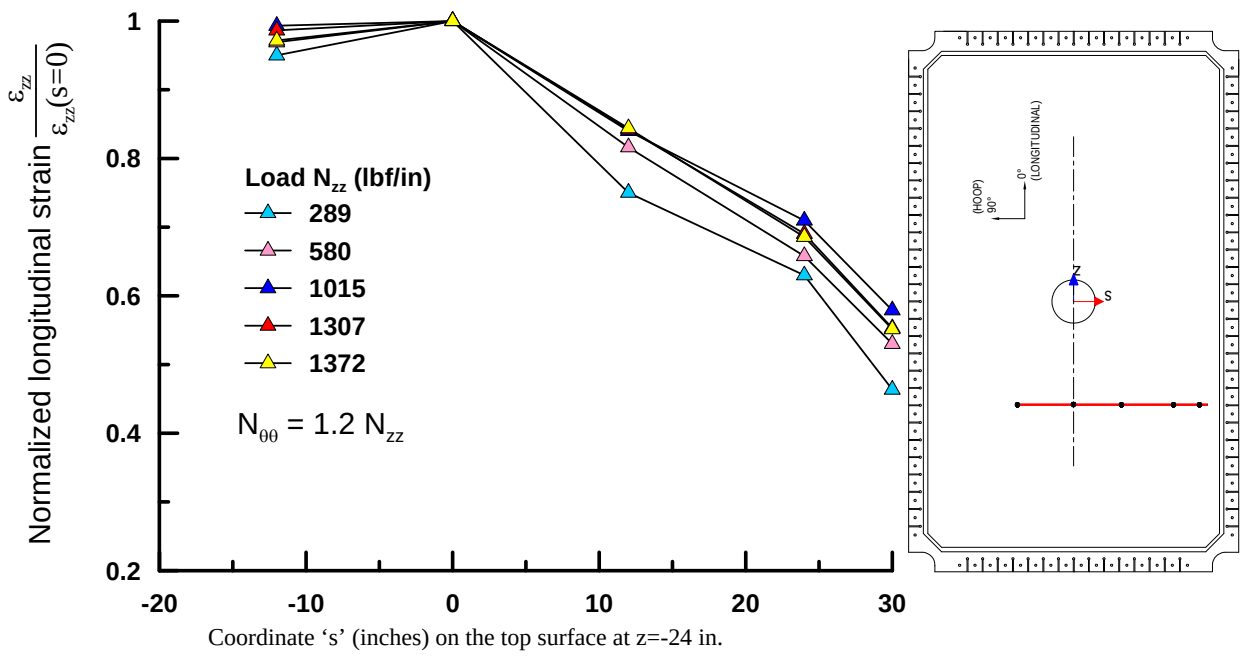

Figure 69. Longitudinal Strain Distribution at z=-24 Inches Under Combined Loading

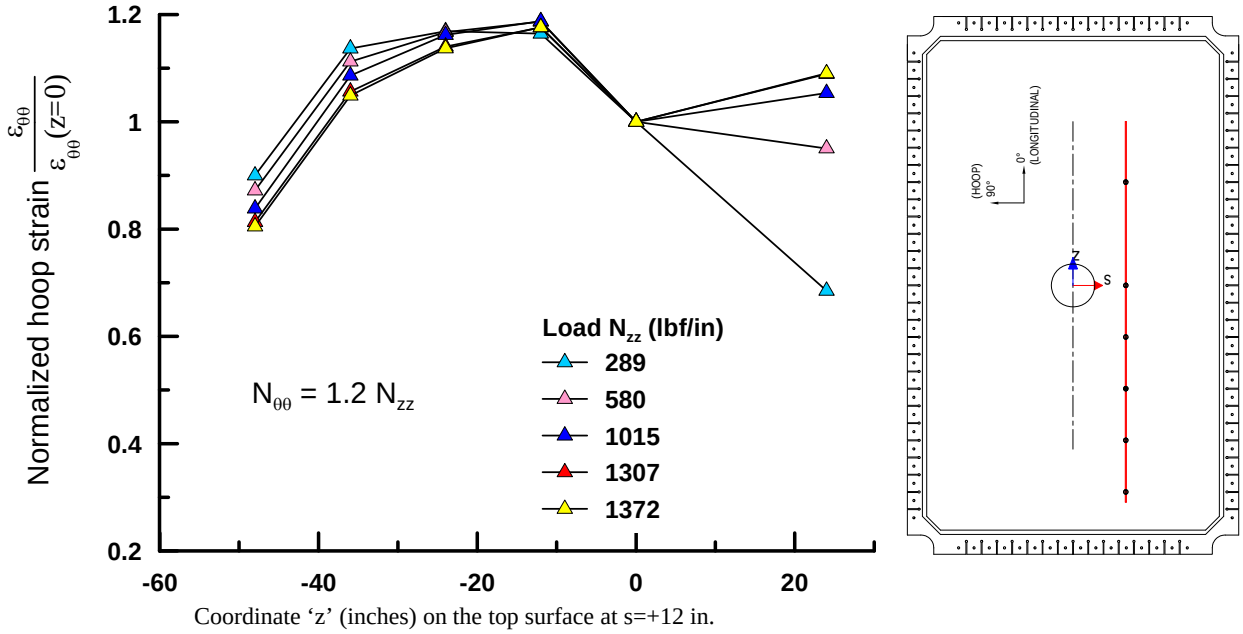

Figure 70. Hoop Strain Distribution at s=+12 Inches Under Combined Loading

The bending of the test panel caused by the presence of the hole and the edge effects due to the stiffened region is presented in figures 71 and 72. The asymmetry in longitudinal strain distribution is further captured by the bending in the r-z plane. Note that some strain gages on the concave/bottom surface were rendered inactive during this test. Thus, bending is evident at only four locations on the panel. Based on the strain gage data, the bending is opposite to the previous loading case in the r-z plane. The bending in the r-z plane was observed to be negative (up to -20%), with the exception of one location, as shown in the figure. The panel bending in the r-θ plane was positive at all locations except on the section (z=0) passing through the hole. The bending deformation closer to the loading edges was observed to be erratic and could be due to the reseating of the panel in the loading arms. The deformation of the panel in the r-θ plane is opposite to that shown in figure 63.

The strains tangential to the hole boundary on the top and bottom facesheet were plotted as a function of the applied longitudinal loads, as shown in figures 73 and 74, respectively. At the maximum applied load of 1373 lbf/in (longitudinal) and 22.7 psi internal pressure, the tangential strains at ϕ=90º and at a distance of 0.25 inch from the boundary, reached about 11,000 $\mu\varepsilon$. This was below the material failure strain presented in table 1. Strain concentration effects can be observed on the top facesheet, with the strain gages nearest to the hole boundary indicating higher strain levels when compared to gages further away from the boundary. The tangential strains (A and B in the figure) at ϕ=0º, were identical, and lower than the tangential strains (E and F in the figure) at ϕ=45º. The far-field strain data along hoop and longitudinal directions are plotted and shown in the same figure to obtain a measure of strain concentration near the hole.

Similar to the previous loading case, on the bottom facesheet, the strain distributions were markedly different from that on the top facesheet. The difference between the strains at a distance of 0.25 inch and 0.75 inch was marginal at ϕ=90º. At ϕ=0º and ϕ=45º, the strains at a distance of 0.75 inch were higher than those at a distance of 0.25 inch. This is attributed to more load being carried in the bottom skin due to the hole in the upper skin.

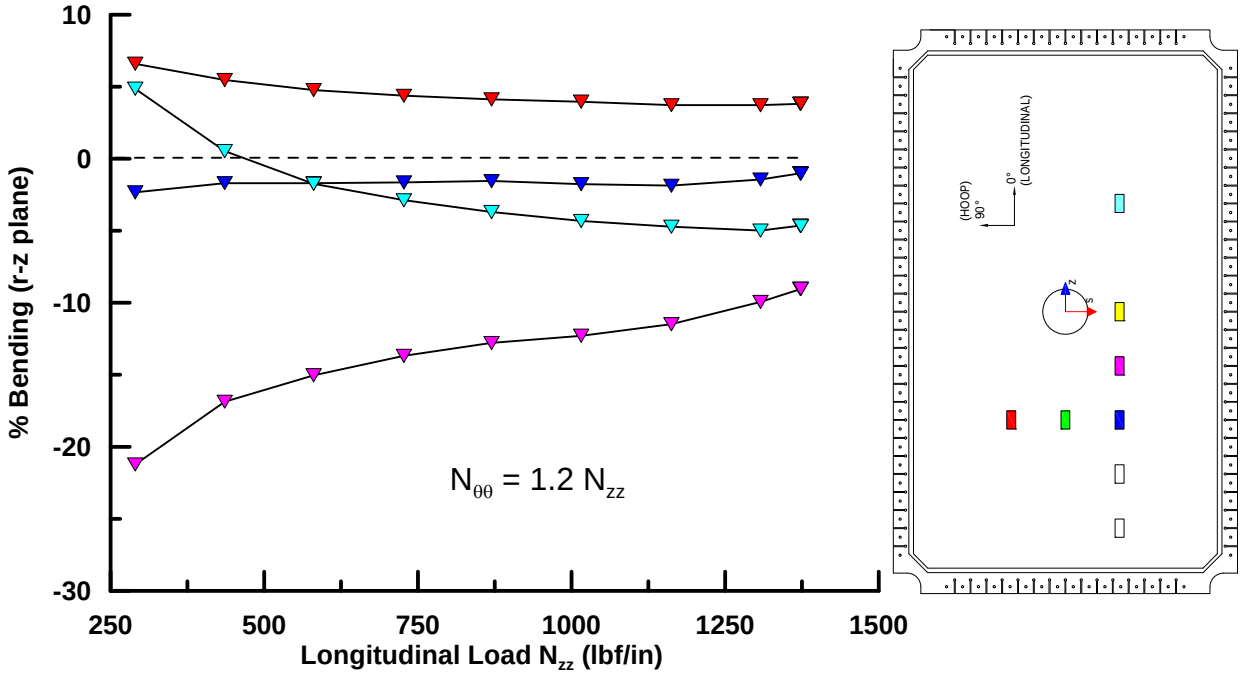

Figure 71. Bending of Test Panel in the r-z Plane Under Combined Loading

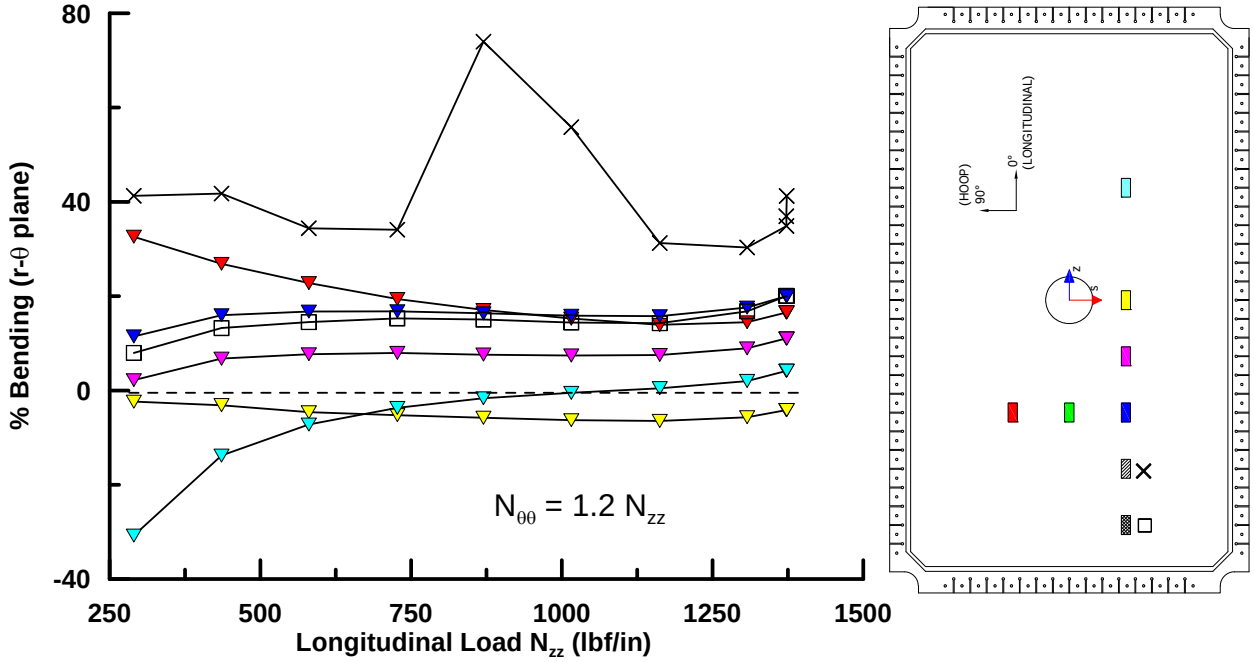

Figure 72. Bending of Test Panel in the r-θ Plane Under Combined Loading

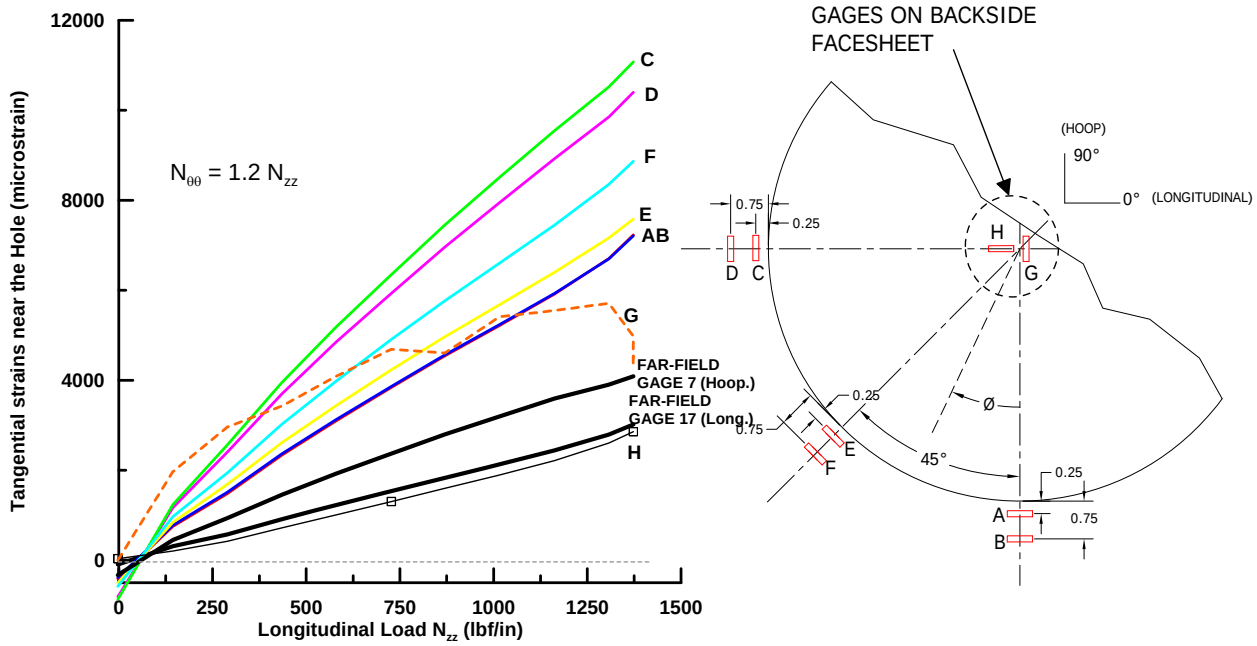

Figure 73. Tangential Strains Near the Hole Boundary on the Top Facesheet

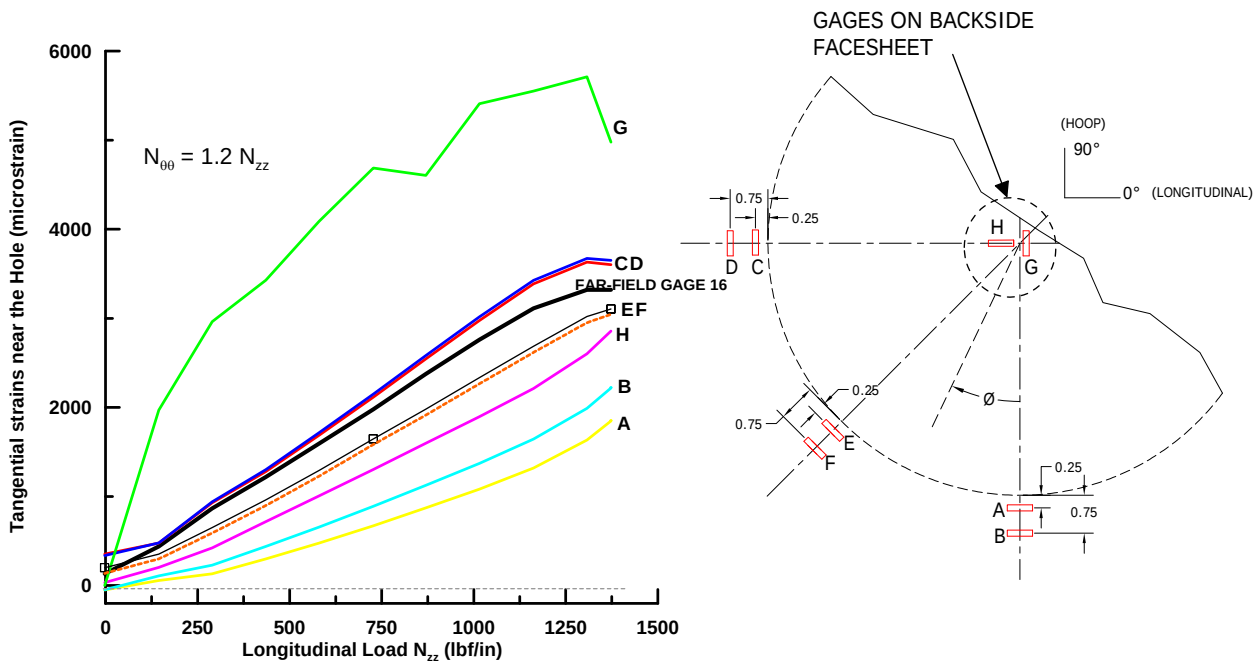

Figure 74. Tangential Strains Near the Hole Boundary on the Bottom Facesheet

5.4.3 Pressurization Loading.

Since the panel could not be loaded to failure under pure longitudinal loading nor under combined longitudinal and hoop loading due to constraints on the test apparatus, the panel was subjected to pure pressurization loading. At a maximum internal pressure of 21.4 psi

(1570 lbf/in hoop load), failure in the form of a crack was initiated at the hole boundary, as shown in figure 75. Also, the failure could not be propagated due to constraints on the test apparatus.

The tangential strains close to the hole boundary were much higher than the previous two load cases. The tangential strains near the hole boundary were plotted as a function of hoop load, as shown in figure 76. The gages along the loading direction indicate strain levels close to the material failure strain.

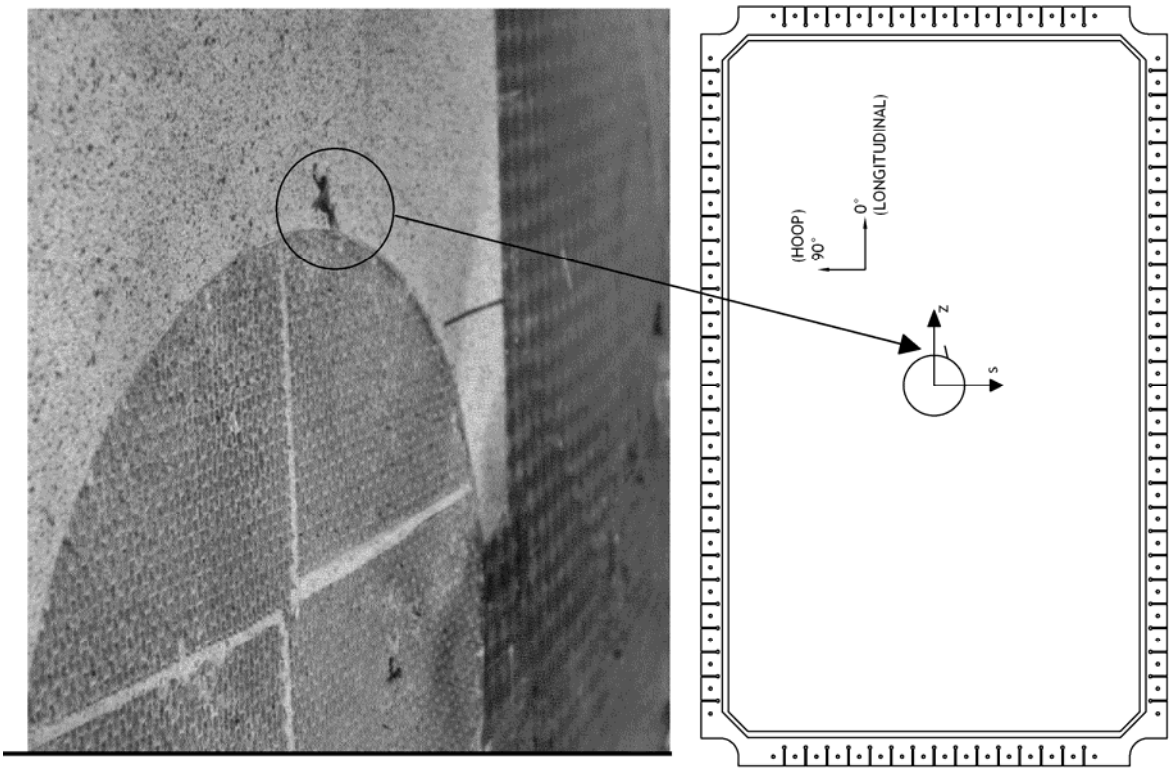

Figure 75. Observed Crack at Hole Boundary Under Pressurization Loading

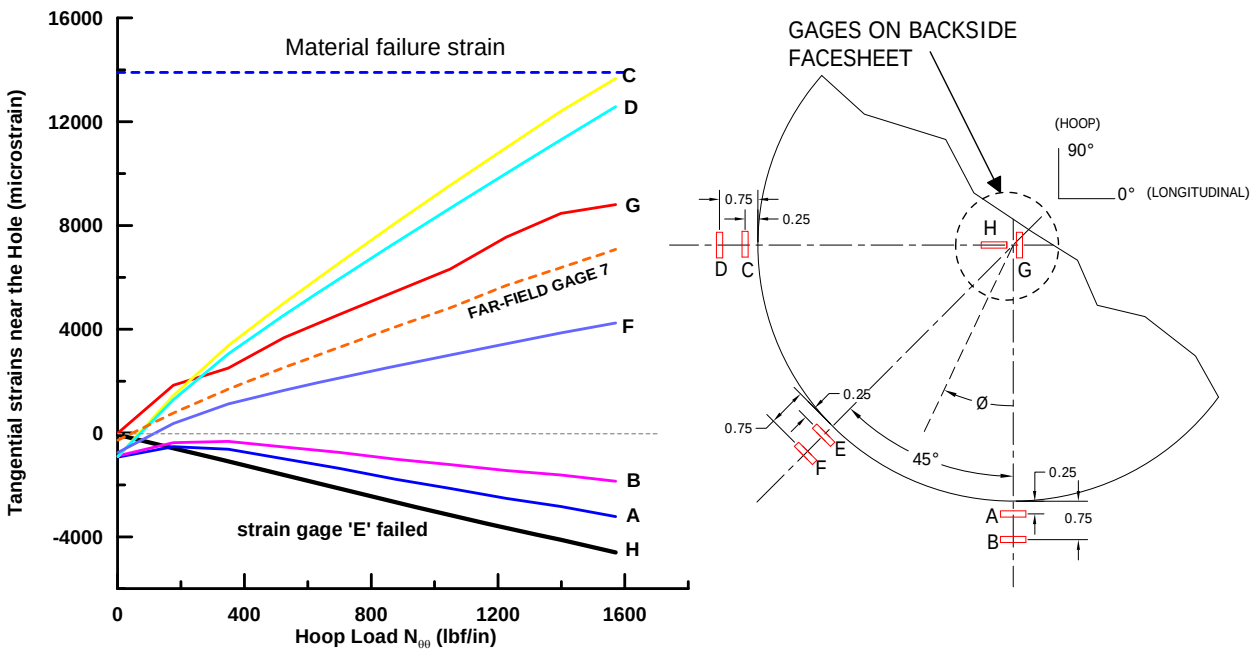

Figure 76. Tangential Strains Near the Hole Boundary on the Top Facesheet Under Pressurization Loading

5.5 TEST PANEL CP3.

The test panel CP3 consisted of a 10-inch circumferential notch with a 0.25-inch notch radius. The test panel was subjected to combined loading, which resembles the loading experienced by a typical pressurized aircraft. The planned loading sequence and the loads recorded during the actual test are shown in figures 77 and 78, respectively. An internal pressure of 8 psi was applied in a quasi-static manner, and the pressure was held at this value for the remainder of the test. Upon reaching an internal pressure of 8 psi, the longitudinal load was increased in a stepwise manner until failure resulted. The panel CP3 failed at a maximum longitudinal load of 1223 lbf/in. The fracture was initiated at the notch root and propagated across the width of the panel resulting in total failure.

Even though the loading indicates that the internal pressure was applied uniformly over the internal surface of the panel, the loading at the notch was not uniform. To contain the pressurizing medium (water), the notch had to be sealed appropriately. Panels that contained through-thickness damage required a seal to be installed on the interior (concave) facesheet to contain the pressurizing medium during tests involving the application of hoop loads and pressurization. A thin, hard plastic sheet was bonded directly to the panel using PR-1422 Class B aircraft fuel tank sealant [13]. The width of the bonded area between the hard plastic sheet and the panel was approximately 2″. The hard plastic layer served to stop the seal from bulging through the through-thickness damage openings. The next layer of the patch was a thin rubber sheet, approximately 20″ by 10″, bonded to the panel and hard plastic sheet by PR-1422 Class B aircraft fuel tank sealant. RTV silicone sealant was applied along the edges of each rubber seal to prevent water ingression under the patch [13]. Thus, a pure normal surface traction condition

does not exist around the notch. The stiffness of the hard plastic layer dictates the load distribution in the vicinity of the notch and is indeterminate in the current study.

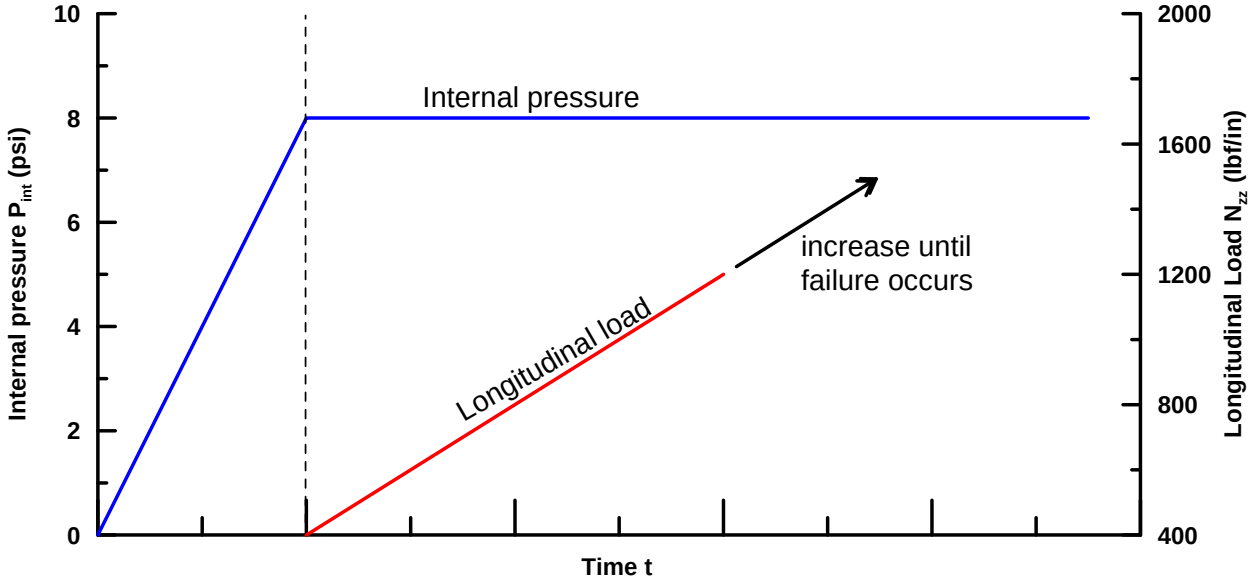

Figure 77. Planned Loading Sequence for Test Panel CP3

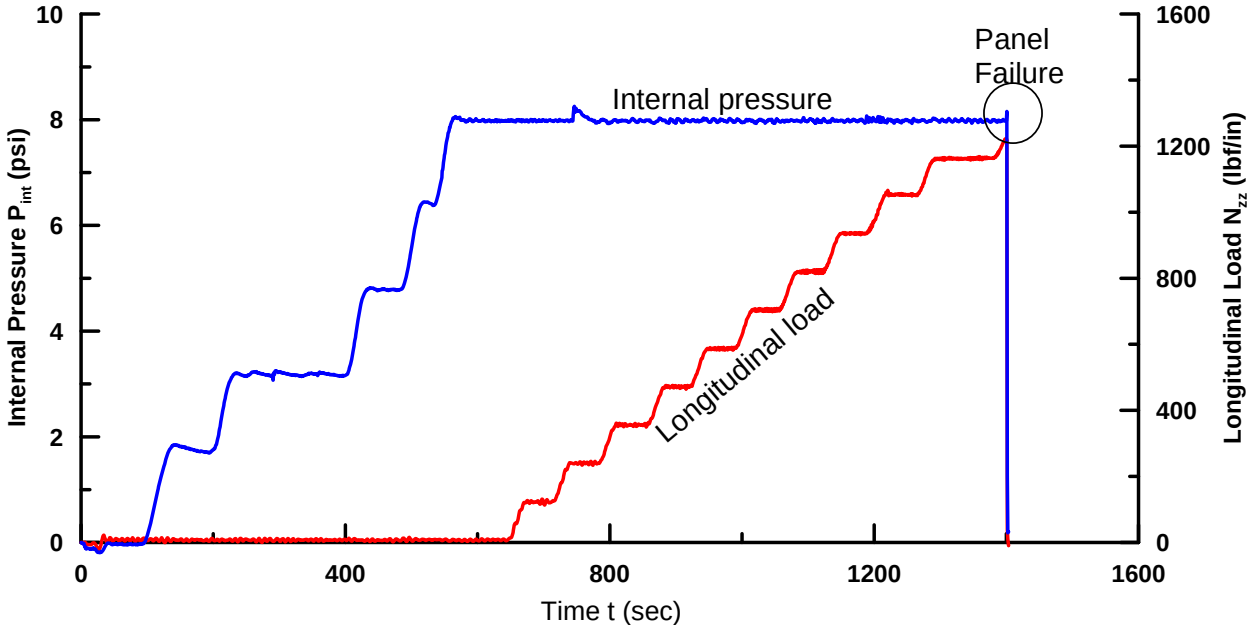

Figure 78. Applied Loading Sequence for Test Panel CP3

The far-field longitudinal and hoop strains recorded during the tests were plotted as a function of test duration, as shown in figures 79 and 80. The strains compare satisfactorily with the CLPT values (for a flat panel) during the initial pressurization stage. However, upon application of longitudinal loads, the magnitude of the strains (longitudinal and hoop) were consistently lower than the CLPT values. The distribution of hoop and longitudinal strains were similar to that of the unnotched panel under combined loading but are not presented in this section for brevity.

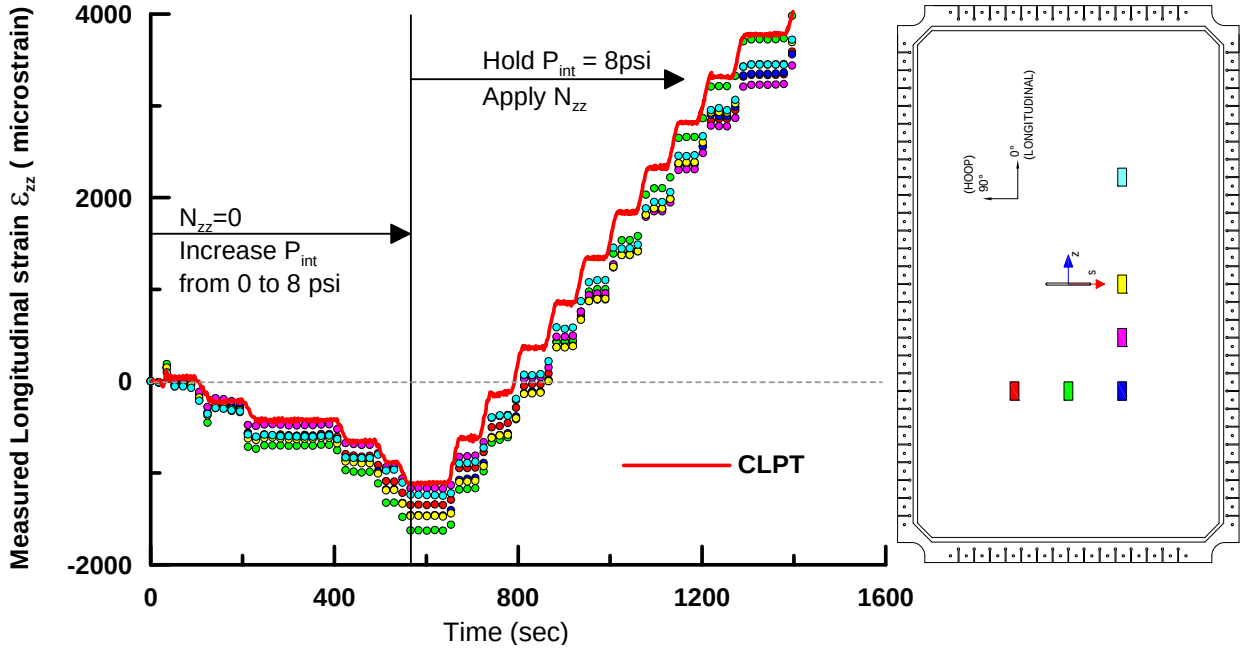

Figure 79. Far-Field Longitudinal Strains in Panel CP3

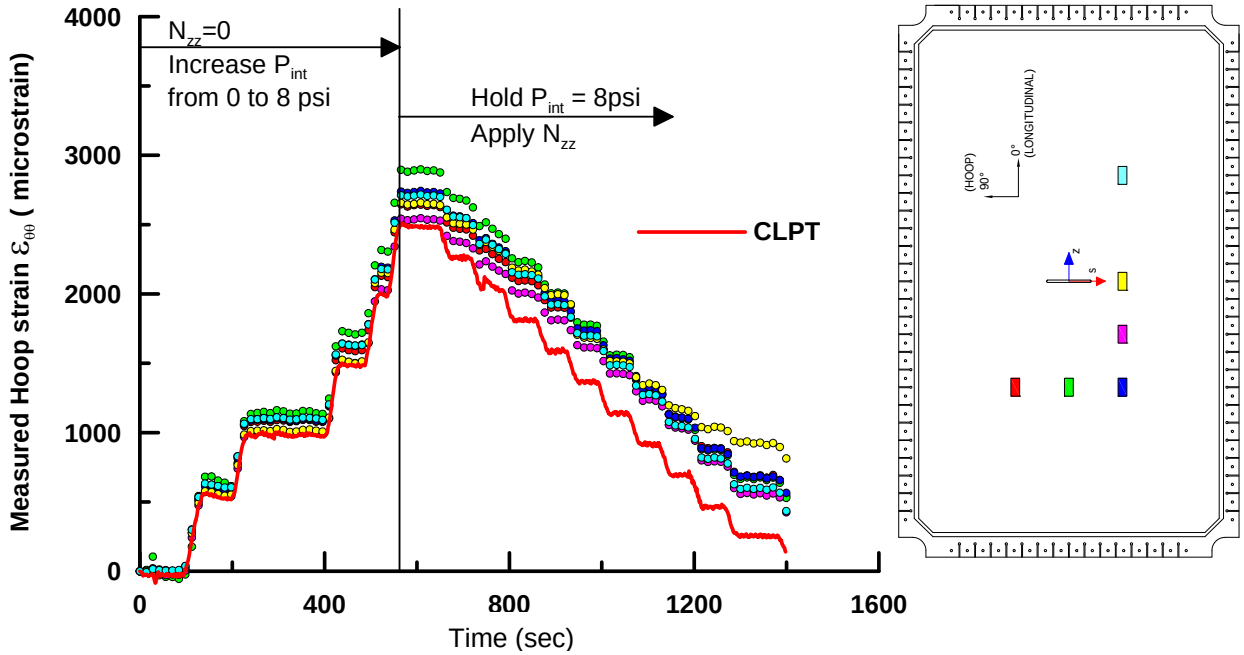

Figure 80. Far-Field Hoop Strains in Panel CP3

The longitudinal strains (back-to-back) in the vicinity of the notch were plotted as a function of the longitudinal load, as shown in figure 81. The strain gage data provides critical information of the failure initiation and propagation in the panel. Based on the strain gage at a distance of 0.25 inch from the notch root, the failure was initiated in the panel at a longitudinal load of 970 lbf/in. This is captured by the sudden drop in the strain value (curve A in the figure). This drop in strain occurs when the fracture occurs above or below the strain gage, thereby relieving the strains locally. However, the strain gage C indicates a sudden spike which occurs when the fracture path passes through the strain gage and severing it in the process. Thus, at the load level of 970 lbf/in, the fracture has progressed at least 0.75 inch from the notch root. A similar observation can be made about the strain gages on the interior/backside (concave) surface. Interestingly, the strain levels on the interior were observed to be consistently lower than those on the outer surface and can be attributed to the bending of the panel. The final failure of the panel occurred at a longitudinal load of 1223 lbf/in, when the panel fractured into two halves.

One half of the panel was returned to WSU for failure mode inspection and analysis. The fracture path was mapped on the geometry of the test panel, as shown in figure 82. The fracture path was observed to follow the critical section for about 2 to 3 inches from the notch root and then, deviated considerably, as shown in figure 82. The close-up of the area near the notch indicates that the failure is distributed over a region on either side of the fracture path.

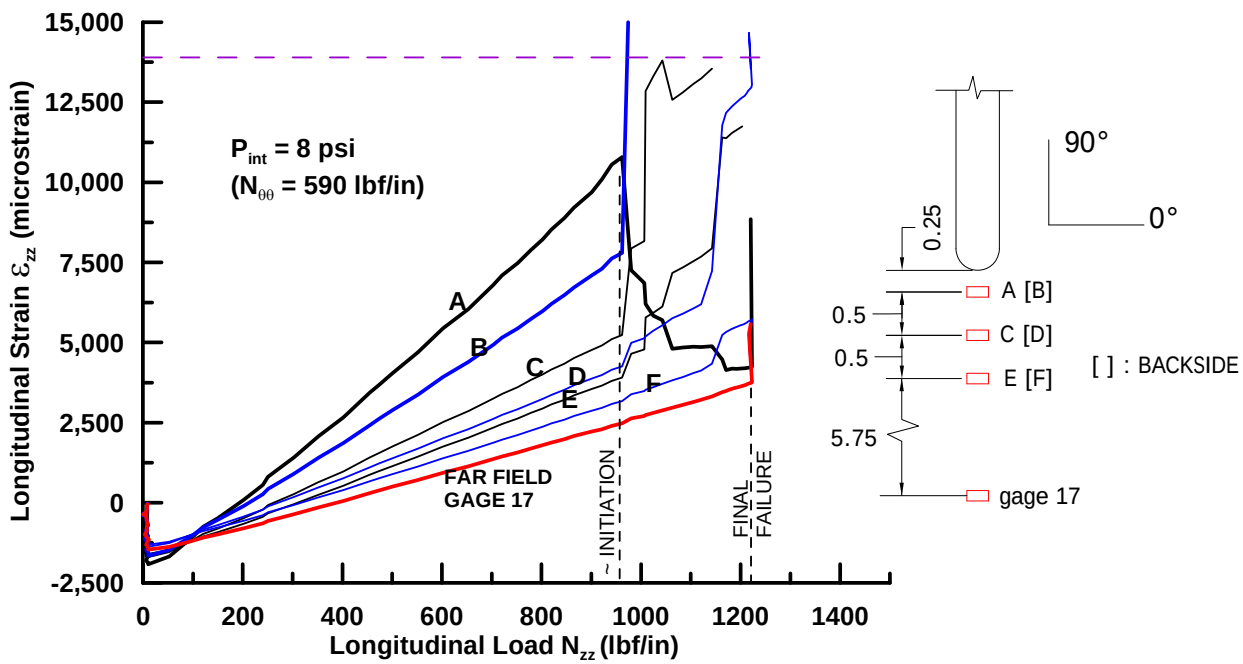

Figure 81. Strains in the Vicinity of the Notch in Panel CP3

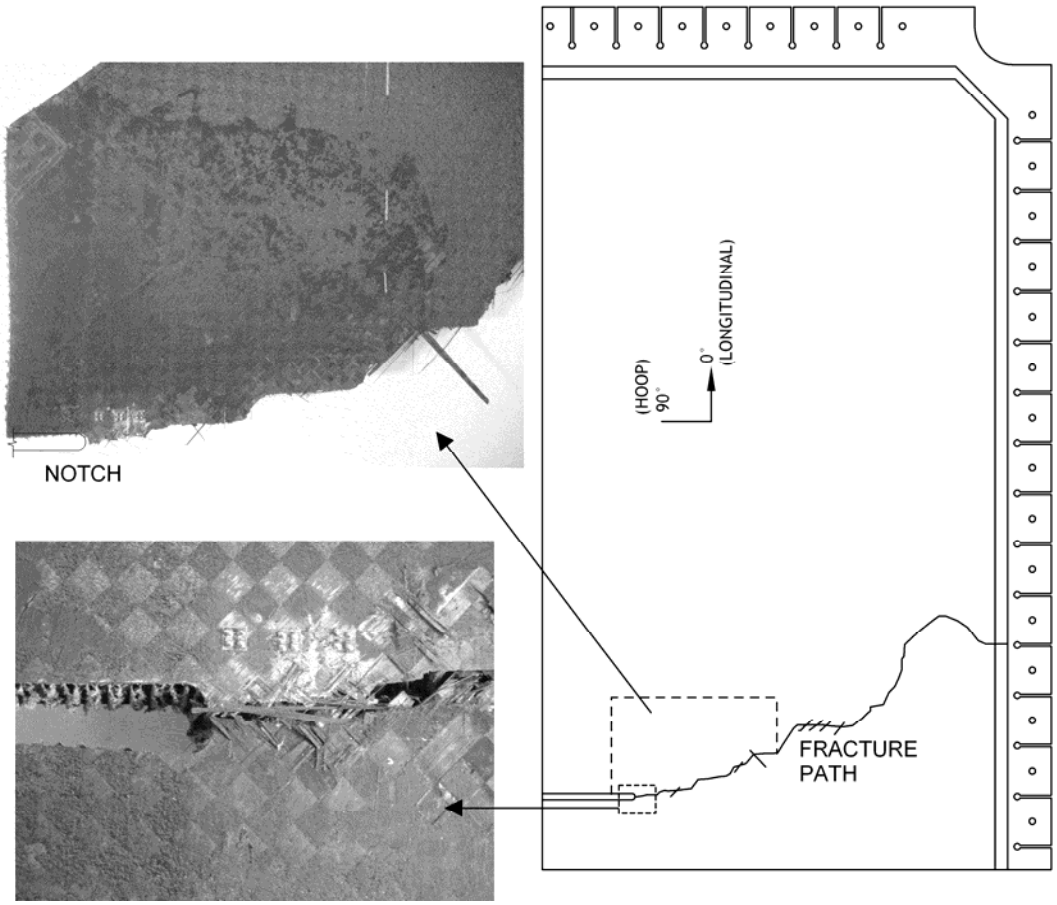

Figure 82. Picture of Observed Failure Mode in One-Half of Panel CP3

5.6 TEST PANEL CP4.

The test panel CP4 consisted of a 10-inch circumferential notch with a 0.25-inch notch radius. The test panel was subjected to longitudinal loading along with a constant internal pressure of 1 psi. The internal pressure was intended to stabilize the panel in the fixture and to produce longitudinal strains symmetric to s=0 (as observed in previous tests). The planned loading sequence and the loads recorded during the actual test are shown in figures 83 and 84, respectively. An internal pressure of 1 psi was applied in a quasi-static manner, and the pressure was held at his value for the remainder of the test. Upon reaching an internal pressure of 1 psi, the longitudinal load was increased in a stepwise manner until failure of the panel resulted. Unlike the previous test, several low-amplitude cycles were applied at selected load steps. These load steps were intended for calibration of nondestructive acoustic emission devices reported in reference 13. The test panel was subjected to a maximum longitudinal load of 1225 lbf/in, at which point additional longitudinal deformation of the test panel could not be accommodated by the test fixture, and the test was stopped.

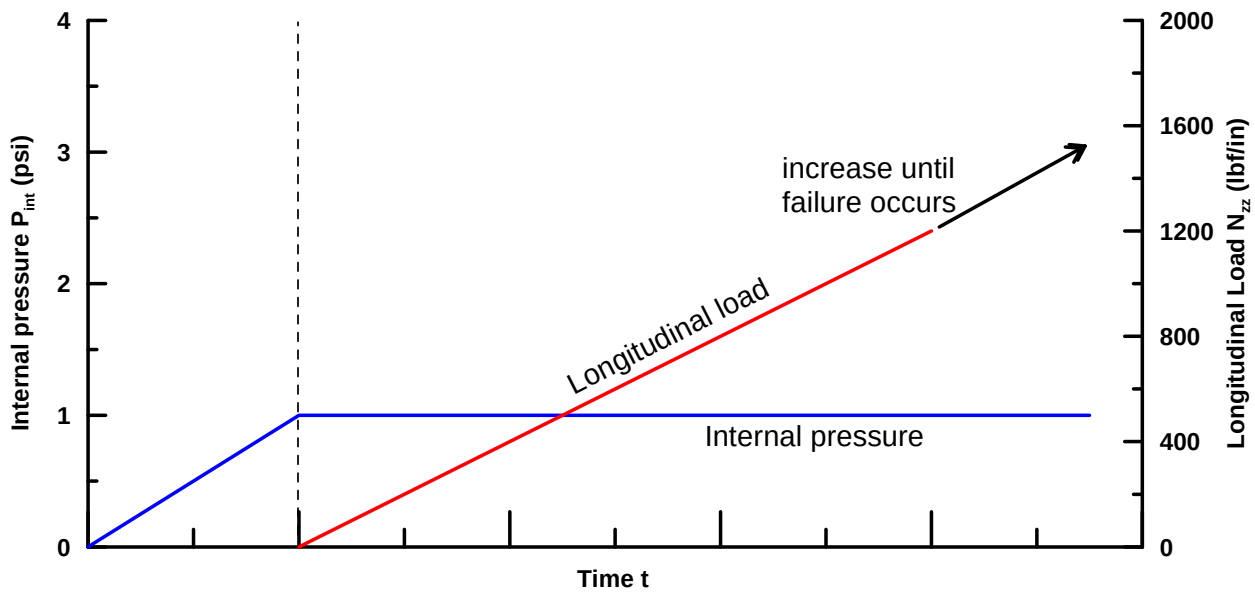

Figure 83. Planned Loading Sequence for Test Panel CP4

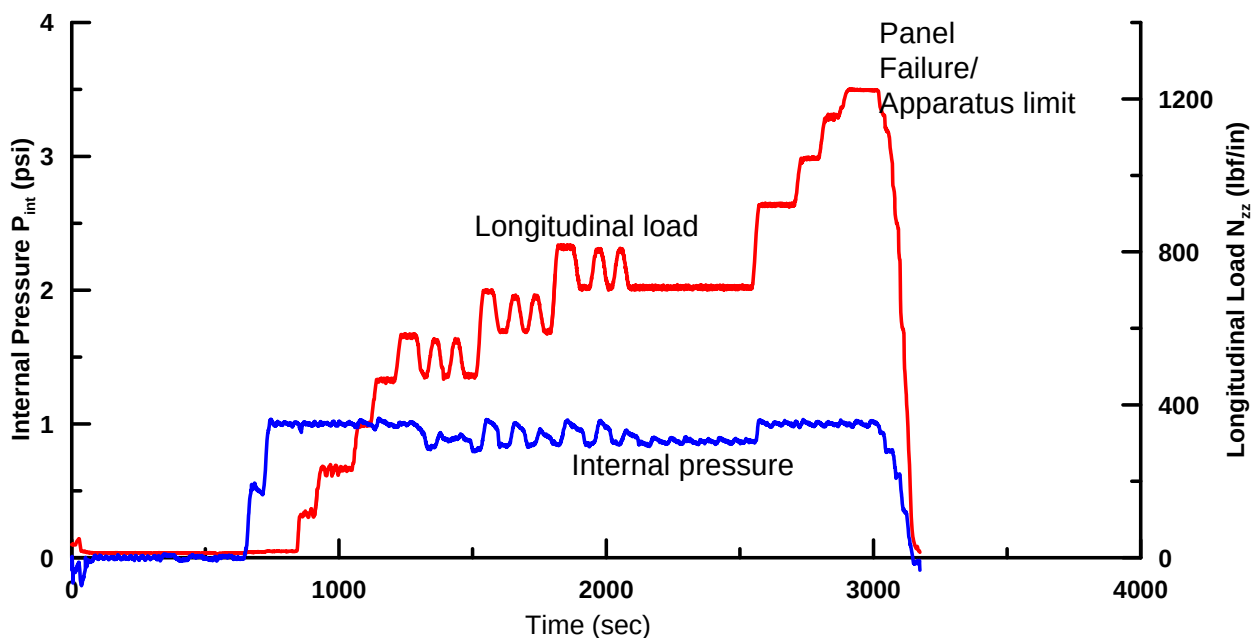

Figure 84. Applied Loading Sequence for Test Panel CP4

The far-field longitudinal and hoop strains recorded during the tests were plotted as a function of test duration, as shown in figures 85 and 86. The longitudinal strains compare reasonably with CLPT predictions, whereas the hoop strains were significantly lower (in magnitude) that the CLPT values. This can be attributed to the edge effects resulting from the stiffened longitudinal edge and the bending of the panel.

The longitudinal strains (back-to-back) in the vicinity of the notch were plotted as a function of the longitudinal load, as shown in figure 87. The strain-load loops corresponding to low-amplitude cycles are identified in the figure. It is interesting to note that these curves do not coincide with the original curve, indicating the presence of a dissipative process. This could indicate the formation of damage ahead of the strain gage. The strain gage data provides critical information of the failure initiation and propagation in the panel. Based on the strain gage at a distance of 0.25 inch from the notch root, the failure initiated in the panel at a longitudinal load of 780 lbf/in. This is captured by the spike in the strain value (curve A in the figure). The corresponding strain spike in the bottom surface is slightly delayed and may be attributed to bending of the panel in the r-z plane. The strains on the bottom facesheet were consistently lower than those of the top facesheet, which is indicative of panel bending. The test was stopped at a longitudinal load of 1220 lbf/in due to constraints on the apparatus.

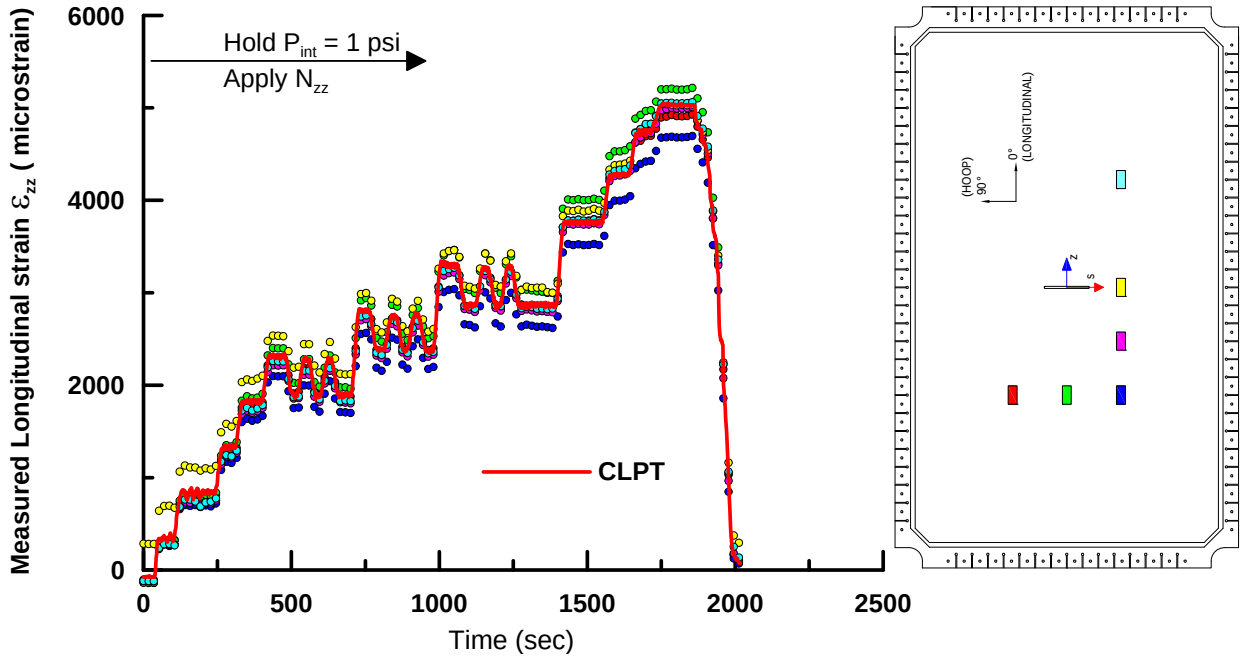

Figure 85. Far-Field Longitudinal Strains in Panel CP4

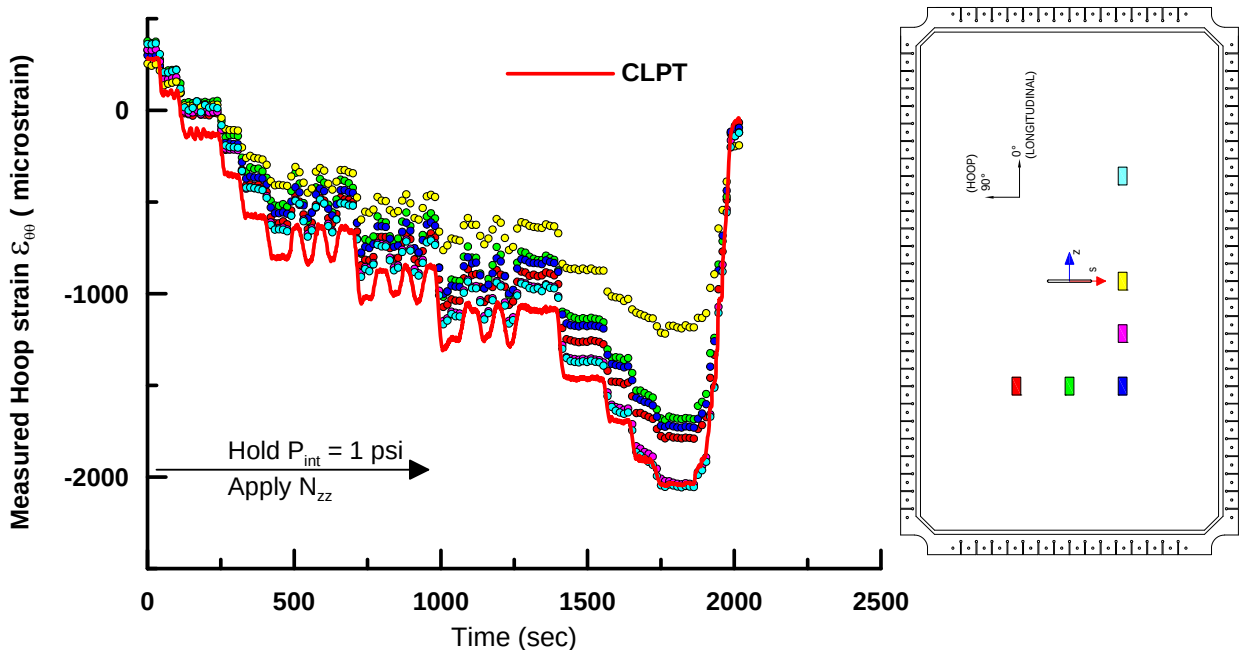

Figure 86. Far-Field Hoop Strains in Panel CP4

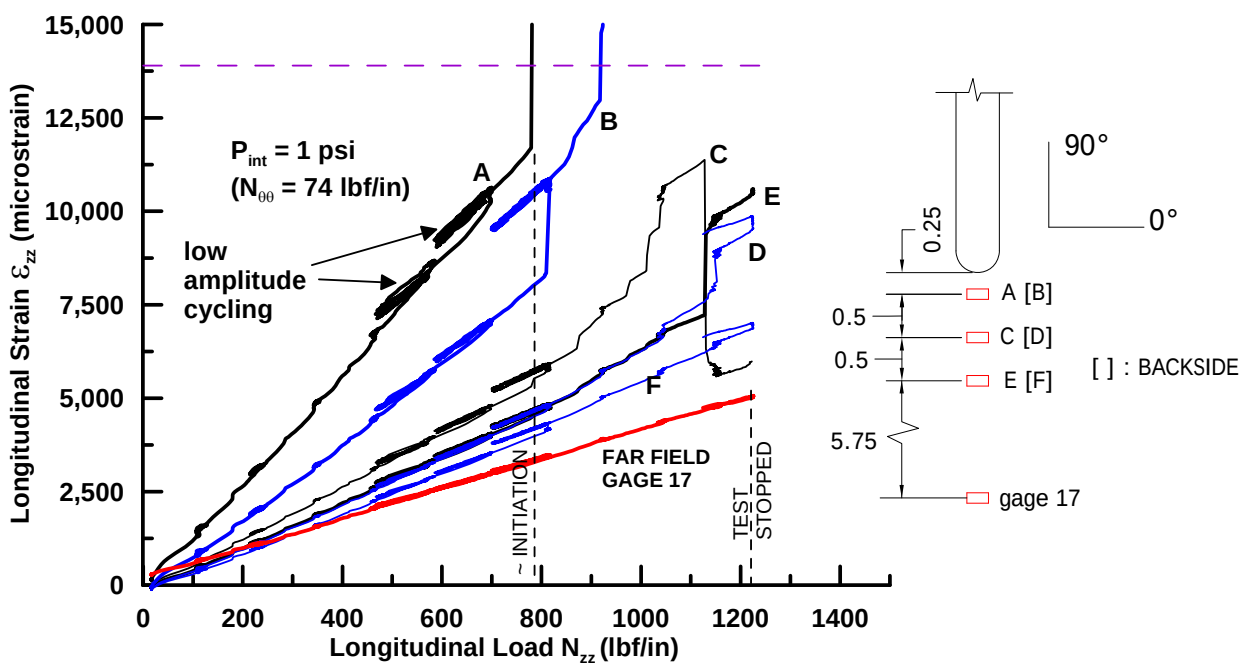

Figure 87. Strains in the Vicinity of the Notch in Panel CP4

5.7 TEST PANEL CP5.

The test panel CP5 consisted of a 10-inch longitudinal notch of length with a 0.25-inch notch radius. Due to the formation of delaminations on the interior (concave) surface over a large area encompassing the center of the panel, the panel had to be repaired, as shown in figure 88. The

repair patch had the same stacking sequence as the test section of the panel. The notch location was offset longitudinally to avoid the effects of scarf region on the stress distribution close to the notch.

The test panel was subjected to pressurization/hoop loading along with a constant longitudinal load of approximately 100 lbf/in. The longitudinal load was intended to stabilize the panel in the fixture and to produce hoop strains symmetric about s=0 (as observed in previous tests). The applied loading sequence during the test are illustrated in figure 89. Similar to the previous test, at selected load levels, low amplitude cycling was conducted for calibrating the nondestructive acoustic emission inspection devices [13]. The test panel fractured at an internal pressure of 13.5 psi (1000 lbf/in hoop load).

The variation of far-field longitudinal and hoop strains on the top surface were plotted as a function of test duration, as shown in figures 90 and 91, respectively. The strains do not compare well with the CLPT strains (for a flat panel) and may be attributed to the panel bending, edge effects, and the presence of a large repair patch.

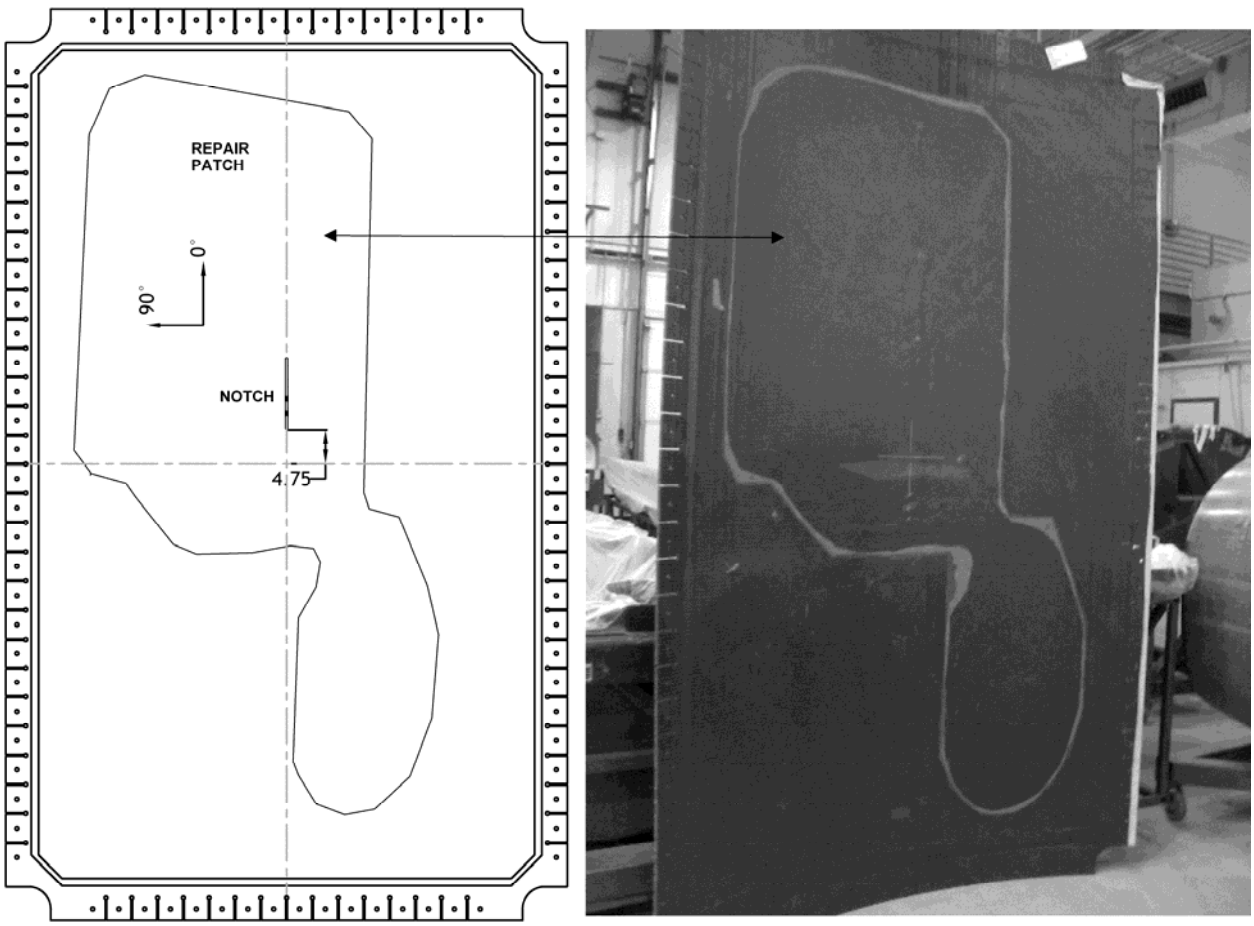

Figure 88. Repair Patch on the Interior (Concave) Side of Panel CP5

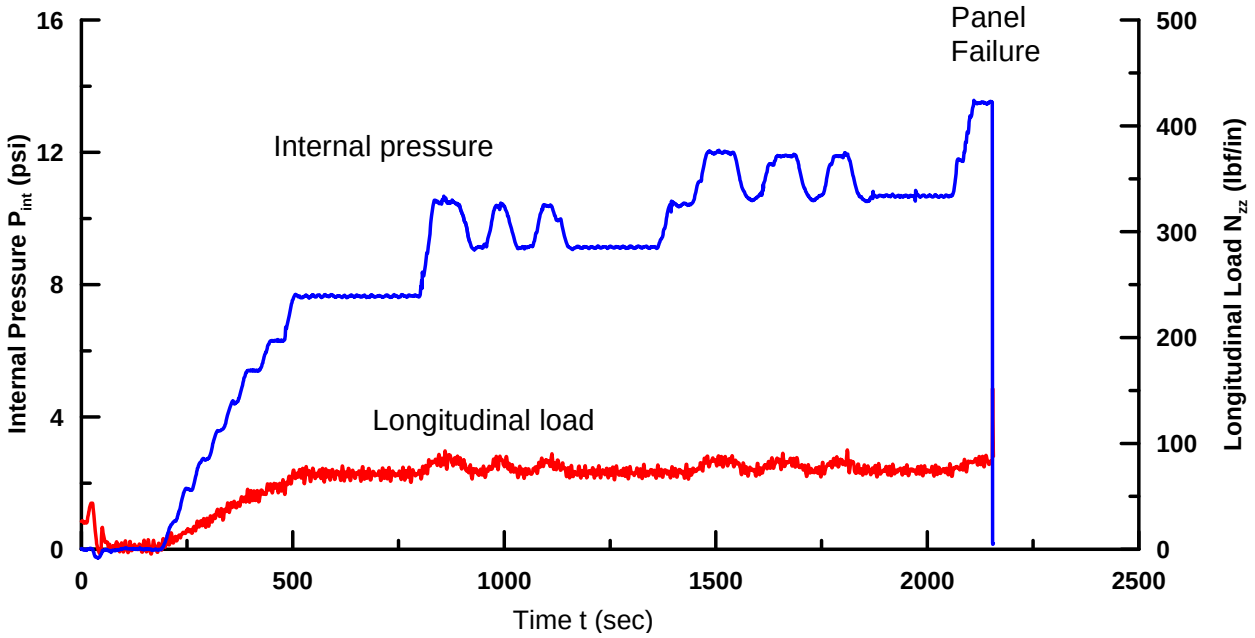

Figure 89. Applied Loading Sequence for Test Panel CP5

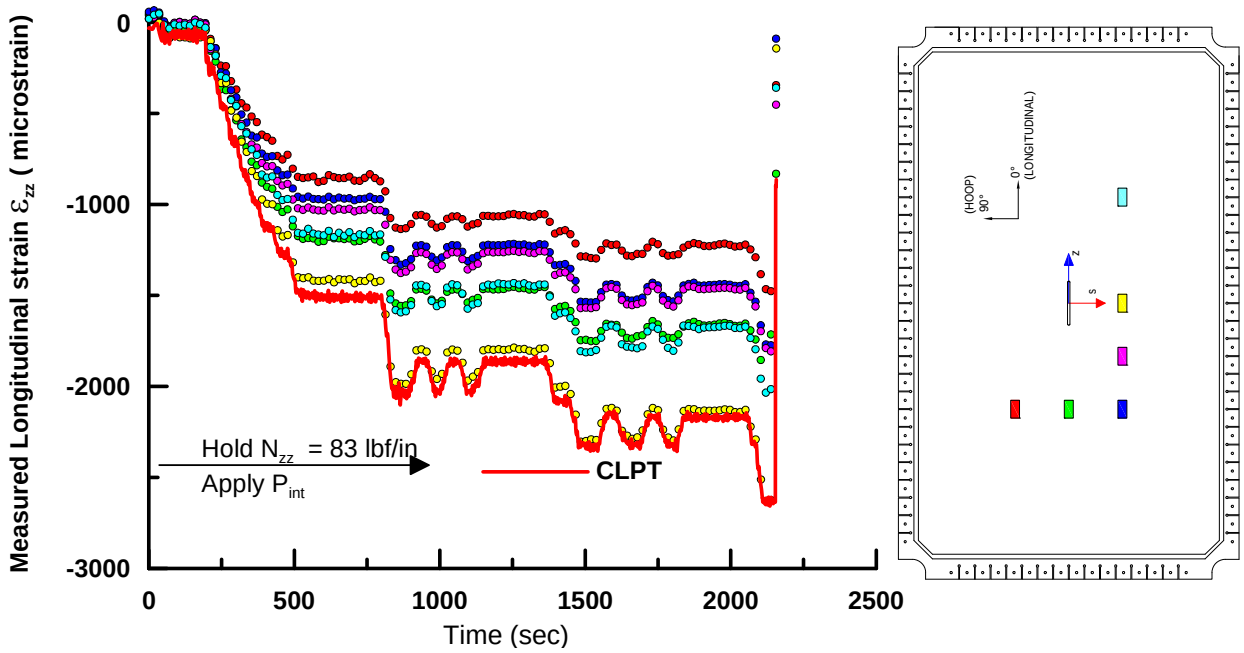

Figure 90. Far-Field Longitudinal Strains in Panel CP5

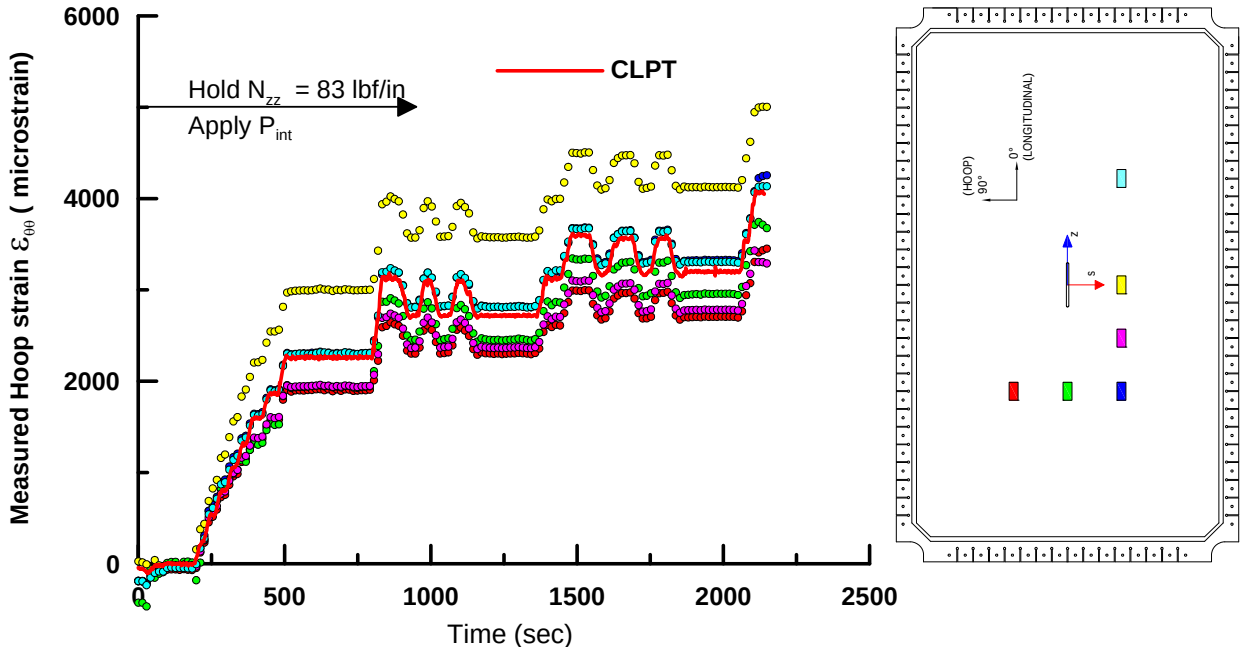

Figure 91. Far-Field Hoop Strains in Panel CP5

The hoop strains in the vicinity of the notch, on the top and bottom facesheets, were plotted as a function of the hoop load, as shown in figures 92 and 93, respectively. Both plots contain strains on the opposite facesheets for comparison. The strain levels on the bottom facesheets were consistently higher than those of the top facesheet. This was expected, as the tangential strains in a cylindrical panel subjected to internal pressure will be maximum on the inner surface [14]. Based on the strain gages at a distance of 0.25 inch from the notch, failure was initiated at a hoop load of 760 lbf/in (10.2 psi internal pressure). Sudden jumps in strain values are evident on the bottom facesheet (curves D and F) indicating propagation of damage. However, on the top facesheet, the gages C and E do not exhibit similar behavior indicating that the fracture propagation in the top facesheet was delayed. In addition, it may be observed that the low amplitude cycles were applied after the initiation of fracture in the bottom facesheet. Upon reaching a hoop load of 1000 lbf/in (13.5 psi internal pressure), the panel fractured in half longitudinally (s=0).

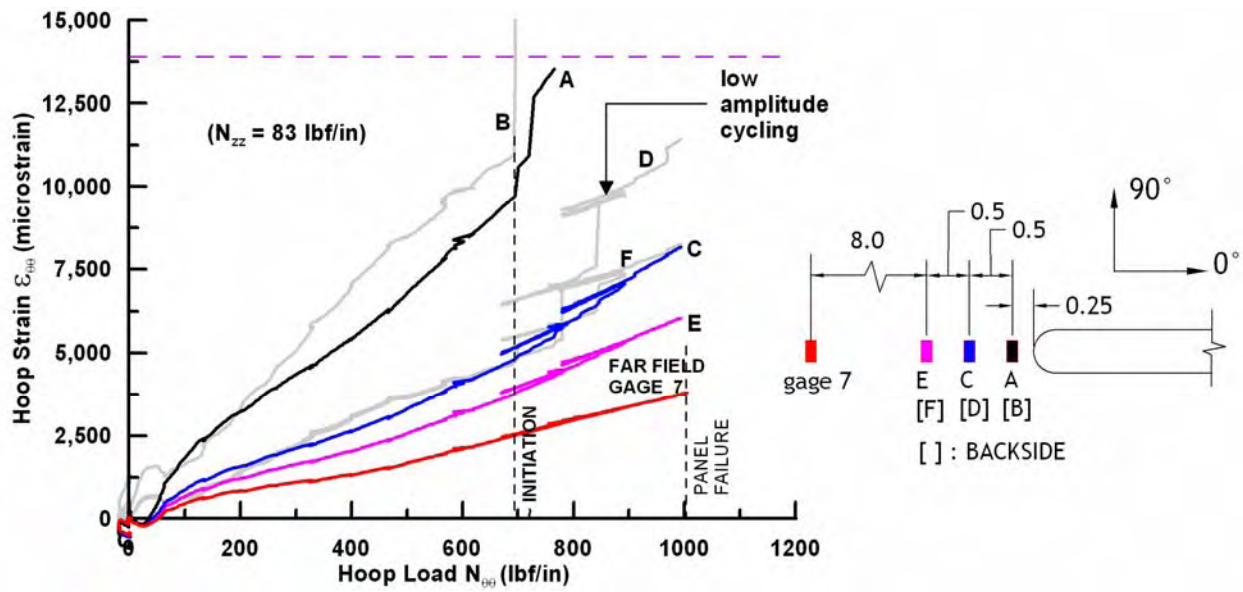

Figure 92. Hoop Strains in the Vicinity of the Notch on the Top (Convex) Facesheet

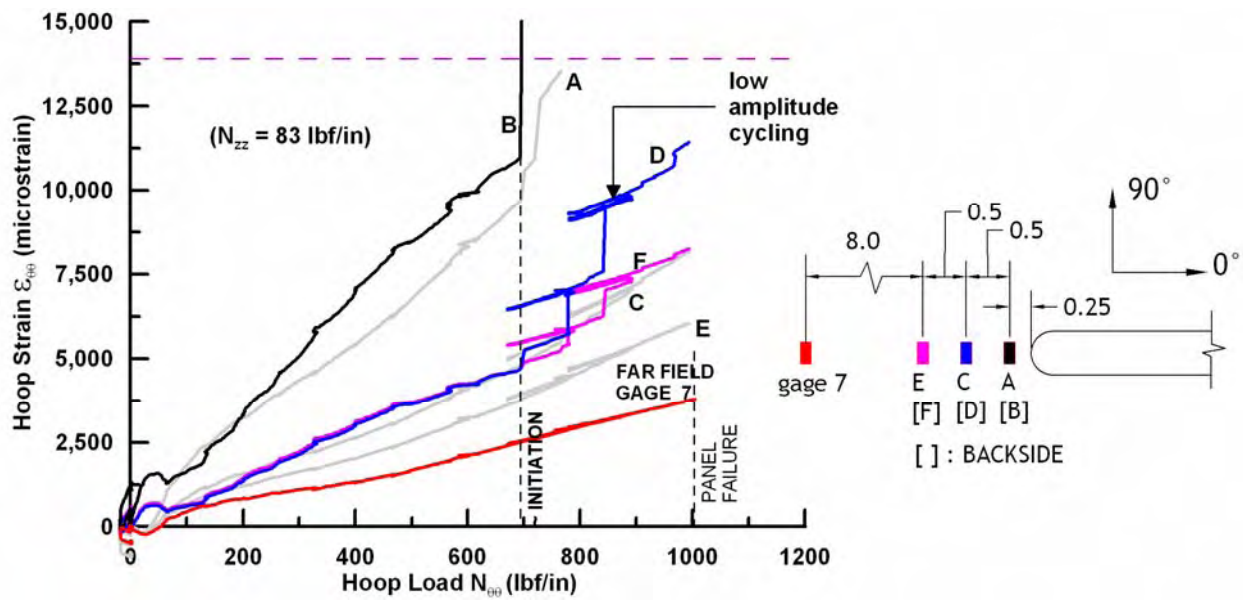

Figure 93. Hoop Strains in the Vicinity of the Notch on the Bottom (Concave) Facesheet

5.8 TEST PANEL CP6.

Test panel CP6 consisted of a 10-inch-long through-the-thickness (both facesheets) inclined/off-axis notch with a 0.25-inch notch radius. The test panel was subjected to combined loading, where the longitudinal load and internal pressure were increased proportionately, as shown in figure 94. The applied load produced a hoop to longitudinal load ratio of 1:2. The test panel fractured when the longitudinal load and internal pressure reached 1153 lbf/in and 18.3 psi, respectively.

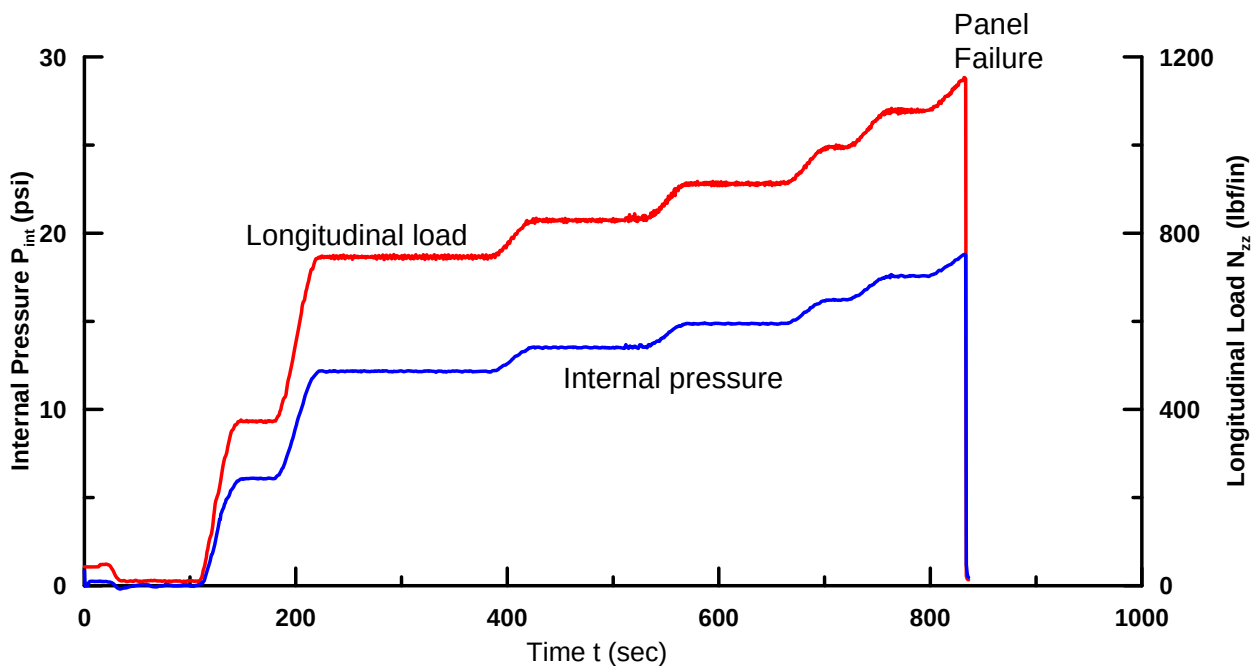

Figure 94. Applied Loading Sequence for Test Panel CP6

The far-field longitudinal and hoop strains recorded during the test were plotted as a function of the test duration, as shown in figures 95 and 96, respectively. The hoop strains compare reasonably well with the CLPT strains, while significant differences can be observed between the measured longitudinal strains and corresponding CLPT values. This may be attributed to the combined effects of the edge effects and asymmetry in the test article due to the orientation of the notch.

The strains in the vicinity of the notch were measured along three directions, which include the longitudinal, hoop, and a direction (N) perpendicular to the length of the notch. The strain components perpendicular to the length of the notch ε_{NN}, on the top and bottom facesheets, were plotted, in figures 97 and 98, respectively. Based on the strains (ε_{NN}) in the top facesheet, it was observed that the failure initiated at a hoop load of 900 lbf/in (12.1 psi internal pressure and 747 lbf/in longitudinal load). However, on the bottom facesheet, a small blip in the strain data was observed, which indicates lack of failure initiation in the bottom facesheet. At a hoop load of approximately 1000 lbf/in, sudden jumps in the strain data were observed in the bottom facesheet. This indicated the failure initiation and propagation in the bottom facesheet. The sudden drop in strain levels indicates that the fracture path bypassed the strain gages, thereby reeducing the strain (loads) locally. The delay in the failure initiation in the bottom facesheet can further be corroborated based on the observed longitudinal and hoop strains shown in figures 99, 100, 101, and 102. The fracture path was observed to propagate at an angle of 45º to the length of the notch, as shown in figure 103. This explains the observed unloading of the strain gages close to the notch. The test panel fractured when the longitudinal load and internal pressure reached 1153 lbf/in and 18.3 psi, respectively.

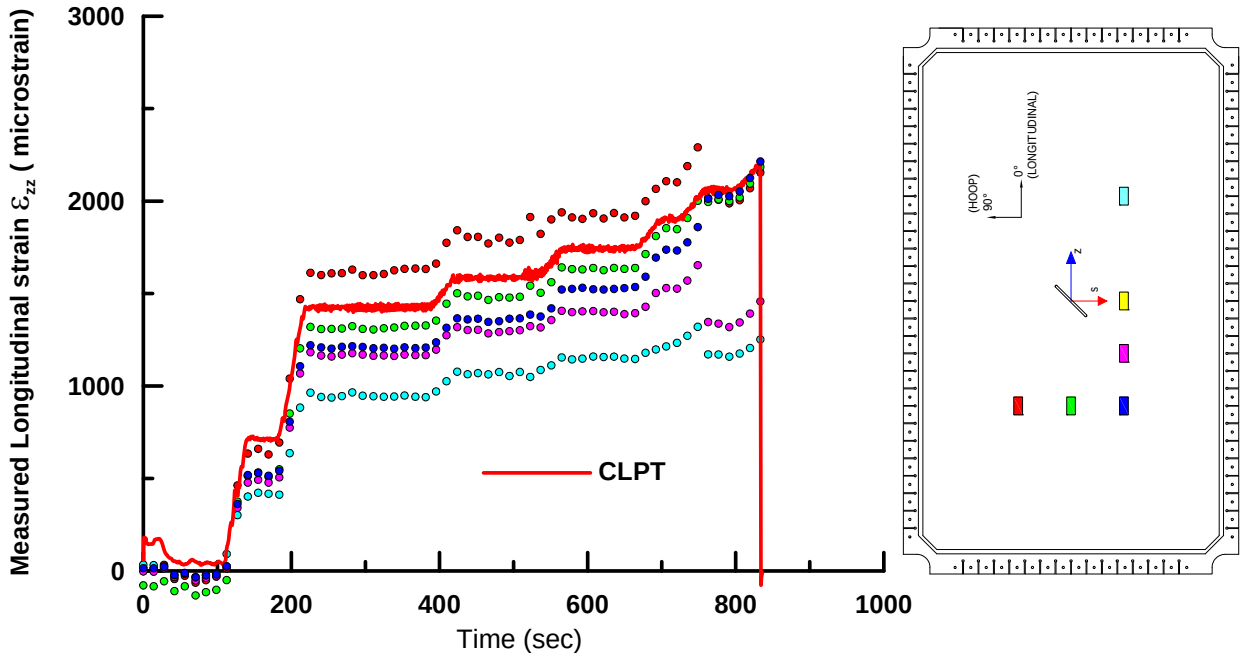

Figure 95. Far-Field Longitudinal Strains in Panel CP6

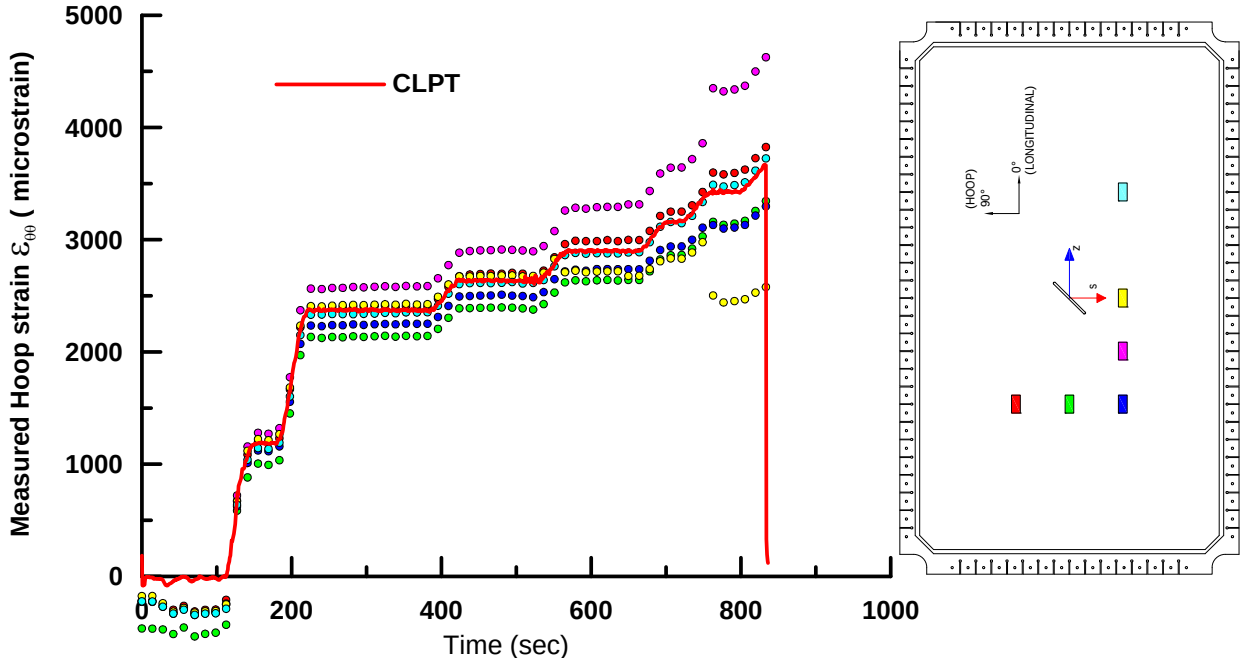

Figure 96. Far-Field Hoop Strains in Panel CP6

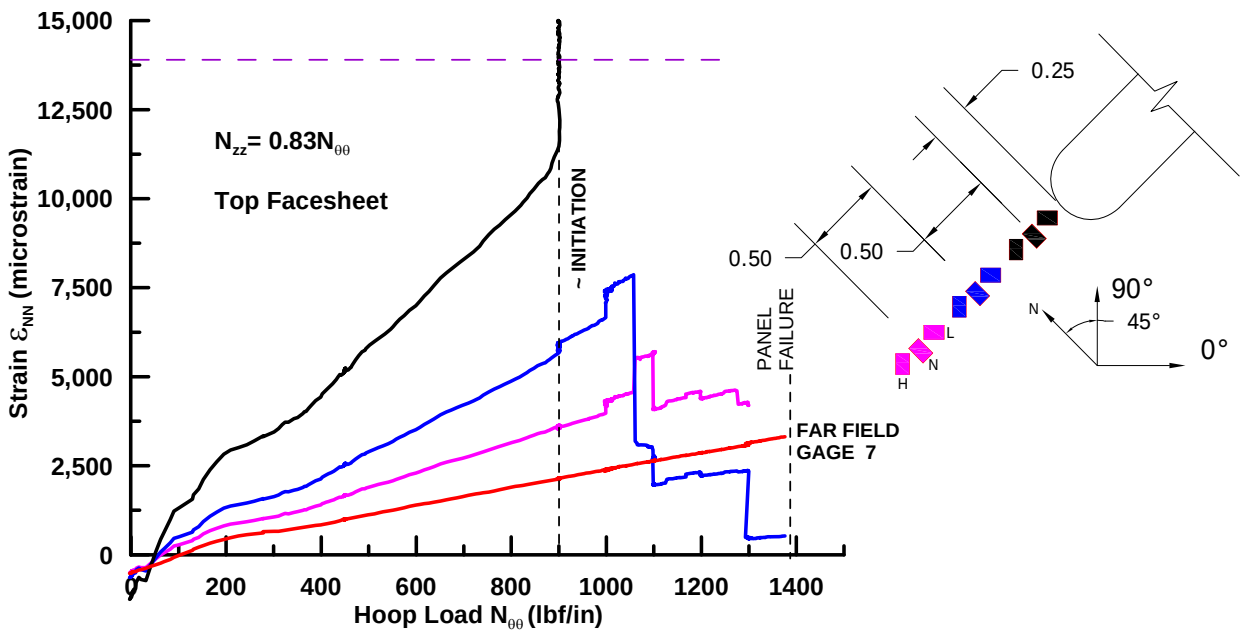

Figure 97. Normal Strains in the Vicinity of the Notch on the Top (Convex) Facesheet

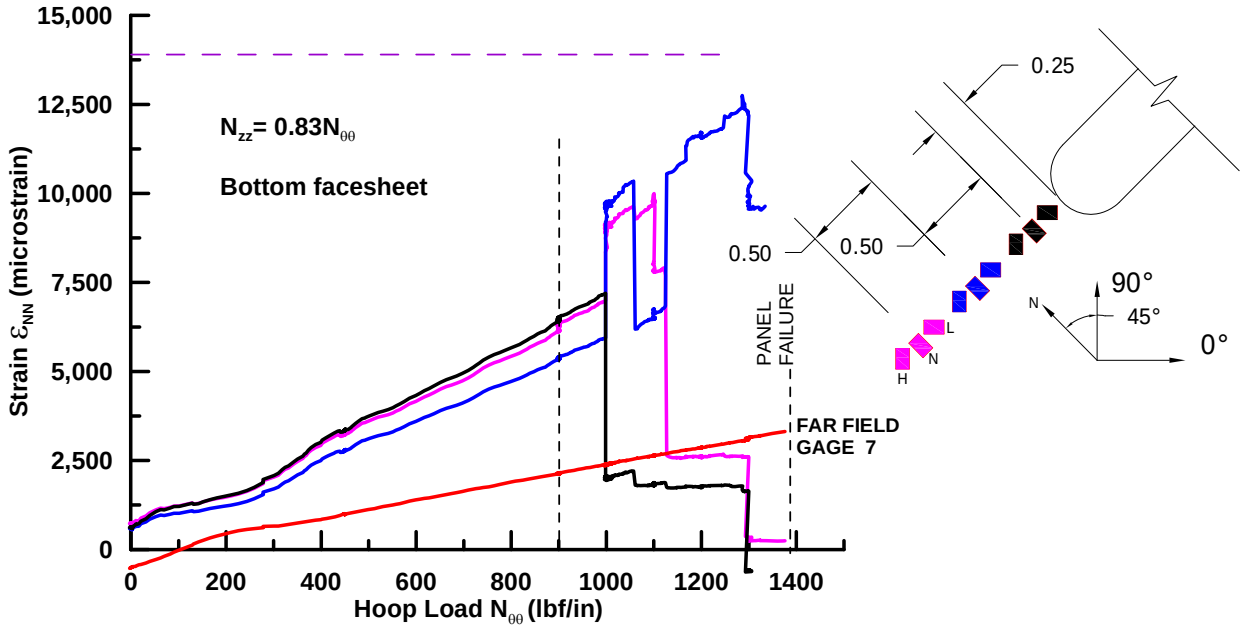

Figure 98. Normal Strains in the Vicinity of the Notch on the Bottom (Concave) Facesheet

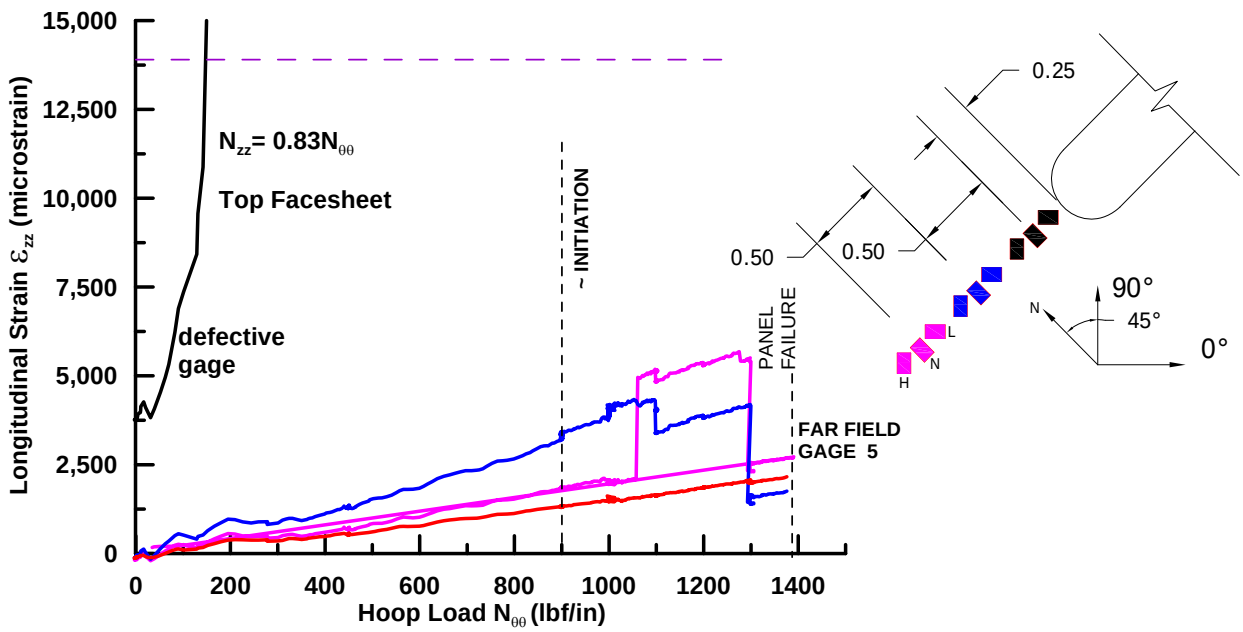

Figure 99. Longitudinal Strains in the Vicinity of the Notch on the Top (Convex) Facesheet

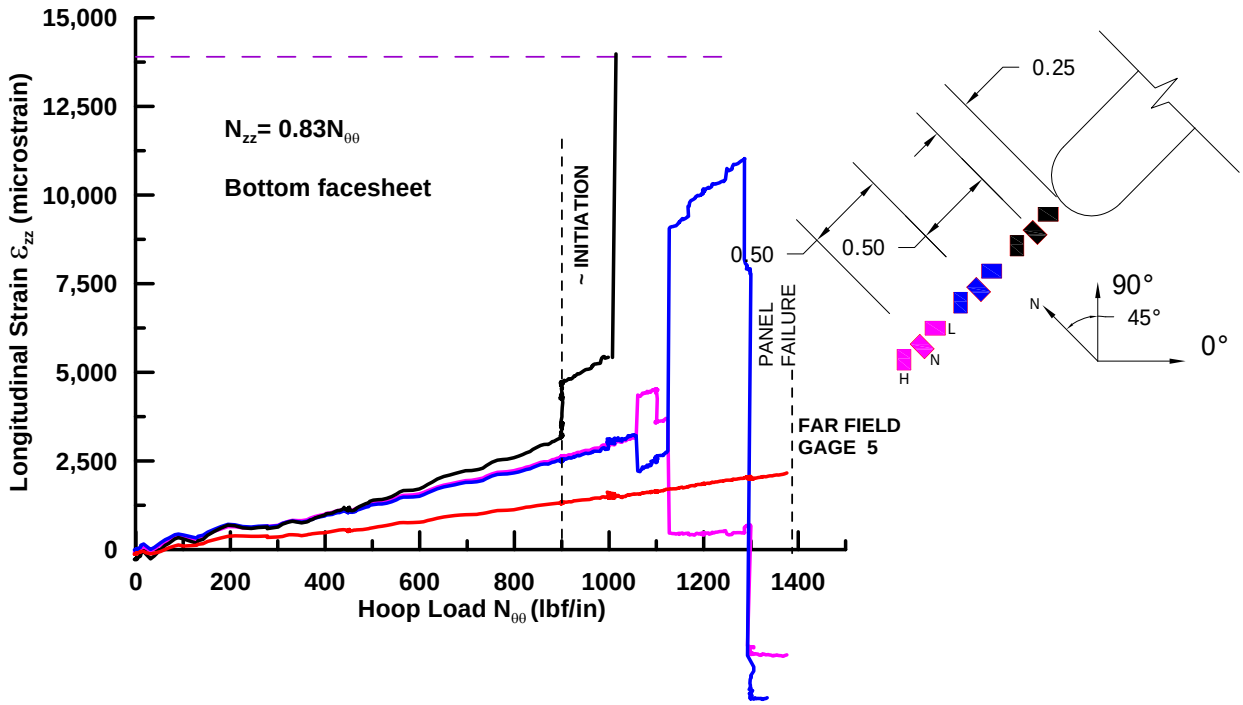

Figure 100. Longitudinal Strains in the Vicinity of the Notch on the Bottom (Concave) Facesheet

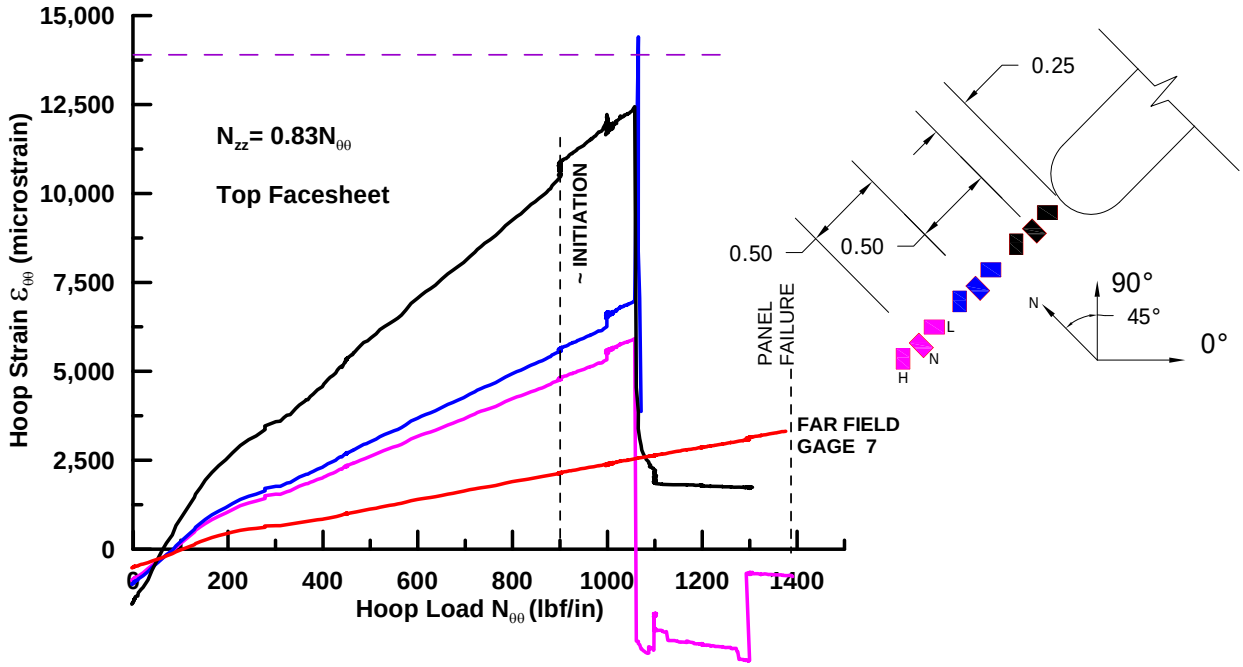

Figure 101. Hoop Strains in the Vicinity of the Notch on the Top (Convex) Facesheet

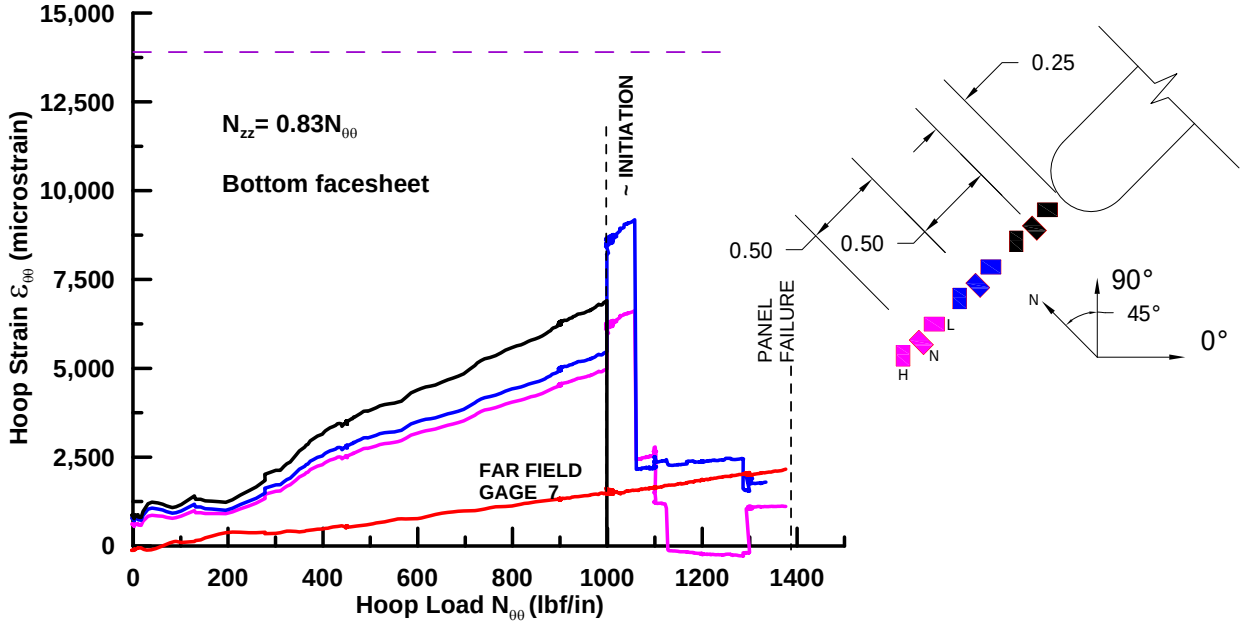

Figure 102. Hoop Strains in the Vicinity of the Notch on the Bottom (Concave) Facesheet

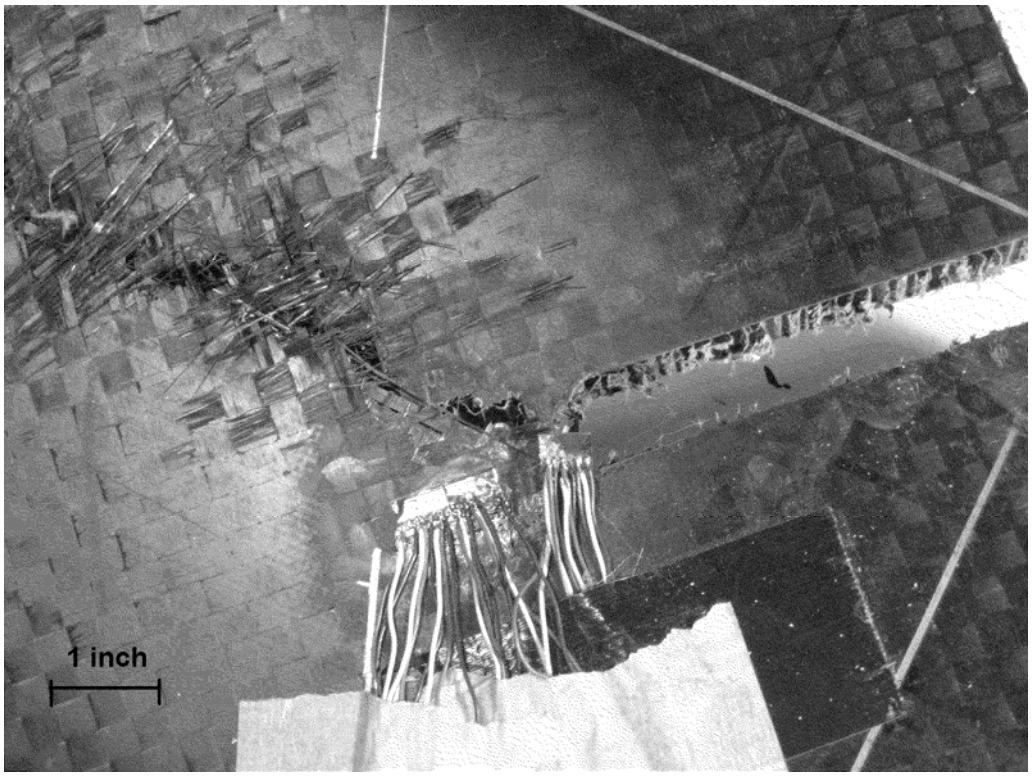

Figure 103. Failure Mode in Panel CP6 With Off-Axis Notch

6. COMPARISON OF TEST AND ANALYSIS OF PANEL FAILURE LOADS.

The loads corresponding to failure initiation based on strain gage readings in the vicinity of the notch/hole and the final failure are compared with the predicted failure loads in table 5. The predicted failure loads based on the finite element analysis are associated with idealized loading conditions where the bending effects were minimal. The predicted failure loads further correspond to failure initiation at the highly stressed regions rather than ultimate failure of the panel.

Table 5. Comparison of Initiation and Final Failure Loads With the Predicted Failure Loads

Panel No.	Damage Type	Load Cases	Initiation and Failure Load from Experiments	Predicted Failure Loads
CP1	Unnotched/baseline	N_{zz}	Elastic loading and unloading	2170 lbf/in
		P_{int}		3315 lbf/in
		$N_{zz}+P_{int}$		2930 lbf/in 39.6 psi
CP1A	3″ x 3″ cross slit, top facesheet	N_{zz}	None	No prediction

Table 5. Comparison of Initiation and Final Failure Loads With the Predicted Failure Loads (Continued)

Panel No.	Damage Type	Load Cases	Initiation and Failure Load from Experiments	Predicted Failure Loads
CP1B	10″ x 1/16″ longitudinal slit	P_{int}	8.1 psi (init) 14 psi (fail)	No prediction
CP2	10″ diameter hole in top facesheet	N_{zz}	No initiation up to 1250 lb/in	1630 lbf/in
		$N_{zz}+P_{int}$	No initiation up to 1160 lbf/in and 18.8psi	1288 lbf/in 17.4 psi
		P_{int}	21.4 psi (init)	16 psi
CP3	10″ x 1/2″ circumferential notch	P_{int} =8 psi N_{zz}	970 lbf/in (init) 1223 lbf/in (fail)	905 lbf /in 12.2psi
CP4	10″ x 1/2″ circumferential notch	P_{int} =1 psi N_{zz}	780 lbf/in (init)	1058 lbf/in
CP5	10″ x 1/2″ longitudinal notch	N_{zz} =83 lbf/in P_{int}	10.2 psi (init) 13.5 psi (fail)	6.2 psi
CP6	10″ x 1/2″ 45º off-axis notch	N_{zz} + P_{int} (1.2:1)	12.5 psi/747 lb/in (init) 18.3 psi/1153 lbf/in (fail)	No prediction

7. SUMMARY.

The behavior of cylindrical sandwich panels with different flaw types under longitudinal and pressurization loads have been investigated experimentally. Test panels were fabricated using Toray T700S-12K-50C/#2510 plain weave carbon fabric prepreg for the facesheets and an overexpanded cell DuPont™ Nomex® honeycomb core (Hexcel Composites, HRH-10/OX-3/16-3.0). Both facesheets had a stacking sequence of [45/0/45] and the core thickness used in the test section was 0.75 inch. The cylindrical panel had a 74-inch internal radius and measured 125 inches long. An undamaged test panel was subjected to longitudinal loading, pressurization and a combination of both loads to study the resulting strain distributions in the panel. Test panels with a 10-inch-diameter open hole, 10-inch-long slit (saw cut) along the longitudinal direction, 10-inch-long longitudinal notch (machined), 10-inch-long circumferential notch, and 10-inch-long notch at 45º to the longitudinal axis were tested under different combination of loads and the residual strengths measured.

The tests on panels without flaws indicated bending of the panel in both r-z and r-q planes, owing to the edge effects produced by the presence of stiffened edges and due to the load introduction region being less wide than the test section. The strains measured along the longitudinal and hoop directions at several locations were compared with the predictions of classical laminated plate theory, albeit for a flat panel. The measured strains compared reasonably well with the CLPT predictions with the differences between the two being maximum at locations closer to the loading edges. After the loading exercises, a 10-inch-long slit was cut

at the center of the panel, while the panel was mounted on the fixture, and loaded to failure under pure pressurization loading. The test panel failed at an internal pressure of 14 psi.

The test panel with a 10-inch-diameter open hole in the top facesheet was subjected to longitudinal, combined longitudinal and pressurization, and pressurization loading scenarios. Due to the constraints on the test apparatus, failure could not be initiated or propagated during the first two loading conditions. Under pressurization loading, a crack was initiated along the boundary of the hole, but due to lack of additional loading capability of the test apparatus, the crack could not be propagated to achieve panel failure. Two test panels with 10-inch-long circumferential notches were tested under different combinations of pressurization and longitudinal loading. The first panel was initially subjected to an internal pressure of 8 psi and longitudinal loads applied while holding the internal pressure. The test panel fractured at a longitudinal load of 1223 lbf/in. The second panel was subjected to a similar loading, except that the internal pressure was 1 psi. While a crack was initiated in the panel, it could not be propagated to achieve panel failure. The test panel had to be unloaded after 1220 lbf/in due to constraints on the test apparatus. The test panel with a 10-inch-long longitudinal notch was subjected to pressurization/hoop loading. A constant longitudinal load of 83 lbf/in was applied to the panel to stabilize the panel in the fixture. The test panel fractured at a pressure of 13.5 psi (hoop load of 1000 lbf/in). The test panel with a 45° off-axis notch was subjected to proportional longitudinal and pressurization loading. The internal pressure was applied such that the longitudinal-to-hoop load ratio was equal to 0.83 at each load step. The test panel fractured when the longitudinal load and internal pressure reached 1153 lbf/in and 18.3 psi, respectively. The fracture path subtended an angle of 45º to the length of the notch.

Analytical predictions of failure load were generally conservative when compared to test results and provide some assurance that analysis can be a useful tool to evaluate the effects of large damage. The predictions are deemed reasonable, as the analysis did not account for local bending effects, did not model the facesheets and honeycomb core individually, and did not model damage progression. The results of analytical modeling that considers those effects will be included in a future report.

8. REFERENCES.

1. Tomblin, J.S., Raju, K.S., Liew, J., and Smith, B.L., "Impact Damage Characterization and Damage Tolerance of Composite Sandwich Airframe Structures," FAA report DOT/FAA/AR-00/44, January 2001.

2. Abrate, S., *Impact on Composite Structures*, Cambridge University Press, 1998.

3. Tomblin, J.S., Raju, K.S., Acosta, J.F., and Romine, N., "Impact Damage Characterization and Damage Tolerance of Composite Sandwich Airframe Structures—Phase 2," FAA report DOT/FAA/AR-02/80, October 2002.

4. Tomblin, J.S., Raju, K.S., and Arosteguy, G., "Damage Tolerance of Composite Sandwich Panels—Scaling Effects," FAA report DOT/FAA/AR-03/75, February 2004.

5. Tomblin, J.S., Raju, K.S., Walker, T., and Acosta, J.F., "Damage Resistance and Tolerance of Composite Sandwich Panels—Additional Results," FAA report DOT/FAA/AR-05/33, October 2005.

6. Bakuckas, John, "Full-Scale Testing and Analysis of Fuselage Structure Containing Multiple Cracks," FAA report DOT/FAA/AR-01/46, July 2002.

7. Rouse, M., Young, R.D., and Gehrki, R.H., "Structural Stability of a Stiffened Aluminum Fuselage Panel Subjected to Combined Mechanical and Internal Pressure Loads," AIAA-2003-1423.

8. Gruber, M.L., Mazur, C.J., Wilkins, K.E., and Worden, R.E., "Investigation of Fuselage Structure Subject to Widespread Fatigue Damage," FAA report DOT/FAA/AR-95/47, February 1996.

9. Tomblin, J., Sherraden, J., Seneviratne W., and Raju, K.S., "A-Basis and B-Basis Design Allowables for Epoxy-Based Prepreg-TORAY T700SC-12K-50C/#2510 Plain Weave Fabric [US Units]," AGATE-WP3.3-033051-131, September 2002.

10. Hexweb® HRH-10 Product Data Sheet, http://www.hexcel.com

11. Hostert Technical Services, 4 Lakeside Blvd., Wichita, Kansas 67207-1012, Tel (316) 682-4231.

12. Measurements Group, Inc., P.O. Box 27777, Raleigh, North Carolina 27611.

13. Leone, Frank A., Bakuckas, John G., Shyprykevich, Peter, and Davies, Curtis, "Structural Testing and Analysis of Honeycomb Sandwich Composite Fuselage Panels," FAA report DOT/FAA/AR-08/51, December 2008.

14. Reismann, H. and Pawlik, P.S., *Elasticity: Theory and Applications*, Krieger Publishing Co., Malabar, Florida 32950, 1991.

APPENDIX A—ANALYIS FOR FAILURE LOAD ESTIMATION

A.1 METHODS OF ANALYSIS.

Room temperature dry analyses were conducted for 12 failure modes, as listed below. All analyses assumed virgin laminate properties (no initial impact damage).

- Core shear was analyzed for combined loading using a modified interaction failure criteria.

$$MS = \frac{1}{\left[\left(\frac{f_{xz}}{F_{xz}}\right)^n + \left(\frac{f_{yz}}{F_{yz}}\right)^n\right]^{\frac{1}{n}}} - 1$$

where: f_{xz} = Applied transverse shear stress in xz plane
f_{yz} = Applied transverse shear stress in yz plane
F_{xz} = Allowable transverse shear stress in xz plane
F_{yz} = Allowable transverse shear stress in yz plane
n = 1.2 for hexagonal core
n = 2.0 for potting

- Core shear crimping for x direction (longitudinal direction) loading was conducted using methods described in reference A-1.

- Core shear crimping for y direction (transverse direction) loading was conducted using methods described in reference A-1.

- Core shear crimping for shear loading was conducted using methods described in reference A-1.

- Compression dimpling analysis, per reference, A-1 was used.

- Shear dimpling analysis, per reference, A-1 was used.

- Combined dimpling analysis, per reference, A-1 was used.

- Facesheet compression wrinkling, per methods described in reference A-1, was conducted using the highest compressive facesheet stress in either the longitudinal or transverse directions. The allowable wrinkling stresses were factored up by 20% to account for conservatism observed from coupon testing.

- Facesheet wrinkling, per reference A-1, was conducted using the minor principal facesheet stress. Material properties were rotated into the minor principal stress direction. The allowable wrinkling stresses were factored up by 20% to account for conservatism observed from coupon testing.

- Laminate analysis using maximum strain failure criteria was conducted in the longitudinal ply direction.

- Laminate analysis using maximum strain failure criteria was conducted in the transverse ply direction.

- Laminate analysis using maximum strain failure criteria was conducted in the shear ply direction.

A.2 RESULTS.

Minimum margin of safety (MS) plots for each panel and loading type are shown in figures A-1 through A-10. These plots reflect the minimum margin of safety considering the 12 failure modes.

A.2.1 UNDAMAGED PANEL, 1000 lb/in LONGITUDINAL LOAD.

The minimum margin of safety plot is shown in figure A-1. The 1.17 minimum MS for principal stress wrinkling failure mode is located at the corner of the 5-ply facesheet region near the loaded edge of the panel.

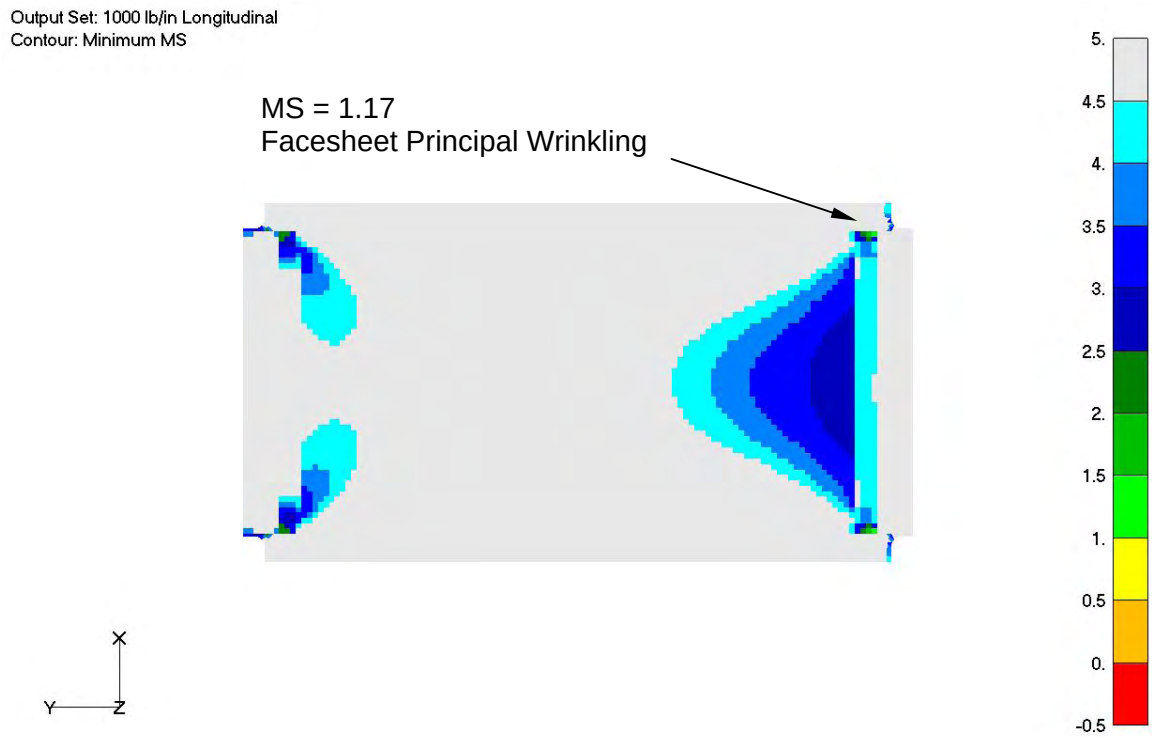

Figure A-1. Undamaged Panel, 1000 lb/in Longitudinal Load

The predicted panel failure load is therefore:

$$\text{Panel Failure Load} = (MS + 1)(1000) = (1.17 + 1)(1000) = 2170 \text{ lb/in}$$

A.2.2 UNDAMAGED PANEL, 13.5 psi PRESSURE LOAD.

The minimum margin of safety plot is shown in figure A-2. The 2.32 minimum MS for core shear is located at a corner radius of the panel.

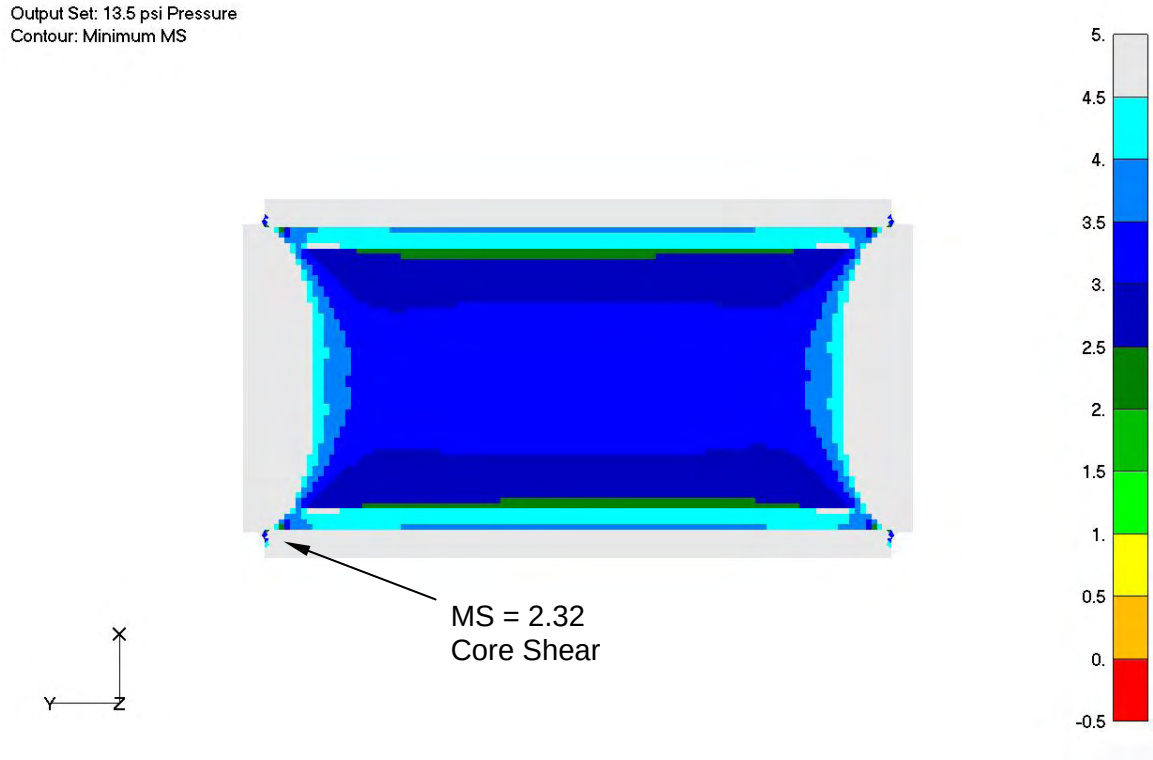

Figure A-2. Undamaged Panel, 13.5 psi Pressure Load

The predicted panel failure load is therefore:

$$\text{Panel Failure Pressure} = (MS + 1)(13.5) = (2.32 + 1)(13.5) = 44.8 \text{ psi}$$

A.2.3 UNDAMAGED PANEL, 1000 lb/in LONGITUDINAL LOAD, 13.5 psi PRESSURE LOAD.

The minimum margin of safety plot is shown in figure A-3. The 1.93 minimum MS for core shear is located at the corner radius of the panel.

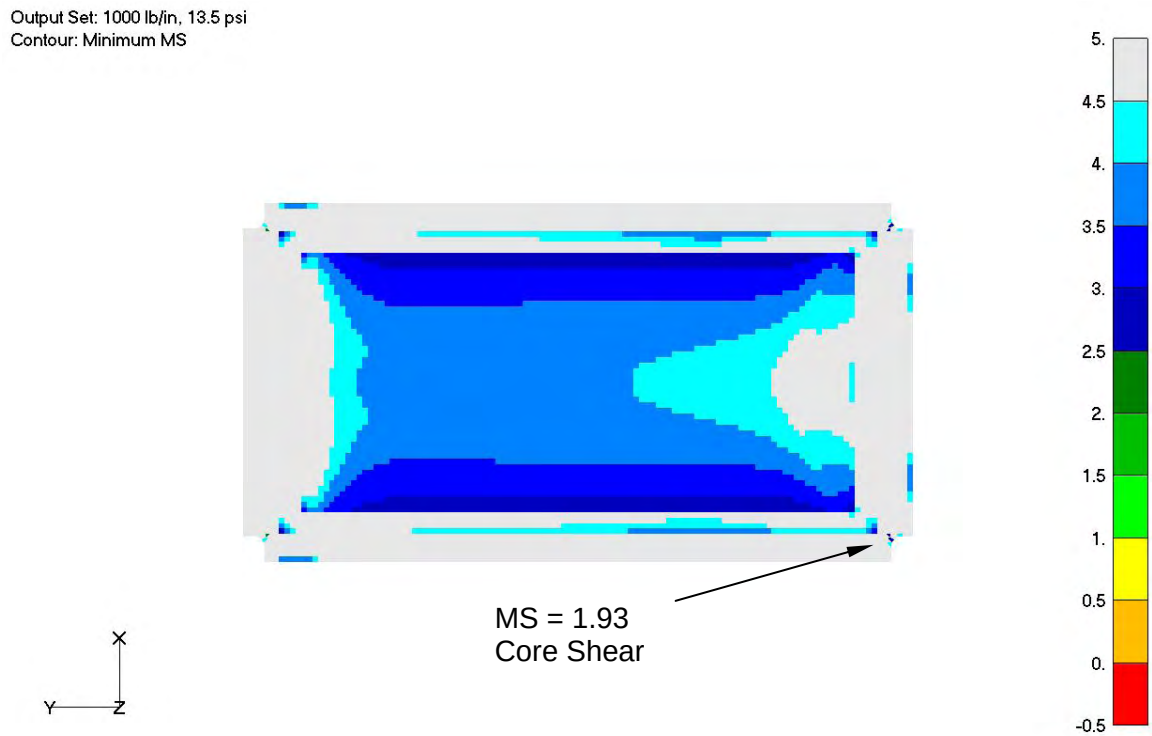

Figure A-3. Undamaged Panel, 1000 lb/in Longitudinal Load, 13.5 psi Pressure Load

The predicted panel failure loads are therefore:

Panel Failure Load = (MS + 1)(1000) = (1.93 + 1)(1000) = 2930 lb/in

Panel Failure Pressure = (MS + 1)(13.5) = (1.93 + 1)(13.5) = 39.6 psi

A.2.4 A 10-INCH CIRCULAR HOLE, 1000 lb/in LONGITUDINAL LOAD.

The minimum margin of safety plot is shown in figure A-4. The 0.63 minimum MS for facesheet principal stress wrinkling is located at panel mid-width at the edge of the circular hole.

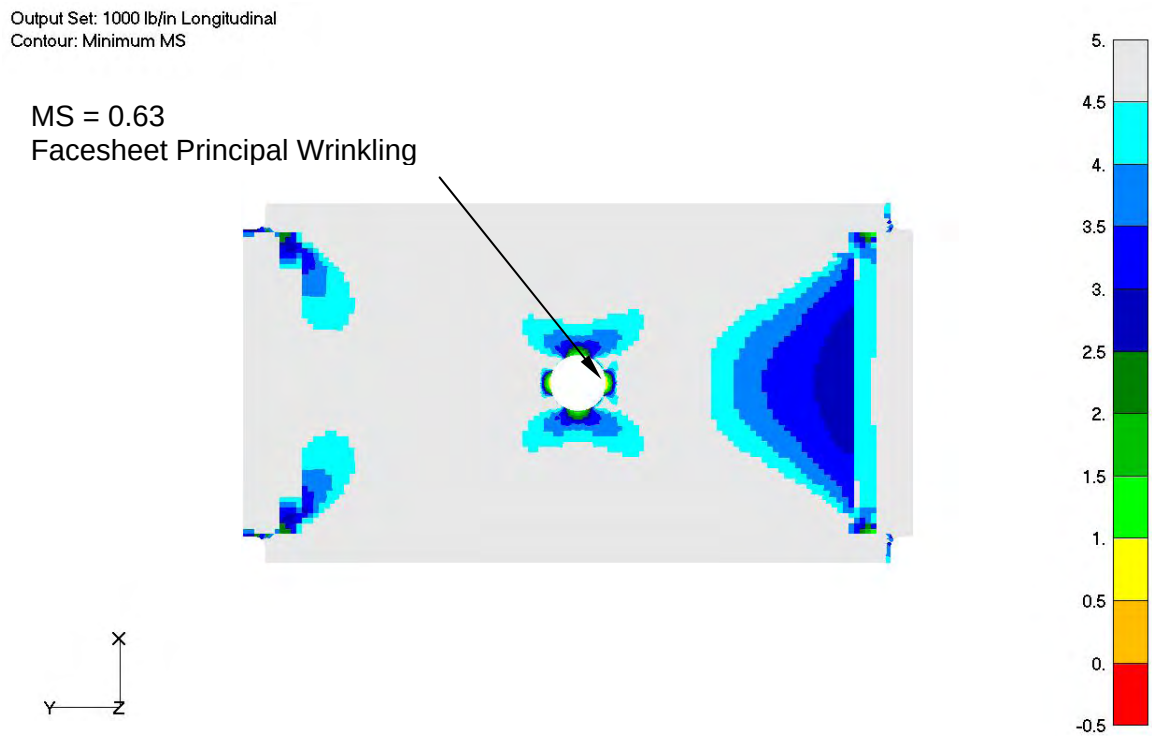

Figure A-4. A 10-Inch-Diameter Circular Hole, 1000 lb/in Longitudinal Load

The predicted panel failure load is therefore:

$$\text{Panel Failure Load} = (MS + 1)(1000) = (0.63 + 1)(1000) = 1630 \text{ lb/in}$$

A.2.5 A 10-INCH CIRCULAR HOLE, 13.5 psi PRESSURE LOAD.

The minimum margin of safety plot is shown in figure A-5. The 0.184 minimum MS for laminate transverse tension fiber strain is located at panel mid-width at the edge of the circular hole.

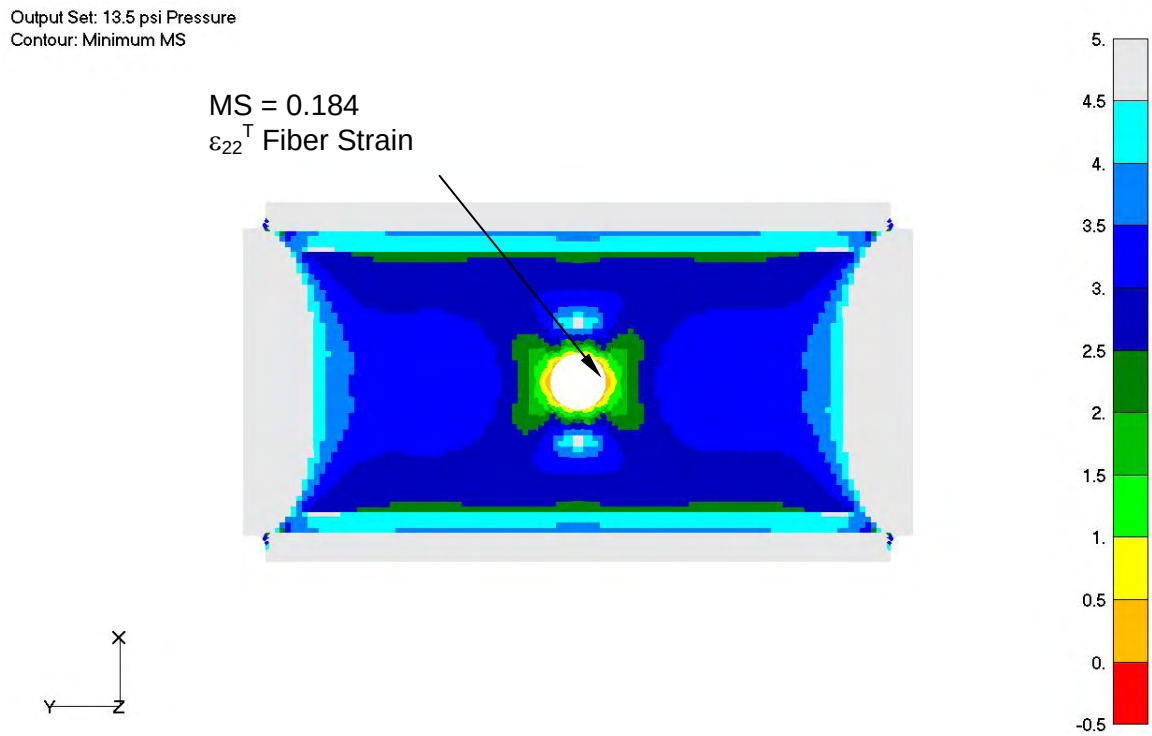

Figure A-5. A 10-Inch-Diameter Circular Hole, 13.5 psi Pressure Load

The predicted panel failure load is therefore:

$$\text{Panel Failure Pressure} = (MS + 1)(13.5) = (0.184 + 1)(13.5) = 16.0 \text{ psi}$$

A.2.6 A 10-INCH CIRCULAR HOLE, 1000 lb/in LONGITUDINAL LOAD, 13.5 psi PRESSURE LOAD.

The minimum margin of safety plot is shown in figure A-6. The 0.288 minimum MS for laminate transverse tension fiber strain is located at panel mid-width at the edge of the circular hole.

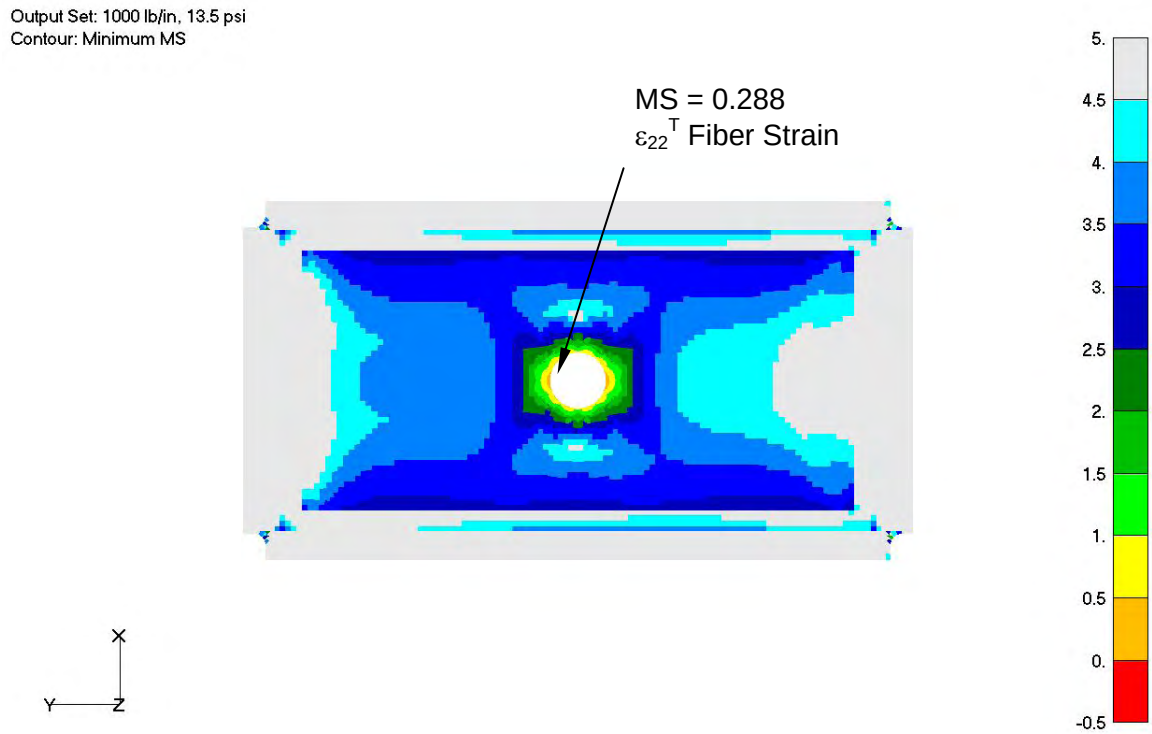

Figure A-6. A 10-Inch-Diameter Circular Hole, 1000 lb/in Longitudinal Load, 13.5 psi Pressure Load

The predicted panel failure loads are therefore:

$$\text{Panel Failure Load} = (MS + 1)(1000) = (0.288 + 1)(1000) = 1288 \text{ lb/in}$$

$$\text{Panel Failure Pressure} = (MS + 1)(13.5) = (0.288 + 1)(13.5) = 17.4 \text{ psi}$$

A.2.7 A 10-INCH LONGITUDINAL NOTCH, 13.5 psi PRESSURE LOAD.

The minimum margin of safety plot is shown in figure A-7. The -0.539 minimum MS for laminate transverse tension fiber strain is located at panel mid-width at the edge of the notch radius.

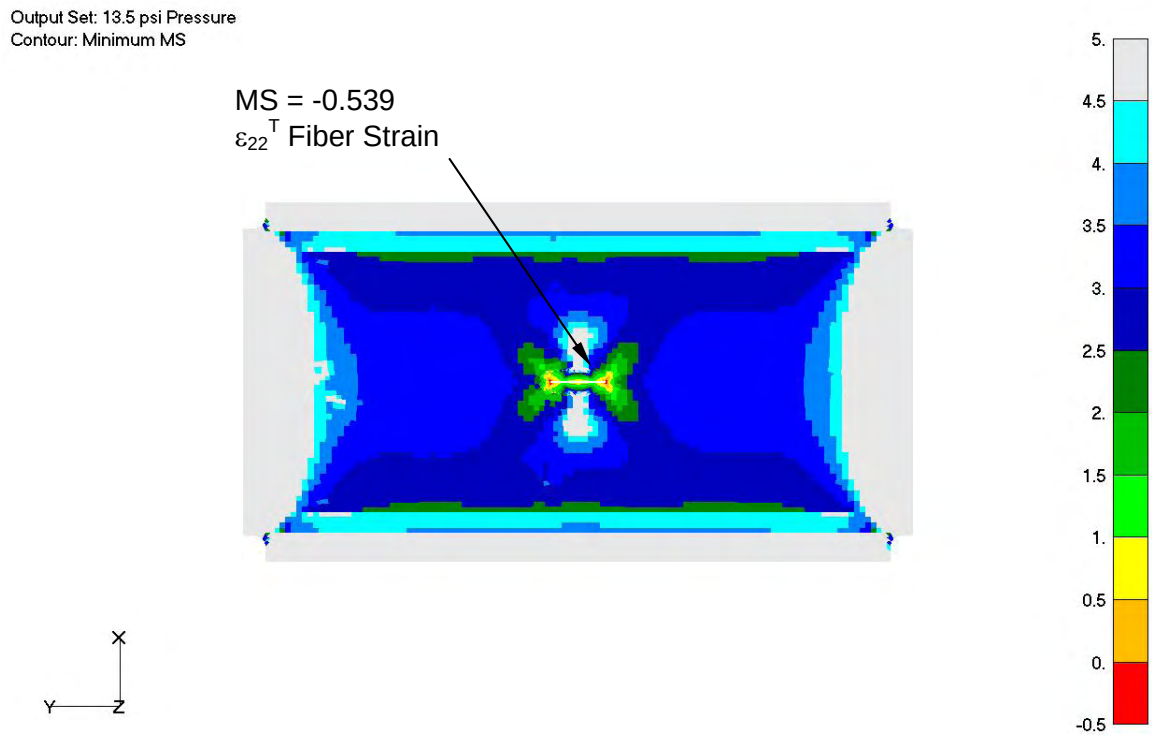

Figure A-7. Longitudinal Slot, 13.5 psi Pressure Load

The predicted panel failure load is therefore:

$$\text{Panel Failure Pressure} = (MS + 1)(13.5) = (-0.539 + 1)(13.5) = 6.2 \text{ psi}$$

A.2.8 A 10-INCH LONGITUDINAL NOTCH, 1000 lb/in LONGITUDINAL LOAD, 13.5 psi PRESSURE LOAD.

The minimum margin of safety plot is shown in figure A-8. The -0.532 minimum MS for laminate transverse tension fiber strain is located at panel mid-width at the edge of the notch radius.

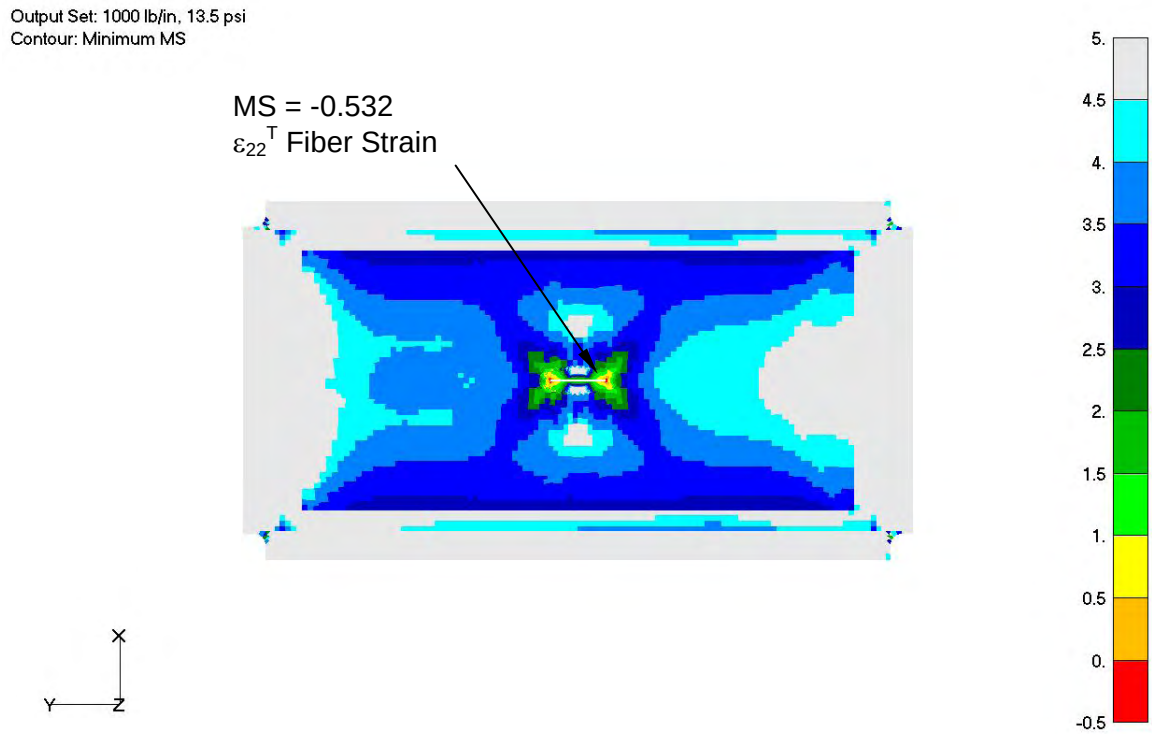

Figure A-8. Longitudinal Slot, 1000 lb/in Longitudinal Load, 13.5 psi Pressure Load

The predicted panel failure loads are therefore:

Panel Failure Load = (MS + 1)(1000) = (-0.532 + 1)(1000) = 468 lb/in

Panel Failure Pressure = (MS + 1)(13.5) = (-0.532 + 1)(13.5) = 6.3 psi

A.2.9 A 10-INCH CIRCUMFERENTIAL NOTCH, 1000 lb/in LONGITUDINAL LOAD.

The minimum margin of safety plot is shown in figure A-9. The 0.058 minimum MS for laminate longitudinal tension fiber strain is located at the extreme edge of the notch radius.

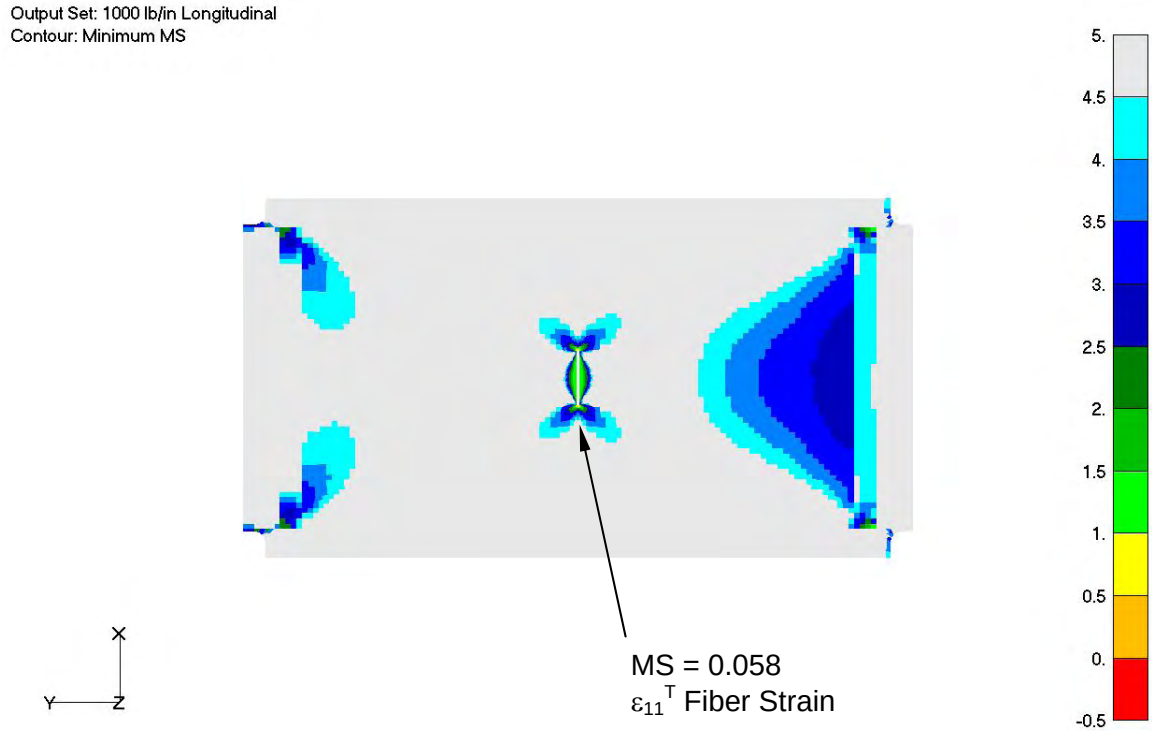

Figure A-9. Circumferential Slot, 1000 lb/in Longitudinal Load

The predicted panel failure load is therefore:

$$\text{Panel Failure Load} = (MS + 1)(1000) = (0.058 + 1)(1000) = 1058 \text{ lb/in}$$

A.2.10 A 10-INCH CIRCUMFERENTIAL NOTCH, 1000 lb/in LONGITUDINAL LOAD, 13.5 psi PRESSURE LOAD.

The minimum margin of safety plot is shown in figure A-10. The -0.095 minimum MS 0.095 for laminate longitudinal tension fiber strain is located at the extreme edge of the notch radius.

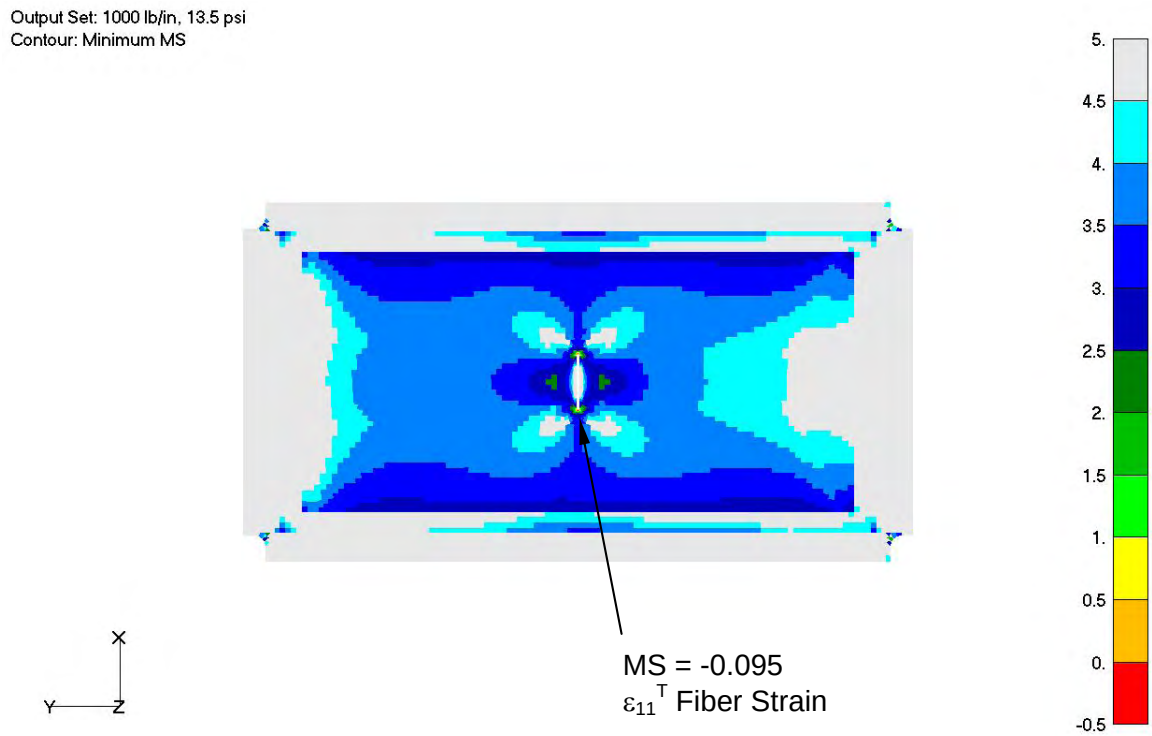

Figure A-10. Circumferential Slot, 1000 lb/in Longitudinal Load, 13.5 psi Pressure Load

The predicted panel failure loads are therefore:

$$\text{Panel Failure Load} = (MS + 1)(1000) = (-0.095 + 1)(1000) = 905 \text{ lb/in}$$

$$\text{Panel Failure Pressure} = (MS + 1)(13.5) = (-0.095 + 1)(13.5) = 12.2 \text{ psi}$$

A.2.11 REFERENCES.

A-1. Ward, S.H., “Sandwich Structure Analysis,” Draft Writeup for MIL-HDBK-17 Meeting–March 1988, San Diego, California.